DEVELOPMENT OF SINTERED TITANIUM POWDER METALLURGY COMPONENTS

Thesis submitted by

ARUNANGSU DAS

Doctor of Philosophy

(Engineering)

DEPARTMENT OF MECHANICAL ENGINEERING

FACULTY COUNCIL OF ENGINEERING & TECHNOLOGY

JADAVPUR UNIVERSITY

KOLKATA, INDIA

2019

JADAVPUR UNIVERSITY

KOLKATA-700032, INDIA

INDEX NO. 84/15/E

1. Title of the Thesis:

DEVELOPMENT OF SINTERED TITANIUM POWDER METALLURGY COMPONENTS

2. Name, Designation and Institution of the Supervisors:

Dr. Goutam Sutradhar
Director
National Institute of Technology, Manipur
Professor (on lien)
Dept. of Mechanical Engineering
Jadavpur University
Kolkata, India

Dr. Susenjit Sarkar
Professor
Dept. of Mechanical Engineering
Jadavpur University
Kolkata, India

3. List of Publications (Referred Journals):

I. **Arunangsu Das, Susenjit Sarkar, Malobika Karanjai, Goutam Sutradhar**, *"An Experimental Investigation into the Role of Sintering Temperature on the Metal Removal Rate of Titanium Powder Metallurgy Products – A Taguchi Approach*" Indian Journal of Engineering & Materials Sciences, Vol. 25, (October 2018), pp. 377-382.

II. **Arunangsu Das, Susenjit Sarkar, Malobika Karanjai, Goutam Sutradhar**, "*Application of Box–Behnken Design and Response Surface Methodology for Surface Roughness Prediction Model of CP-Ti Powder Metallurgy Components through WEDM*"; Journal of the Institution of Engineers (India) Series D (Springer), Vol.99, Issue-1, (April 2018), pp. 9-21.

III. **Arunangsu Das, Susenjit Sarkar, Malobika Karanjai, Goutam Sutradhar**, "*RSM Based Study on the Influence of Sintering Temperature on MRR for Titanium Powder Metallurgy Products using Box-Behnken Design*"; Materials Today: Proceedings (Elsevier), Vol. 5, Issue -2, Part-1 (2018), pp. 6509-6517.

IV. **Arunangsu Das, Malobika Karanjai, Susenjit Sarkar, Goutam Sutradhar**, ''*Investigation of the Wire-EDM characteristics on CP-Titanium powder metallurgy components - an RSM approach*''; Transactions of Powder Metallurgy Association of India, Vol. 43 (1), (June 2017), pp. 24-32.

V. **Arunangsu Das, Susenjit Sarkar, Malobika Karanjai, Goutam Sutradhar**, ''*Experimental Investigation of the Compressibility and Mechanical Properties of Cp-Ti Powder Metallurgy Components*''; Transactions of Powder Metallurgy Association of India, Vol. 42 (1), (June 2016), pp. 32-38.

VI. **Arunangsu Das, Suman Sarkar, Susenjit Sarkar, Goutam Sutradhar**, ''*Optimization of the Wire-EDM Characteristics on Press and Sintered Pure Titanium Powder Metallurgy Components Using Grey Relational Analysis*''; International Journal of Advanced Manufacturing Technology, (Communicated).

4. List of patents:

Nil

5. List of Presentations in National/International/Conferences/Workshops:

I. **Arunangsu Das, Malobika Karanjai, Susenjit Sarkar, Goutam Sutradhar**, "*Sensitivity Analysis of MRR during Wire-EDM of Sintered Titanium Powder Metallurgy Parts*"; Proceedings: 1st International Conference on Mechanical Engineering (INCOM 2018), Jadavpur, Kolkata, pp 477-481.

II. **Arunangsu Das, Susenjit Sarkar, Malobika Karanjai, Goutam Sutradhar**, "*RSM Based Study on the Influence of Sintering Temperature on MRR for Titanium Powder Metallurgy Products using Box-Behnken Design*", Souvenir of 7th International Conference on Materials Processing & Characterization (ICMPC) 2017, Hyderabad, pp 48.

III. **Arunangsu Das, Malobika Karanjai, Susenjit Sarkar, Goutam Sutradhar**, "*Investigation of the Wire-EDM characteristics on CP-Titanium powder metallurgy components - an RSM approach*" presented at the International Conference on Powder Metallurgy & Particulate Materials (PM17) 2017, New Delhi.

IV. **Arunangsu Das, Malobika Karanjai, Susenjit Sarkar, Goutam Sutradhar**, "*Investigation of the Compressibility and Machinability of Sintered Titanium Powder Metallurgy Components vis-à-vis cast Titanium Products*", Transactions of 65th Indian Foundry Congress (IFC) 2017, Kolkata, pp 162-169.

V. **Arunangsu Das, Susenjit Sarkar, Malobika Karanjai, Goutam Sutradhar**, "*Experimental Investigation of the Compressibility and Mechanical Properties of Cp-Ti Powder Metallurgy Components*", presented at the International Conference on Powder Metallurgy & Particulate Materials (PM16) 2016, Pune.

VI. **Suswagata Poria, Arunangsu Das, Goutam Sutradhar**, "*Development of Sintered Titanium Powder Metallurgy Products for Medical Applications*", presented at the All India Seminar on Recent Advancement in Manufacturing and its Management (RAMM-14), 2014, Dhanbad.

DEPARTMENT OF MECHANICAL ENGINEERING

FACULTY COUNCIL OF ENGINEERING & TECHNOLOGY

JADAVPUR UNIVERSITY

KOLKATA, INDIA

CERTIFICATE FROM THE SUPERVISOR/S

This is to certify that the thesis entitled ***"Development of Sintered Titanium Powder Metallurgy Components"*** *submitted by* ***Shri Arunangsu Das****, who got his name registered on* ***06.04.2015*** *for the award of* ***Ph.D. (Engineering)*** *degree of Jadavpur University is absolutely based upon his own work under the supervision of* ***Prof. (Dr.) Goutam Sutradhar*** *and* ***Prof. (Dr.)Susenjit Sarkar*** *and that neither his thesis nor any part of the thesis has been submitted for any degree/diploma or any other academic award anywhere before.*

_____

Prof. (Dr.) Goutam Sutradhar
Director
National Institute of Technology, Manipur
Professor (on lien)
Dept. Mechanical Engineering
Jadavpur University, Kolkata
Supervisor

_____

Prof. (Dr.) Susenjit Sarkar
Professor
Dept. of Mechanical Engineering
Jadavpur University
Kolkata
India
Supervisor

"This page is intentionally left blank"

ABSTRACT

In the last 6 decades, after the emergence of titanium in commercial quantities in the early 1950's, there has been an ever increasing demand in titanium use as a substitute over many metals in the aerospace, automotive, petrochemical, chemical, oil and biomedical industries. Titanium and its alloys play an important role in the aerospace industry in the construction of airframes and aero engines where weight, safety and fuel economy is highly prioritized. In automotive, chemical and biomedical industries, titanium is typically used to manufacture valves, valve springs, connecting rods, bolt fasteners and exhaust system of automobiles, heat exchangers, tanks, structural parts, process vessels and medical implants for human body. Other areas of application are in spectacle frames, cameras, watches, and golf club heads.

Titanium is also widely used for the production of orthopedic or dental implants because direct contact occurs between bones and implant surfaces. Titanium is biocompatible, highly corrosion resistant and durable. Moreover, it is easily prepared in many different shapes and textures without affecting its biocompatibility.

The powder metallurgy technique aims to transform metallic powders, using pressure and heat, by means of a thermal treatment (sintering) that substitutes the classic melting and that is carried out below the melting point of the most important metal. The use of the powder metallurgy in the biomedical area is recent and its great advantage is the production of prosthesis near to the final format (near net shapes), dense or with controlled porosity and generally less expensive than the conventional processes.

Powder Metallurgy is a near net shaping technology, where high material waste is reduced and close proximity of final dimensions and elimination / minimization of machining processes are achieved. In addition, the final properties of a sintered powder metallurgy material can be easily controlled to suit some applications, for example in biomedical applications where the density is controlled in order to produce porous material into which bone can grow.

Powder metallurgy processes typically use metal powders that are formed into final shape. The most common powder metallurgy process is press-and-sinter where the powders are pressed into shape under high pressures and then the compacted shape is sintered in a protective atmosphere.

The present thesis focuses on the processing, characterization, forging behavior, machining analysis and corrosion behavior of press and sinter formed commercially pure titanium powder metallurgy parts. The forging behavior has been validated by mathematical analysis with the help of 'upper bound theory'. The machining analysis has been performed in a Wire-cut EDM, since conventional machining is difficult for hard materials like titanium. The corrosion behavior of the titanium samples has been tested in Hank's solution to analyze its effects as prosthesis when implanted in human body.

“This page is intentionally left blank”

ABOUT THE AUTHOR

Name: ARUNANGSU DAS
Address: 12/1D, Dakshinpara Road
P.O. Thakurpukur
Kolkata - 700063
West Bengal, India

Email: dasarunangsu@gmail.com

Education:

B.E. (Mechanical) (2004)
Jadavpur University, Kolkata, West Bengal

M.E. (Design of Mechanical Equipment) (2011)
Birla Institute of Technology, Mesra
Ranchi, Jharkhand

Experience:

Mr. Arunangsu Das is presently working as Lecturer in Mechanical Engineering at Ranaghat Government Polytechnic, Ranaghat, Nadia from 05.01.2019 to till date. Earlier, Sri Das had worked in the capacity of Lecturer and Head of the Mechanical Engineering Department at Iswar Chandra Vidyasagar Polytechnic, Jhargram, Paschim Medinipur from 01.11.2007 to 31.10.2013 and at Acharya Prafulla Chandra Ray Polytechnic, Jadavpur, from 01.11.2013 to 04.01.2019. He had previously worked at Public Health Engineering Dte., Govt. of West Bengal from 08.09.2000 to 31.10.2007.

He is an Associate Member of the **Institution of Engineers (India).** He is also a member of **The Institute of Indian Foundrymen**. He is a Life Member of the **Indian Association for the Cultivation of Science** and also Life Member of the **Powder Metallurgy Association of India**. He is also a **paper setter** of various engineering admission tests and corporate recruitment examinations.

“This page is intentionally left blank”

ACKNOWLEDGEMENT

I wish to express my profound regards to my supervisor, Prof. (Dr.) Goutam Sutradhar, Director, National Institute of Technology Manipur, and Professor on-lien, Department of Mechanical Engineering, Jadavpur University, Kolkata, for his unconditional support, guidance and advice towards me during preparation of this dissertation. No word would be sufficient to express my gratitude towards him.

I would like to express my sincere thanks to my co-supervisor, Prof. (Dr.) Susenjit Sarkar, Professor, Department of Mechanical Engineering, Jadavpur University, Kolkata, for his important suggestions, encouragement, and constant motivation in completing this research work. Without him, this research work would never have been completed.

I would like to express my most sincere thanks to my another mentor, Dr. Malobika Karanjai, Senior Scientist, International Advanced Research Centre for Powder Metallurgy and New Materials (ARCI), Hyderabad and her staff, without whose support the sintered samples could not have been made. It has been a distinct privilege for me to work with Prof. Goutam Sutradhar, Prof. Susenjit Sarkar and Dr. Malobika Karanjai.

Words are inadequate to express deep sense of gratitude to the members of the doctoral committee, Mechanical Engineering Dept., Jadavpur University, Kolkata.

I am grateful to C.S.I.R., New Delhi for providing the financial support under Major Research Project titled 'Investigation of forgeability and machinability of sintered titanium components', Sanction Letter No. 22(0587)/12/EMR-II dated 02.04.2012 to P.I. Prof. Goutam Sutradhar, without which this work could not have been attempted.

I am thankful to Dr. Prabal Kumar Das, Retired Scientist, Central Glass and Ceramic Research Institute (CGCRI), Kolkata and Mr. S. K. Dalui for providing the facilities to conduct various experimental works in the concerned laboratories of CGCRI.

I am also thankful to Mr. A. K. Samanta, Senior Manager, Central Tool Room and Training Centre (CTTC), Kolkata, for providing the facilities to conduct various machining works in the concerned workshops of CTTC.

A work of this nature and size requires a help from others. I am lucky to receive unconditional help from so many persons.

My sincere thanks are due to Dr. Suman Sarkar, Senior Scientist, S. N. Bose National Centre for Basic Sciences, Kolkata, who helped me in performing the microstructural examinations.

I would like to thank all my laboratory-mates in Jadavpur University, specially Dr. Hillol Joardar, Dr. Shamim Haider, Dr. Tanmoy Sarkar, Dr. Suswagata Poria, Mr. Sudip Banerjee, Ms. Sasmita Tripathy, Mr. Asim Kumar Dhar; all of them helped me directly or indirectly during the fabrication and testing of the Titanium Components.

I am also thankful to Mr. Titas Nandi, Workshop Superintendent, Blue Earth Workshop, Mechanical Engineering Department, Jadavpur University, Sri Jayanta Bhattacharya and Sri Amit Sarkar of Metallurgy Department, JU, for their kind cooperation during conducting necessary experimental work.

It is my pleasure to express heartfelt thanks to all my departmental colleagues in Ranaghat Govt. Polytechnic, A.P.C. Ray Polytechnic, Jadavpur and I.C.V. Polytechnic, Jhargram specially Mr. Mayukh Nath Mishra, Mr. Arun Kumar Sarker, Mr. Rohininandan Jana, Mr. Biswanath Paul, Mr. Sumon Roy, Mr. Nirmalendu Majhi, Mr. Utpal Chakraborty, Mr. Sudipta Mondal, Mr. Subrata Das, Mr. Samir Dutta, Mr. Barun Bhattacharya, Dr. Pradyut Kundu, Mr. Khagendra Nath Mahato and my former Principals Dr. Amit Ranjan Ghatak, Dr. Pujan Sarkar and my students Sri Ramen Banerjee and Sri Saikat Pal for their support in carrying out the present research work.

I am greatly indebted to my parents-in-law, my aunts and uncles, my sister Arunima, brother-in-law Barun and niece Bipasha for their continuous inspiration and moral support.

Lastly, I would like to thank my wife Papia and son Arkopravo for their saintly patience and constant inspiration.

ARUNANGSU DAS

DEDICATED TO

My Parents

Late Mira Das and Late Arun Kumar Das

"This page is intentionally left blank"

TABLE OF CONTENTS

BRIEF NOMENCLATURE

Symbols	Details
h	Instantaneous thickness of perform
b	Radius of the preform
r_m	Sticking zone radius or mean radius
μ_1	Coefficient of friction of upper surface
μ_2	Coefficient of friction of lower surface
μ	Coefficient of friction at both upper and lower surfaces = $\mu_1 = \mu_2$
P	Die load
τ	Shear stress
λ	Flow stress of the metal powder preform
p	Ram pressure
σ_0	Yield stress of the non-work hardening matrix metal
J_2'	Second invariant of deviatoric stress
r, θ, z	Cylindrical co-ordinates
n	A constant quantity ($n \geq 1$)
ρ_0	A dimensional ratio (ρ_r / ρ^*)
ϕ_0	Specific cohesion of a contact surface
k	Constant equal to 2 in yield criterion
ρ^*, ρ_r	Densities of apparent and real contact areas
η	Constant and a function of ρ only
ρ	Relative density of the perform
ε_r', ε_θ', ε_z'	Principal strain increment
x	a factor (in upper bound analysis, $0 < x < 1$)
y	y intercept (in density variation plots)
x	x intercept (in density variation plots)
R	regression value

LIST OF FIGURES

LIST OF TABLES

"This page is intentionally left blank"

CHAPTER 1

INTRODUCTION

Outline of the Chapter: *1.1 Background, 1.2 Objective and scope of the present research work, 1.3 Outline of the thesis, 1.4 Closure*

1.1 Background

Titanium was discovered between 1791-1795 by English chemist and mineralogist William Gregor and German chemist Martin Heinrich Klaproth separately and independently. It is found as rutile (TiO_2) and ilmenite ($FeTiO_3$) form in nature. Titanium is the ninth most abundant element, constitutes 0.44% of the earth's crust, and found in almost all biological things, rocks, soils and natural water [1-4].

Nilson and Pettersson processed impure titanium in 1887. The pure form (99.9%) of metal was isolated by metallurgist Matthew A. Hunter in 1910 by heating titanium tetrachloride ($TiCl_4$) in presence of sodium in an airtight cylinder. Kroll commercially produced the metal in 1946, by reducing titanium tetrachloride ($TiCl_4$) with magnesium [2]. Titanium dioxide is a photocatalyst and widely used in the manufacture of white pigments. Other titanium compound e.g. titanium tetrachloride ($TiCl_4$) is used in skywriting and producing smoke screens; and titanium trichloride ($TiCl_3$) is used as a catalyst in the making of polypropylene [1, 3].

Titanium (atomic number 22; atomic weight 47.88 amu) may be compounded with iron, aluminium, vanadium, and molybdenum to produce strong, light-weight alloys for aerospace industries (e.g. jet engines, missiles, spacecraft bodies, etc.), industrial process plants (e.g. chemicals and petro-chemicals industries, de-salination plants etc.), automobile industries, agricultural and food products, medical prostheses, orthopedic and dental implants, dental instruments, sporting goods (like golf stick, tennis racket, etc.), jewelry, mobile phones, and other applications [1-4].

Titanium is as strong as steel, but its density (4.51 g/cm^3) is almost half the density of steel. Titanium has high strength-to-density ratio and very good corrosion resistance among other metallic elements. High strength-to-density ratio, good corrosion resistance and biocompatibility make titanium an excellent metal for bio-medical implants [1-4]. Also its surface properties agree with spontaneous build-up of a stable and inert oxide layer [5]. Mirvis et al. [6] studied that titanium is non-ferromagnetic, so patients with titanium made

prosthetic implants can be thoroughly treated with MRI and CT scan. The melting point of titanium is 1668 °C; its boiling point is much higher at 3287 °C. It will ignite in air at 1200 °C and also burn in an atmosphere of nitrogen [3], so difficult to cast in open atmosphere at elevated temperature [7]. The powder metallurgy processing technique is probably the best method to produce various components. Machining titanium and its alloys is very difficult as the shear angle changes with temperature. So, manufacturing of prosthesis into near net shapes with controlled porosity is possible by powder metallurgy route. It also provides good biological adaptability through bone tissue in-growth into the porous network [8].

1.2 Objective and scope of the present research work

Objective: The main focus of this research work is to produce titanium bio-implants through press and sinter powder metallurgy process. Therefore, the basic objective of the work is to indigenously manufacture P/M titanium samples and study the effects of variation of compaction load, sintering temperature on density, micro hardness, formability, corrosion and machining.

Scope of work and statement of the problem

- To fabricate titanium samples through the press and sinter powder metallurgy route.
- To characterize the properties like densities, micro-hardness of P/M titanium samples formed through press and sinter powder metallurgy method.
- To study the formability characteristics of the P/M titanium samples experimentally.
- To corroborate the experimental values of formability data with mathematical analysis in case of titanium sintered preforms.
- To study the machining behavior like surface roughness and metal removal rate (MRR) of the P/M titanium samples machined by Wire-EDM process.
- An effort has been made to find the relationships between sintering temperature and surface roughness as well as sintering temperature and metal removal rate (MRR).
- To study the corrosion behavior of the P/M titanium samples.

1.3 Outline of the thesis

Chapter 1 gives a brief description of titanium metal and highlights the various aspects of this unique metal. This chapter provides a brief insight to the history, properties and potential application of this metal. At the end, a brief report regarding the limitations of previous studies and present research objectives, are presented.

Chapter 2 presents an updated view of the research work carried out in the field of titanium. Extensive literature review has been carried out to find out the present state of research in the field. All the available literatures have been classified into three categories; titanium production (P/M as well as cast titanium), its characterization and applications, its mechanical properties like density, hardness, tensile and compressive properties as well as its machining behavior.

Chapter 3 presents the detailed design and experimental methodology adopted for manufacturing P/M titanium. It includes the analysis of the raw material that is used in the process, and details of the P/M titanium sample manufacturing equipment, facilities etc.

Chapter 4 includes the findings of physical as well as formability characteristics P/M titanium samples under cold condition. The density and micro-hardness of the developed samples are determined and an experimental study of the formability properties along with mathematical validation is reported in this chapter.

Chapter 5 discusses the Design of Experiment technique for statistical analysis of the effect of various process parameters like sintering temperature, pulse on-time & pulse-off time on the surface roughness and metal removal rate of the samples, by Response Surface Methodology (RSM) through Box-Behnken Design method to optimize the output. The responses predicted by RSM approach have been presented and compared with experimental results.

Chapter 6 gives a detailed report on the corrosion characteristics of titanium powder metallurgy samples. The potentiodynamic polarization curves and Nyquist plots were discussed elaborately.

Chapter 7 presents the conclusions from the present work, a detailed discussion on the outcome of the results and suggestions for future investigations.

It is expected that the research work presented in this thesis will be highly useful for all researchers, scientists and industry personnel working in this area in understanding the fabrication and characterization of P/M titanium parts formed through press and sinter method.

CHAPTER 2

LITERATURE REVIEW

Outline of the Chapter: *2.1 Titanium basics, 2.1.1 General Properties, 2.1.2 Classification of titanium alloys, 2.2 Titanium production from its ore, 2.3 Introduction to Powder Metallurgy, 2.3.1 Advantages of powder metallurgy process, 2.3.2 Applications of Powder Metallurgy, 2.4 Titanium powder metallurgy, 2.4.1 Non-melt angular titanium powder production, 2.4.2 Forming of titanium powder into near net shapes, 2.5 Biomaterials and biomedical implants, 2.5.1 Metallic implants, 2.6 Fabrication of P/M titanium components, 2.6.1 Powder Production and characterization, 2.6.2 Blending, 2.6.3 Compaction, 2.6.4 Sintering, 2.6.5 Finishing and other secondary operations, 2.7 Characterization and mechanical properties of P/M Titanium, 2.7.1 Mechanical properties of P/M Titanium prepared through conventional press and sinter method, 2.7.2 Forging behavior of sintered P/M Titanium, 2.7.3 Machining characteristics of Titanium parts, 2.7.4 Surface roughness of Titanium parts after machining, 2.7.5 Corrosion in titanium implants, 2.8 Closure*

2.1 Titanium basics

2.1.1 General Properties

Titanium is paramagnetic, low electrical & thermal conductive, lustrous grey & white colored metal. Commercially pure (99.2% pure) grades of titanium have ultimate tensile strength of about 434 MPa, with low density comparing to steel.

Table 2.1 Comparison of Titanium, Iron and Aluminium on some selected properties

Properties	Density (gm/cm^3)	Melting Point (°C)	Crystal structure at room temp.
Titanium	4.51	1668	HCP
Iron	7.87	1538	BCC
Aluminum	2.70	660	FCC

Titanium is not as hard as some grades of heat-treated steel. Machining requires precautions, because the material can swell unless sharp tools and proper cooling agents are used.

The metal is a dimorphic allotrope of hexagonal α-form that changes into a BCC lattice β-form at 882 °C. The specific heat of the α-form increases rapidly as it is heated to the transition temperature but then falls and remains fairly constant for the β-form, regardless of the temperature [4]. Figure 2.1 shows influence of various alloying elements on phase diagram of titanium alloys.

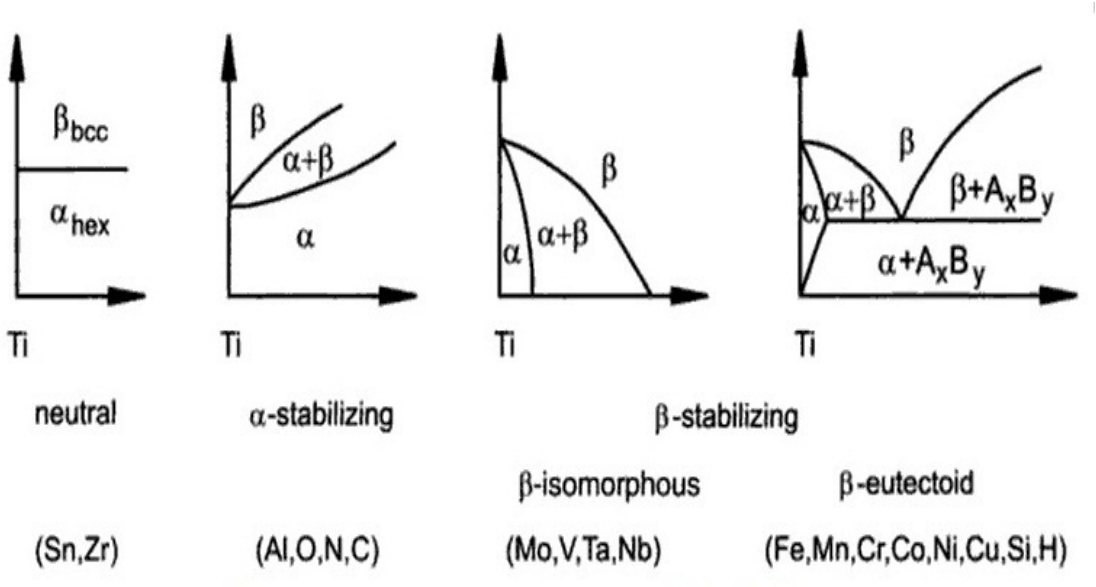

Figure 2.1 Influence of alloying elements on phase diagram of titanium alloys [9]

Titanium has great affinity to oxygen and nitrogen, and readily absorbs them at elevated temperatures, which increases its strength but simultaneously reduces its ductility. On the other hand, hydrogen is always avoided as it causes stress-cracking by precipitation of hydrides [10].

2.1.2 Classification of titanium alloys

Depending upon the amount of alloying with beta stabilizers, titanium alloys may retain some β phase at room temperature. Thus, titanium alloy compositions are classified as near-alpha (α) alloys, beta (β) alloys, or alpha-beta (α + β) alloys. Of the three broad classes of titanium alloys, grouping is done according to the levels of alpha or beta stabilizing elements. Typically, beta content by volume is approximately:

- Near-alpha (α) alloys: <10% β
- (α + β) alloys: 10 to 25% β
- beta (β) alloys: > 25% β

Commercially pure titanium

Commercially pure titanium (98.9 to 99.6% Ti) consists of all α-phase (HCP crystal structure). It has relatively low strength and high ductility. Yield strengths of CP-Ti grades (Table 2.2) vary from 170 to 480 MPa, simply because of variations in the interstitial impurity levels. Oxygen and iron are primary variants in these grades; strength increases with increasing oxygen and iron contents. Applications of CP-Ti grades include pacemaker

housings, implantable infusion drug pumps, dental implants, maxillofacial and craniofacial implants etc. [10].

Table 2.2 Tensile properties and impurity levels for ASTM F67 unalloyed Titanium [10]

Designation	**Tensile strength, min**	**0.2% yield strength, min**	**Elongation, %**	**Impurity limits, max, 0.2%**				
	MPa	**MPa**		**N**	**C**	**H**	**Fe**	**O**
ASTM Grade 1	240	170	24	0.03	0.08	0.015	0.20	0.18
ASTM Grade 2	340	280	20	0.03	0.08	0.015	0.30	0.25
ASTM Grade 3	450	380	18	0.05	0.08	0.015	0.30	0.35
ASTM Grade 4	550	480	15	0.05	0.08	0.015	0.50	0.40

α and near-α alloys

α and near-α alloys have not been used for biomedical applications. Their utilities for medical devices have been limited due to their low ambient temperature strength when compared with α+β alloys or β alloys. Unlike α+β alloys and β alloys, the α-titanium alloys cannot be significantly strengthened by heat treatment [10].

α+β alloys

α+β alloys contain one or more α stabilizers or α-soluble elements plus one or more β stabilizers. These alloys retain more β-phase after solution treatment than that of near-α alloys. The amount depends on the quantity of β-stabilizers present and on heat treatment process. Ti-6Al-4V and Ti-6Al-4V-ELI are the most commonly used alloys mainly for hip or knee replacements. In the future, it is likely that Ti-6Al-4V implants will be replaced by beta-titanium alloys, which have some advantages over alpha-beta alloys.

One limitation of alpha-beta alloys (relative to beta alloys) in orthopedic applications is the mismatch of their elastic modulus relative to that of bone. The distribution of stress around an orthopedic implant bone improves when the elastic modulus of the biomaterial more closely matches cortical bones. Stress shielding occurs when there is mismatch between the moduli of the implant and adjacent hard tissue. Relative motion occurs at the biomaterial-tissue interface because of difference in the elastic moduli, and serious deterioration of the biomaterial tissue interface or a total failure may result. Ideally, a material used for replacement of bony tissues should have an elastic modulus that is similar to that of bone.

The elastic modulus of a cortical bone is close to 18 GPa, while the modulus of Ti-6Al-4V alloy is 110 GPa, or half the modulus of cobalt-base alloys. In contrast, beta alloys have a much lower modulus and are thus more suitable to bone. The use of Ti-6Al-4V as permanent implants also has potential concerns with toxicity of vanadium and aluminum. Vanadium was replaced by niobium and iron as a beta stabilizer, leading to alloys Ti-6Al-7Nb and Ti-5Al-2.5Fe. The alloys Ti-6Al-7Nb and Ti-5Al-2.5Fe are metallurgically quite similar to Ti-6Al-4V, although they contain aluminum (as an alpha stabilizer) that may pose a concern in terms of toxicity.

β alloys

Beta alloys are richer in β stabilizers and leaner in α stabilizers than α+β alloys. They are characterized by high hardenability due to β phase. Beta alloys have excellent forgeability and cold-rolling capabilities. The 1990s witnessed considerable advances in the development of β alloys for orthopedic implant applications. The β alloys offer lower elastic moduli and enhanced biocompatibility when compared to Ti-6Al-4V and other α-β alloys. The moduli of β-type titanium alloys are lower than the alpha-beta alloys and have a closer match to the moduli of cortical bones, the β-type titanium alloys are, in general, desirable for use in orthopedic applications. Table 2.3 compares the elastic modulus values for a variety of natural and synthetic joint materials.

Table 2.3 Elastic moduli of natural and synthetic joint materials

Joint material	**Elastic modulus (GPa)**
Articular cartilage	0.001-0.17
PTFE	0.5
UHMWPE	0.5
Bone Cement (PMMA)	3.0
Bone	10-30
TNZT alloys	55-66
New generation β-Ti alloys	74-85
Ti-6Al-4V	110
Zirconia	200
Stainless steel	205
Co-Cr-Mo alloy	230
Alumina	350

PTFE = polytetrafluroethylene, UHMWPE = Ultra-high-molucular-weight-poly-ethylene, PMMA = polymethyl methacrylate, TNZT = Titanium-niobium-zirconium-tantalum.

The principal alloying elements in beta alloys are niobium, zirconium, molybdenum, tantalum, and iron, all of which exhibit excellent biocompatibility. A typical β-type titanium alloy developed for biomedical applications is Ti-15Mo-5Zr-3Al, which has been developed as a structural titanium alloy. Properties of some common titanium beta alloys are stated as below:

- Ti-15Mo alloy has good corrosion resistance and good toughness.
- Ti-12Mo-6Zr-2Fe (TMZF) has a lower modulus, good strength, good corrosion resistance and good wear resistance.
- Ti-13Nb-13Zr has a lower modulus, high corrosion resistance, and high fatigue limit.

2.2 Titanium production from its ore

Titanium mill products like sheets, plates, bars, wire, etc., castings and forgings are made by Hunter process since the inception of titanium industry in 20th century. This process necessitates reducing of titanium tetrachloride ($TiCl_4$) with sodium in a batch reactor within an inert gas atmosphere at a temperature of 1000 °C [4]. The major volume of this metal is made using a process developed by Dr. Wilhelm J. Kroll in the 1930's [11]. Figure 2.2 shows titanium sponge produced by Kroll Process.

(a) (b)

Figure 2.2 Titanium sponge produced by Kroll Process, a) before and b) after crushing

Sponge is a primary raw material used in the melting operations producing ingot or slab. It is available in various grades, with varying levels of impurities. The difference between the reactions of Hunter and Kroll process is illustrated in Table 2.4.

Table 2.4 Difference between Kroll and Hunter process's reactions

Method	Reaction	Temperature
Kroll	$TiCl_4 + 2Mg = Ti + 2MgCl_2$	900 °C
Hunter	$TiCl_4 + 4Na = Ti + 4NaCl$	700 – 800 °C

2.3 Introduction to Powder Metallurgy

Powder metallurgy (P/M) is defined as the technology of producing metal powders and making semi-finished or finished products from individual, mixed or alloyed powders with or without addition of non-metallic ingredients. Production of P/M parts involve mixing of elemental or alloy powders with additives and lubricants, compaction of the mixture in a suitable die and heating the resulting green compacts in a controlled atmosphere furnace in order to bond the particles metallurgically. The resulting parts are solid bodies of materials with sufficient strength and density to use in diverse fields of applications. Highly porous parts, precise high-performance components and composite materials can be produced by P/M route [12].

2.3.1 Advantages of powder metallurgy process

The powder metallurgy process has certain basic advantages over conventional melting and casting method of producing metals, alloys and finished articles. These advantages include:

Process Advantages:

1. Eliminates or minimizes machining (little or no scrap)
2. Efficient material utilization – above 95% material is utilized
3. Enables close dimensional tolerances – near net shapes possible
4. Produces good surface finish
5. Facilitates manufacture of complex shapes, which would be impossible with other metal working processes
6. No requirement of highly skilled personnel
7. Composite materials of insoluble metals (for e.g. Cu-W, Cu-Ag, Cu-Fe & Ag-Cd) can be produced through P/M route
8. Refractory metals can be easily formed into desired shapes without melting
9. Components of hard materials which are difficult to machine can be readily manufactured, e.g. tungsten wires for incandescent lamp

Metallurgical Advantages:

1. Powder compacts with uniform chemical composition and desired characteristics are obtained, preventing segregation during solidification
2. Elemental and pre-alloyed powders can be used for production
3. Parts with controlled porosity can be formed
4. Materials with improved magnetic properties can be generated

Functional Advantages:

1. Ferrous and non-ferrous P/M parts can be oil impregnated to function as self-lubricating bearings
2. Parts can be resin-impregnated to seal inter-connected porosity for improving density
3. P/M parts can be infiltrated with lower melting point metal for greater strength or shock resistance and for making electrical products
4. Parts can be heat-treated and plated if required

2.3.2 Applications of Powder Metallurgy

Followings are some application areas of PM components:

Refractory Metals: Components made of tungsten by powder metallurgy are widely used in the electric light bulbs, fluorescent lamps, oscillator valves, mercury arc rectifiers and x-ray tubes in the form of filament, radio valves, anode & cathode, screen and control grids.

Refractory Carbides: Refractory carbide made by P/M used in various parts of lathes, drilling and threaded guides, etc.

Automotive Applications: In the developed countries, it is the motor industry which relies heaviest upon powder metallurgical components, (for example, in USA motor uses 100 P/M parts per 1000 while the UK motor industry uses 48 P/M parts per 1000).

Aerospace Applications: Metal powders are playing an important role in rocket, missiles, satellites and space vehicles.

Atomic Energy Applications: P/M has played a significant role in the development of nuclear power reactors. Composite materials are applied in various fuel elements and control rod systems (for example, the distribution of uranium oxide throughout the stainless steel matrix).

2.4 Titanium Powder Metallurgy

An indication of where PM stands into the broad scenario of fabrication techniques is shown in Figure 2.3 [15].

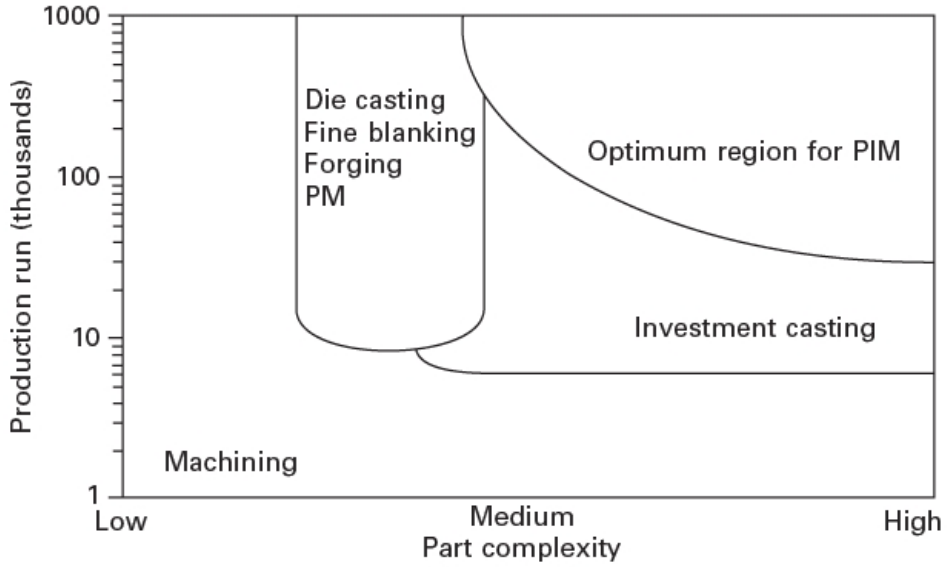

Figure 2.3 Diagram showing where powder metallurgy (PM) and powder injection moulding (PIM) stands in comparison with other fabrication processes [15]

2.4.1 Non-melt angular titanium powder production

Table 2.5 shows the characteristics of the different types of titanium powders that are either available or under development today. This table is based in part on a recent review of powder production methods co-authored by McCracken [16].

Table 2.5 Characteristics of different types of titanium powders [17]

Type/Process	Powder type	Advantages	Status/Disadvantages
Hunter process (pure sodium)	Elemental	Low cost; excellent for cold press and sinter	Limited availability; high chloride
Hydride Dehydride (HDH) Kroll process (pure magnesium)	Elemental	Lower cost; good compactability; readily available; low chloride	
HDH powder produced from alloys	Prealloyed	Readily available	High cost; fair compactability
Atomized	Prealloyed	High purity; available	High cost; not cold compactable
Rotating Electrode	Prealloyed	High purity	High cost; not cold

Powder (REP)/Plasma Rotating Electrode Powder (PREP)			compactable
ITP (International Titanium Powder)/ Armstrong	Elemental and Prealloyed	Compactable; moderate cost; potential for low cost	Processibility/quality; production scale-up
Fray	Elemental and Prealloyed	Yet To Be Decided	Developmental
MER Corp. Tucson, Ariz	Elemental and Prealloyed	Yet To Be Decided	Developmental
CSIRO Melbourne, Australia	Elemental and Prealloyed	Yet To Be Decided	Developmental
ADMA Products Hydrided Powder	Elemental and Prealloyed	Lower cost; better compactability	Semi-commercial
CHINUKA, Cambridge, UK	Alloy possible but difficult	Can use impure ores	Developmental
CSIR, Pretoria, SA	May be possible	Moderate cost	Developmental

2.4.2 Forming of titanium powder into near net shapes

The processes that are available for near net shapes (NNS) production are usable with various types of titanium powders that include conventional press-and-sinter method, Cold Isostatic Pressing (CIP) and Hot Isostatic Pressing (HIP). The future prospects for PM titanium lies in the application of Blended Elemental (BE), Pre-alloyed (PA) or Additive Manufacturing approach. PA titanium is useful in case of TiAl alloys that are difficult to fabricate. On the other hand, Additive Manufacturing approach will see significant growth in near future, in comparison with the BE and PA techniques [19].

2.5 Biomaterials and biomedical implants

Biomaterials are materials of natural or artificial origin that can be used to replace living tissues [20]. Different uses of biomaterials are artificial hip joints, kidney dialysis machines, bone plates, screws, cardiac pacemakers, intraocular lens, probes, catheters, etc. Implants now are used in dentistry, orthopedics, reconstructive surgery, ophthalmology and cardiovascular surgery (Figure 2.4) [22].

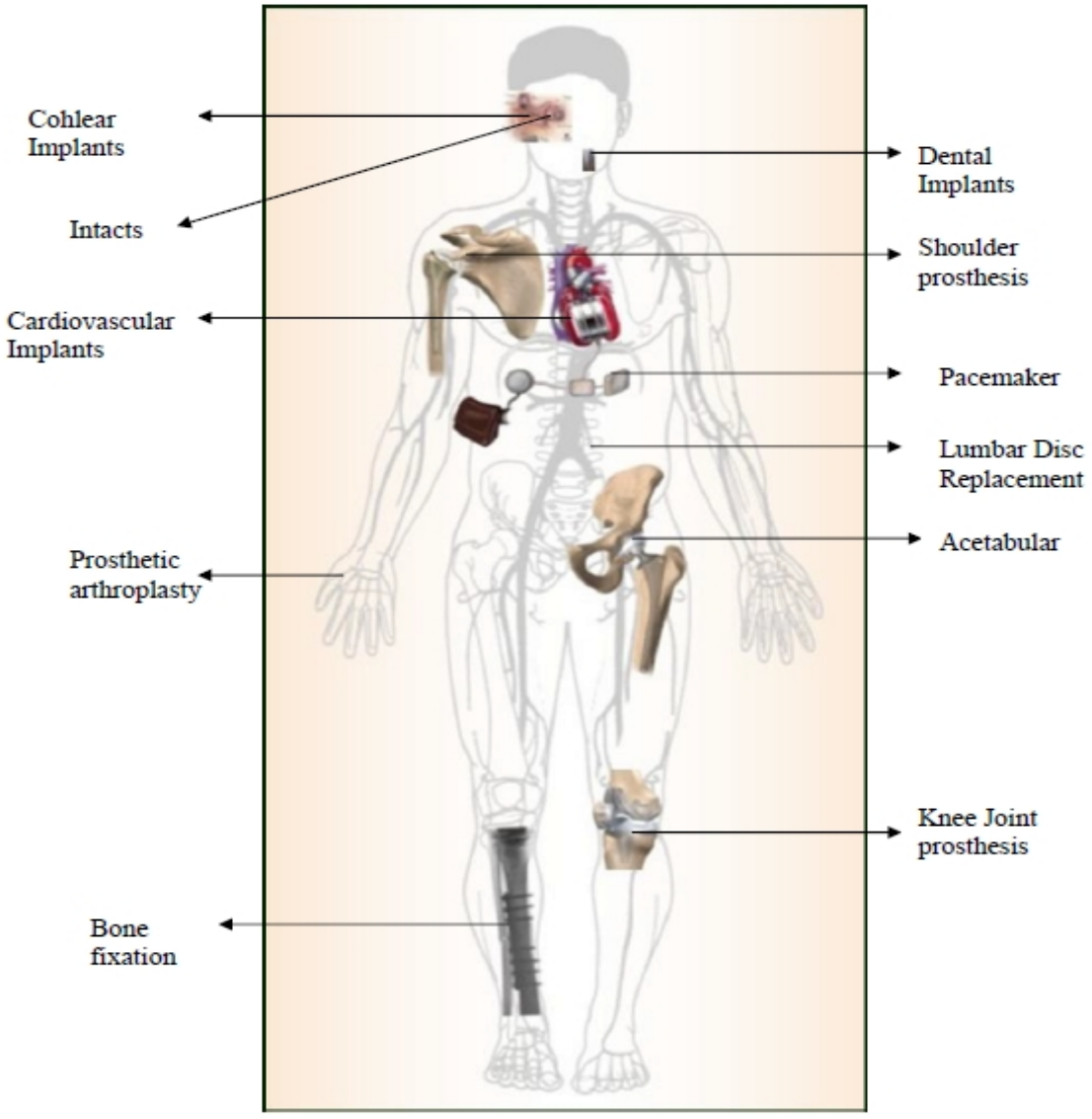

Figure 2.4 Biomaterials for human applications [22]

Biomedical implants should meet some special requirements to serve for longer period without rejection from human body [23, 24]. The first requirement is that the material must be biocompatible, that does not cause any adverse reaction with the body and can integrate well with surrounding tissues. The second requirement is that the material must be corrosion resistant to the body's aggressive environment. Corrosion resistance should ensure that metal

ions will not release into the body that may lead to inflammation of organs and tissues. Moreover, the implanted device will retain its integrity and not degrade due to corrosion. The third requirement is that the device must have sufficient mechanical strength. This should guarantee matching of elastic modulus between bones and foreign implants. The fourth requirement is the appropriate design for the intended use. Crevices should be avoided to provide good corrosion resistance. The fifth requirement is the proper surface treatment. Once the device is implanted into the bone, its surface directly comes in contact with body fluids and tissues. Surface treatment controls the nature of surface and is important for improving biocompatibility.

Metallic materials as pure metals and alloys are widely employed to produce many types of biomedical devices [25-32]. Table 2.6 shows the type of metals which are generally used for different implants division.

Table 2.6 Implants' category and type of used metals

Division	**Implants**	**Type of metal**
Orthopedic	●Bone fixation (plate, screw, pin)	SS316L; Ti; Ti-6Al-4V
	●Spinal fixation	SS316L; Ti; Ti-6Al-4V; Ti-6Al-7Nb
	●Artificial joints	Co-Cr-Mo; Ti-6Al-4V; Ti-6Al-7Nb
Craniofacial	●Plate and screw	SS316L; Co-Cr-Mo; Ti; Ti-6Al-4V
Cardiovascular	●Artificial valve	Ti-6Al-4V
	●Stent	SS316L; Co-Cr-Mo; Ti
	●Pacemaker case	Ti; Ti-6Al-4V
	●Stent graft	SS316L
Otorhinology	●Artificial eardrum	SS316L
	●Artificial inner ear (electrode)	Pt
Dentistry	●Filling	Ag-Sn-(Cu) amalgum, Au
	●Inlay, crown, bridge	Au-Cu-Ag; Au-Cu-Ag-Pt-Pd; Ti; Co-Cr
	●Orthodontic wire	SS316L; Co-Cr-Mo; Ti-Ni; Ti-Mo
	●Dental implant	Ti; Ti-6Al-4V; Ti-6Al-7Nb; Au

Figure 2.5 shows the elastic modulus of biomedical alloys commonly used in biomedical implants [26].

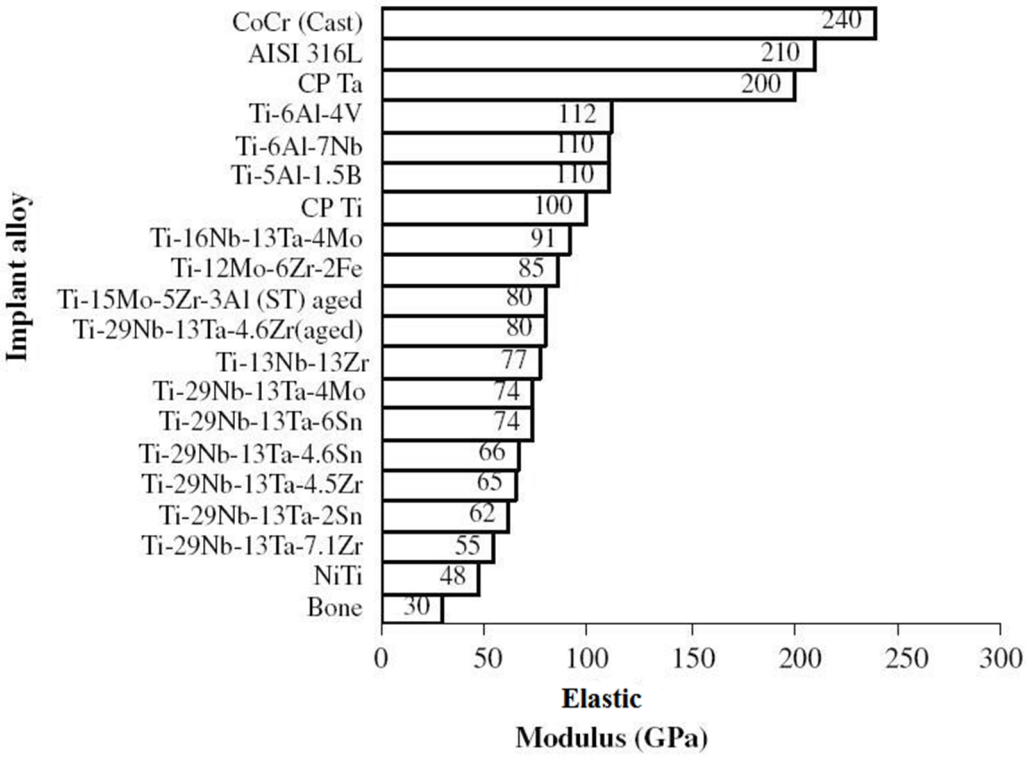

Figure 2.5 Elastic Modulus for different metallic alloys [26]

Titanium and its alloys as bio-implants

In comparison with stainless steel and Co-Cr alloys, titanium has lower modulus which varies from 48 GPa to 112 GPa. The density of titanium is only 4.506 g/cm^3 as compared to 7.9g/cm^3 for 316 stainless steel and 8.3 g/cm^3 for cast Co-Cr-Mo alloy. Titanium can be alloyed with many elements, like iron (Fe), aluminium (Al), vanadium (V) and molybdenum (Mo), to produce strong, lightweight alloys as required for the application of medical prostheses, orthopedic and dental implants. Table 2.7 gives a concise understanding about the excellent mechanical properties CP-Ti and some of its important alloys employed in the field of biomedical devices.

Table 2.7 Mechanical properties of biomedical titanium alloys

Material	Standard	Elastic (GPa)	Tensile (MPa)	Alloy type
CP-Ti (Grade 1-4)	ASTM1341	100	240-550	α
Ti-6Al-4V ELI	ASTM F1472	112	895-930	α+β
Ti-6Al-7Nb	ASTM F1295	110	900-1050	α+β
Ti-5Al-2.5Fe	…	110	1020	α+β

Ti-13Nb-13Zr	ASTM F1713	79-84	973-1037	Metastable β
Ti-12Mo-6Zr-2Fe	ASTM F1813	74-85	1060-1100	β
Ti-35Nb-7Zr-5Ta	…	55	596	β
Ti-29Nb-13Ta-4.6Zr	…	65	911	β
Ti-35Nb-5Ta-7Zr-0.4O	…	66	1010	β
Ti-15Mo-5Zr-3Al	…	82	…	β
Ti-15Mo	ASTM F2066	…	…	…

ASTM = American Society for Testing and Materials

2.6 Fabrication of P/M titanium components

The main steps involved in production of various powder metallurgy components including titanium are explained in figure 2.6. They are:

- **Powder production and characterization**
- **Blending**
- **Compaction**
- **Sintering**
- **Finishing and other secondary operations**

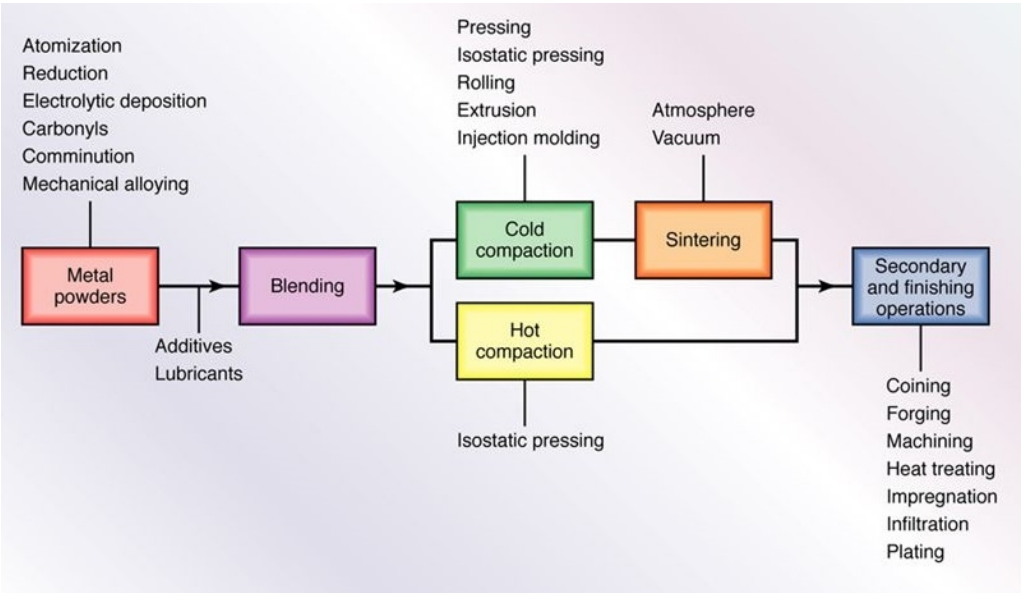

Figure 2.6 Outline of processes and operations involved in making PM titanium parts

2.6.1 Powder Production and characterization

Practically any material can be made into a powder by using any one of the methods discussed previous literatures [17]. The particular method chosen depends upon the types of

raw materials readily available, the desired properties and structure, type of application. The processes of manufacturing P/M articles depend largely on the physical and chemical characteristics of the initial metal powders. The characteristics of metal powders depend upon the method used in producing these metal powders. There are various methods of manufacturing metal powders and consequently there is a wide range in their characteristics [15-17]. A choice regarding the suitability of manufacturing techniques of metal powders can be made only after considering the required finished product for a specific job. The main purpose of powder testing is to ensure that the powder is suitable for subsequent processing. A sample of metal powder is always selected for the determination of its characteristics and control of these characteristics is necessary for maintaining the (required) uniformity in different powder lots.

The basic characteristics of a metal powder are:

a) Chemical composition and purity
b) Particle size and its distribution
c) Particle shape
d) Particle porosity
e) Particle microstructure

The other characteristics which are dependent entirely or a large extent on the above primary properties of metal powders:

a) Specific surface
b) Apparent density
c) Tap density
d) Flow rate
e) Pressing properties
f) Sintering properties

Primary properties such as the particle size distribution and the important secondary properties such as apparent density and flow rate are most widely used in specification and control routine. Other properties such as permeability regarding liquids and gases, magnetic properties, electrical and thermal conductivity, etc. are also of importance for special applications of P/M parts.

2.6.2 Blending

Blending (mixing) powders is the second step in powder metallurgy processing and is carried out for the following purposes:

Powders of different metals and materials may be blended to impart specific physical and mechanical properties and characteristics. Proper mixing is essential to ensure uniformity of properties throughout the part. Even when a single metal is used, the powders may significantly vary in shape and size; hence they must be blended to obtain uniformity from part to part. The ideal mix is one in which all the particles of each material, and of each size and morphology are distributed uniformly. Also lubricants can be mixed with the powders to improve their flow characteristics during processing. Thus reduce friction between the metal particles and improve flow of the powder metals into the dies, and improve die life. Lubricants are typically stearic acid or zinc stearate, in a proportion ranging from 0.25 to 5% by weight. Various additives, such as binders as in sand moulds, are used to develop sufficient green strength and facilitate sintering. Some typical blending machines are illustrated in figure 2.7.

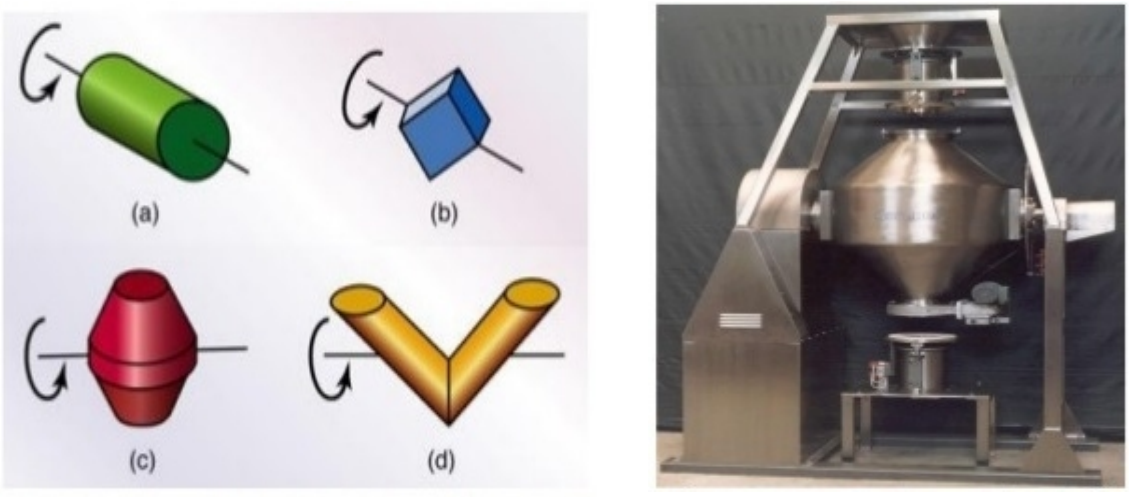

Figure 2.7 Some common equipment geometries used for blending powders (a) cylindrical (b) rotating cube (c) double cone (d) twin shell

2.6.3 Compaction

Compaction is the step in which the blended powders are pressed into desired shapes using dies and punches that are either hydraulically or mechanically actuated (Figure 2.8). Pressing is generally carried out at room temperature, although it can be done at elevated temperatures as well. The purposes of compaction are to obtain shape, density and particle to particle contact and to make the part sufficiently strong to handle for further processing. The initial pressed powder is known as **green compact**.

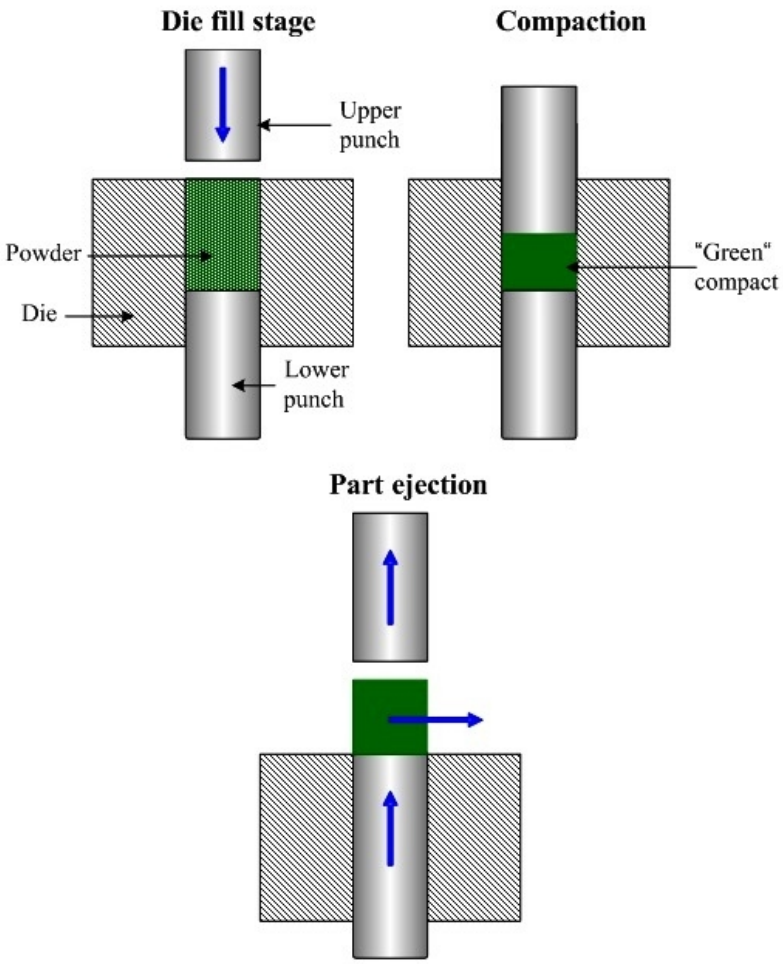

Figure 2.8 Powder compaction process

2.6.4 Sintering

Sintering is the process of heating compacted metal powder in a controlled atmosphere to a temperature below its melting point, but sufficiently high to allow bonding or fusion of the individual metal particles. Prior to sintering, the compact is brittle and its strength, known as *green strength*. The nature and strength of the bond between the particles, of the sintered compact depends on the mechanisms of diffusion, plastic flow and evaporation of volatile materials, recrystallization, grain growth and pore shrinkage.

The density of the sintered part mainly depends on the green density and on the sintering temperature, time and furnace atmosphere. The sintered density increases with increasing temperature and time. Sintering temperatures are generally within 70 to 90% of the melting point of the base metal or alloy. Sintering time ranges from a minimum of 10 minutes for iron and copper alloys to as long as 8 hours for tungsten and tantalum. Continuous sintering furnaces are used nowadays for production purposes. These furnaces have three chambers: a)

a burn-off chamber, to volatilize the lubricants in the green compact in order to improve bond strength and prevent cracking; b) a high temperature chamber for sintering; and c) a cooling chamber. A continuous sintering furnace is shown in Figure 2.9.

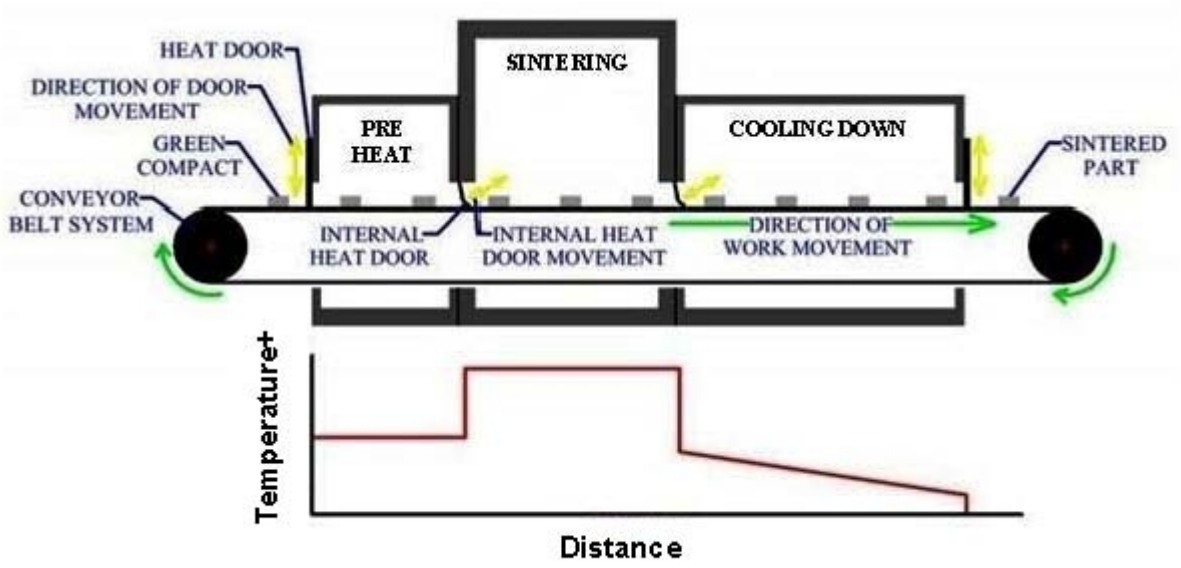

Figure 2.9 Continuous sintering furnace

Sintering mechanisms

Sintering mechanisms are complex and depend on the composition of the metal particles as well as process parameters. As the temperature increases, two adjacent particles begin to form a bond by diffusion. As a result, the strength, density, ductility, thermal and electrical conductivities of the compact increases. At the same time the compact shrinks; hence allowances should be provided for shrinkage, as in castings [12, 33]. Figure 2.10 explains phase material transport mechanism during particle bonding.

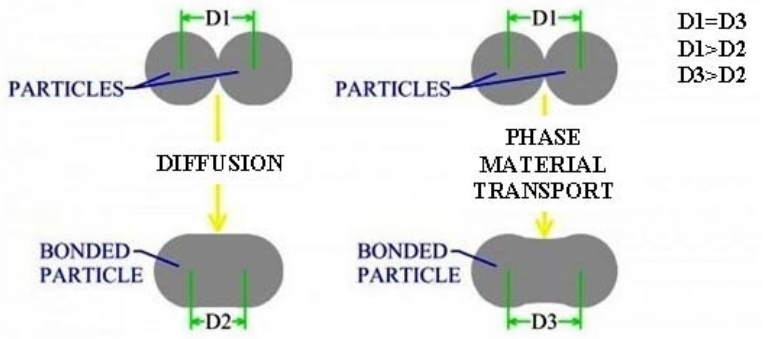

Figure 2.10 Bonding mechanisms in powder sintering

2.6.5 Finishing and other secondary operations

In order to improve the properties of sintered powder metallurgy products or to impart certain specific characteristics, several additional operations may be carried out after the sintering process:

- **Re-pressing,** also called coining and sizing, is an additional compaction operation, performed under high pressure in presses. The purposes of this operation are to improve dimensional accuracy and surface finish of the sintered part and to increase the part's strength.
- **Forging** involves the use of un-sintered or sintered alloyed-powder preforms that are subsequently hot forged in heated, confined dies to the desired final shapes. This forging process is generally referred to as *powder metallurgy forging* (P/F), and when the un-sintered preform is later sintered, the process is usually referred to as *sinter forging*. Ferrous and non-ferrous powders can be processed in this manner resulting in full-density products with 99.9% relative density.
- **Impregnating** is the procedure by virtue of which fluid is inserted into the inherently porous powder metallurgy products. A typical application is to impregnate the sintered part with oil, which is usually done by immersing the part in heated oil. Internally lubricated bearings thus have a continuous supply of lubricants through its service life. Universal joints are now made with grease-impregnated P/M techniques, as a result of which these parts no longer require grease fittings.
- **Infiltration** is a process whereby a metal slug, with a lower melting point, is placed on top of the sintered part, and the assembly is heated to a temperature sufficient to melt the slug. The molten metal infiltrates the pores of the sintered part through capillary action, resulting in a relatively pore-free part with good density and strength. The most application is the infiltration of iron-based compacts with copper.
- **Powder-metal** parts may be subjected to various other operations like heat-treating, machining, deburring, plating, coating, etc.

2.7 Characterization and mechanical properties of P/M Titanium

2.7.1 Mechanical properties of P/M Titanium prepared through conventional press and sinter method

Torres et al. [34] contemplated the impact of the processing parameters (compacting pressure and sintering temperature) on the microstructure (size, type, morphology, and level of

porosity), just as on the mechanical properties (compressive yield quality, as well as conventional and dynamic Young's modulus). The outcomes demonstrated that there was an improvement in density, roundness of pores and mean free-way between the particles as compacting pressure and/or sintering temperature have been increased. An assessment of porosity and Young's modulus in a tube shaped sample demonstrated that it was probable to acquire titanium with reviewed porosity.

Elias et al. [35] detailed that Titanium (CP-Ti) is the best bio-perfect material, since its surface properties prove unconstrained development of a steady and idle oxide layer. Mohammed et al. [36] checked on and revealed that titanium and its alloys are utilized broadly in biomedical applications dependent on their high specific strength, great corrosion obstruction and lower elastic modulus when contrasted with different biomaterials like stainless steel, cobalt based alloys, polymers and composites. Niinomi et al. [37] examined the mechanical and biological similarity of Ti-29Nb-13Ta-4.6Zr alloy created by Levicast technique. Greger et al. [38] examined the production of nano-structured titanium through equal channel angular pressing (ECAP) process. Zherebtsov et al. [39] looked at the mechanical properties of Ti-6Al-4V with microcrystalline and sub-microcrystalline structures created by extreme plastic deformation in the temperature range 20 – 600°C. Scientists like Threrujirapapong et al. [40] have considered the mechanical properties of titanium matrix composites fortified with low cost carbon black through powder metallurgy technique. Santulli et al. [41] performed normal and off-axis compression tests on titanium dental inserts. Scarcely any researchers [42, 43] have focused their work on high cycle weakness of Ti-6Al-4V.

Chen et al. [44, 45] concentrated the cold compaction conduct of Armstrong process CP-Ti and Ti-6Al-4V powders for cylindrical shape sintered items with three diverse aspect ratios, namely, 0.5, 1, and 2. Behrens et al. [46] inspected the consolidation of tool-die vibration on the mechanical properties of titanium P/M parts. Choe et al. [47, 48] examined the mechanical properties of Ti-6Al-4V alloys strengthened with W/TiC. Afrin et al. [49] investigated the HA and Ti compound relations under different conditions. Ghorbani and others [50] examined the interface behaviour of plasma sprayed hydroxyapatite coating on Ti-6Al-4V.

2.7.2 Forging behavior of sintered P/M Titanium

Imayev et al. considered the forging characteristics of near alpha titanium alloy (VT18U) which was cast with TiB and TiC. The samples were exposed to 2-stage 3D forging at 950°C

and 800°C and in this manner heat-treated. The heat treated samples exposed extensively higher strength, creep resistance and lower ductility when contrasted with Ti-base alloys [51, 52]. Dahar et al. researched the impacts of thermal and thermo-mechanical preparation, sample orientation and load ratio in room temperature fatigue crack development and crack pattern of third generation gamma titanium aluminide (TNM) [53]. Bambach et al. investigated the hot forgeability of TNB-V5 created by Spark Plasma Sintering (SPS) from pre-alloyed powder utilizing the idea of processing map. Their examination offered another investigation that could stabilize ductile stage [54]. Miura et al. multi-directionally forged (MDFed) CP-Ti Grade-2 at room temperature with no breaking to a combined strain of $\Sigma\delta\varepsilon = 2.0$. They accomplished tensile strength of 710 MPa and 21% ductility [55]. Bézi et al. [56] handled Grade-2 titanium with multiple forging and ensuing plane rolling and announced that the utilization of this innovation multiplied its strength without significant loss in ductility.
Lu et al. [57], in their examination, recognized 3-dimensional micro void assessment amid and after warm-forging of Ti-6Al-4V segment by utilizing a high-resolution micro-focus X-ray CT framework. Sizova et al. [58] examined the microstructure advancement amid heat treatment and hot-working of Ti-6Al-4V samples which were prepared by Selective Laser Melting (SLM). Ducato et al. [59] advanced the die geometry for manufacturing a complex shaped aeronautical part made of Ti-6Al-4V by methods for numerical simulation. Mamedov et al. [60] introduced a numerical modelling of Ti-6Al-4V forging process and examined the impact of the procedure parameters on mechanical and microstructural properties of the compound.

2.7.3 Machining characteristics of Titanium parts

Titanium is hard to machine through the ordinary course. It is a poor conductor of heat. Heat, produced by the cutting activity, does not dissipate rapidly. Therefore, a large portion of the heat gets gathered on the cutting edge and face. Titanium has a solid alloying propensity with cutting tool materials at machining temperatures. This causes welding of chips at the cutting edge. It has low elastic modulus. This implies that the work-piece will in general move away from the cutting tool under substantial cutting forces. Thin parts will in general divert under tool pressure and this causes machine tool chatter and vibration prompting tolerance issues. Rigidity of the whole machining framework is thus imperative, while machining titanium. Titanium's work-hardening attributes are such that, while machining, a high shearing angle is formed.

Isik et al. [61] considered the heat changes in Ti-6Al-4V, based on feed, depth of cut and cutting velocity, amid drilling, with the assistance of a thermal camera. Rahim et al. [62] examined the machinability of Ti-6Al-4V and Ti-5Al-4V-0.6Mo-Fe alloys by drilling with uncoated WC/Co carbide drill. Shetty et al. [63] performed machinability examination on Ti-6Al-4V compound utilizing L9 orthogonal array.

For different challenges encountered amid regular machining, non-traditional machining can be a substitute technique for machining titanium, of which, Wire-cut Electric Discharge Machining (WEDM) can be a reasonable alternative. Kumar et al. [64, 65] built up a quadratic model for dimensional deviation to connect the dominating machining process parameters: e.g., pulse on time, pulse off time, spark volt, peak current, wire feed, and wire tension in the WEDM procedure of grade-2 pure titanium. They watched pulse on time, peak current decayed the reliability of the machined surfaces bringing about cavities, scars, trash, and miniaturized scale cracks. Badkar et al. [66] revealed that, heat input (HI) assumes a critical role in choosing the tensile strength of the laser-hardened CP-Ti.

Manjaiah et al. [67] considered the improvement of surface harshness and MRR through Wire-EDM of TiNi Shape Memory Alloys (SMA). They performed analysis of means (ANOM) and e analysis of variance (ANOVA) on signal to noise (S/N) ratio to decide ideal parameter levels. The optimization procedure of Wire-EDM of TiNi SMA showed that pulse duration altogether influenced the material removal rate and surface harshness parameters of the machined parts. Rahaman et al. [68] built up an optimization model to examine the impacts of peak current, pulse on time and pulse off time in EDM of Ti-6Al-4V compounds with copper tungsten electrode. As peak current increased, surface harshness of the workpiece increased, in a similar manner, surface roughness increased with pulse on time. Nourbakhsh et al. [69] considered the impact of zinc-covered metal wire on the execution of WEDM as contrasted with brass. Garg et al. [70] contemplated the impact of procedure parameters on cutting rate in WEDM of Ti 6-2-4-2 combination with Box-Behnken design. They considered six control factors viz. spark voltage, pulse on time, pulse off time, peak current, wire feed and wire tension at three unique dimensions. An exact equation was acquired for cutting rate (CR) utilizing regression analysis.

Bhaumik et al. [71], amid their examination, completed a comparative report on electro discharge machining (EDM) of grade 6 titanium alloy utilizing distinctive kind of electrodes for example copper, brass and zinc. The procedure output has been surveyed by methods for material removal rate and tool wear rate. Baroi et al. [72] focussed on the Electric Discharge Machining of Grade 2 Titanium composite to discover the output variation of metal removal

rate, tool wear rate and surface harshness because of variety of info parameters like current and pulse on time.

Kieren-Ehses et al. [73] in their examination demonstrated the constructive outcome of utilizing metal working fluid (MWF) when smaller scale milling of CP-titanium with 50 μm diameter micro end-mills. Isopropanol, sodium dodecyl sulfate (SDS) and industrially accessible cutting oil were investigated and contrasted with dry condition. Among the MWF utilized, isopropanol demonstrated the best capacities to conduct heat away from the contact zone. To balance out and increment the effectiveness of machining titanium compound, Jing et al. [74] built up a Multiple-input multiple output (MIMO) adaptive control framework for EDM.

2.7.4 Surface roughness of Titanium parts after machining

Yang et al. [75] constructed a mathematic model by the response surface methodology to fit the relationship between the process parameters and the surface roughness. He chose cutting speed, feed rate and depth of cut as process input parameter. The prediction accuracy was verified by one-way ANOVA. The results showed that the feed was the most important effect on surface roughness, followed by cutting speed. The cutting depth has minimal effect. Sun et al. [76] studied machined surface integrity during orthogonal turning of titanium alloy TB6. The effects of cutting parameters and process system vibration on the machined surface roughness and defects were investigated. Micro-hardness and microstructure of the machined surface were also studied. The results showed that it was not the cutting speed, but feed rate had significant impacts on the surface roughness, residual stress and micro-hardness. The roughness increased from 0.2 to 0.4 μm, the residual compressive stress also increased by 10% and the location depth of the peak, increased from 50 to 70 μm, when feed rate was varied from 0.05 to 0.1 mm/rev. Kumar et al. [77] optimized the surface roughness of titanium alloy during turning in a CNC Machine through L9 Taguchi orthogonal array. Yang et al. [78] characterized surface topography in peripheral milling of Ti-6Al-4V.

2.7.5 Corrosion in titanium implants

Titanium is an exceedingly reactive metal and an oxide layer is effectively shaped because of its strong chemical affinity to oxygen. It was accounted for that an oxide layer with a thickness more prominent than 10 $\mathring{A}$ can form quickly on in under a microsecond in environment [79]. Titanium rapidly forms an oxide of 2-7 nm thickness in air or water at room temperature. This oxide layer, which is basically TiO_2, holds fast firmly to the titanium

substrate surface. The adhesion and adhesive quality are constrained by the oxidation temperature, thickness of the oxide layer and presence of nitrogen in the oxidation procedure [80-82]. TiO_2 has a tetragonal structure and known as the steadiest phase.

As per the passivity theory, the titanium material framework has both the dynamic and latent surfaces simultaneously in contact with electrolytes [82-84], and experiences a nonstop procedure of halfway disintegration and re-precipitation in the aqueous environment. It was additionally discovered that calcium, phosphorous and sulfur are joined in the oxide layer on titanium embedded in bones [85, 86]. Calcium phosphates viewed as the primary composition of characteristic bone are precipitated on titanium and its composites in simulated body liquids. The formation of calcium phosphate can advance the osseointegration (integration with bones) of biomedical embeds and stretch its life span under in vivo condition.

Dalmau et. al. [87] researched the electrochemical conduct of rolled and sintered Ti– 6Al–4V combination by various electrochemical strategies so as to ponder the impact of the manufacture procedure on the corrosion mechanisms of these titanium composites. Prior to performing out the electrochemical tests, they did an actuation of the electrode surface to limit the impact of the unconstrained formation of titanium oxides. The consequences of examination demonstrated that the rolled and the sintered composites have comparable electrochemical conduct, yet the sintered compound displays higher corrosion opposition than the rolled one. Powder metallurgy is a promising fabrication system to acquire titanium biomedical alloys offering the near ideal corrosion opposition.

Utilization of titanium composites as biomaterials is picking up enthusiasm because of their unrivaled biocompatibility and improved corrosion opposition when contrasted with customary stainless steels and cobalt-based alloys [88]. The physical, mechanical and topographical properties of the metallic surface assume an imperative role in the life span of prosthesis; additionally, these highlights decide the marvels happening at the interface between the embedded device and the natural environment. The corrosion conduct of titanium alloys relies upon the arrangement of an oxide film predominantly made out of TiO_2 with some measure of TiO and Ti_2O_3, which in a split second covers the outside of titanium and its compounds in presence of oxygen. The thickness of the oxide layer relies on the oxidation potential [89]. Liu et al. inspected the different surface adjustment strategies relating to titanium composites like mechanical treatment, thermal spraying, sol-gel, chemical/electro-chemical treatment and ion implantation from the point of view of bio-therapeutic methodology [90].

Nowadays, permeable titanium has turned into a well-known careful embed material, as it has been known to have the roughness and the porosity of the material, vital for expanding the coordination of the embedded implant into the bone [91]. The permeable surface solid cored Ti-64 inserts have a lot higher compressive strength when contrasted with human teeth and bone [92-94]. Bandyopadhyay et. al. created penetrable Ti-6Al-4V utilizing Laser Engineered Net Shaping and performed in vivo examination, acquiring higher porosity of the samples, with rich calcium concentration inside the pores, recommending a quicker rate of tissue generation and integration as contrasted with samples with lower pore volume [95].

2.8 Research Gap

From the literature survey (Survey Table given in Annexure 1), it is found that, plainly researchers and specialists have widely examined on manufacture, characterization, forging, machining and corrosion of cast titanium compounds and have improved the machining parameters. However, not many works have been accounted so far on manufacturing, characterization, forging, machining and corrosion of Commercially Pure Sintered Titanium (CP-Ti) powder metallurgy items. CP-Ti is effectively available as rods and bars, however, manufacturing of bio-medical prosthesis, for example, hip-joints or dental inserts, from those rods or bars requires lot of machining, which is troublesome. Accordingly, it would be advantageous, if a close net shape segment of hip-joint or dental implant can be at first made through powder metallurgy route, and from there on, forging and minor machining of the same component can easily be done through the non-conventional route to acquire the final shape.

CHAPTER 3

EXPERIMENTAL PROCEDURE

Outline of the Chapter: *3.1 Fabrication of P/M Samples, 3.2 Microstructural Examination, 3.3 Mechanical Properties, 3.3.1 Density Measurement, 3.3.2 Microhardness, 3.3.2 Formability, 3.3.4 Machinability, 3.3.5 Surface Roughness, 3.4 Closure*

3.1 Fabrication of P/M Samples

As received Titanium powder (of 325 average particle mesh size, 99% metal basis, of make: Alfa Aesar) were utilized as the test material for manufacture through powder metallurgy process. The metal powders were mixed with a binder ACRAWAX (0.01 % by weight) in a drum with a round blender (measurement: 40 mm diameter and 35 mm height), at a steady speed of 1500 revolutions per minute for 60 minutes.

A short time later, the blend of the titanium particles and binder was filled in a high carbon high chromium steel tubular shaped die, the die having 30 mm thickness, 90 mm external diameter and 14.5 mm internal diameter. The detail dimensions of the die and punch set is given in Figure 3.1.

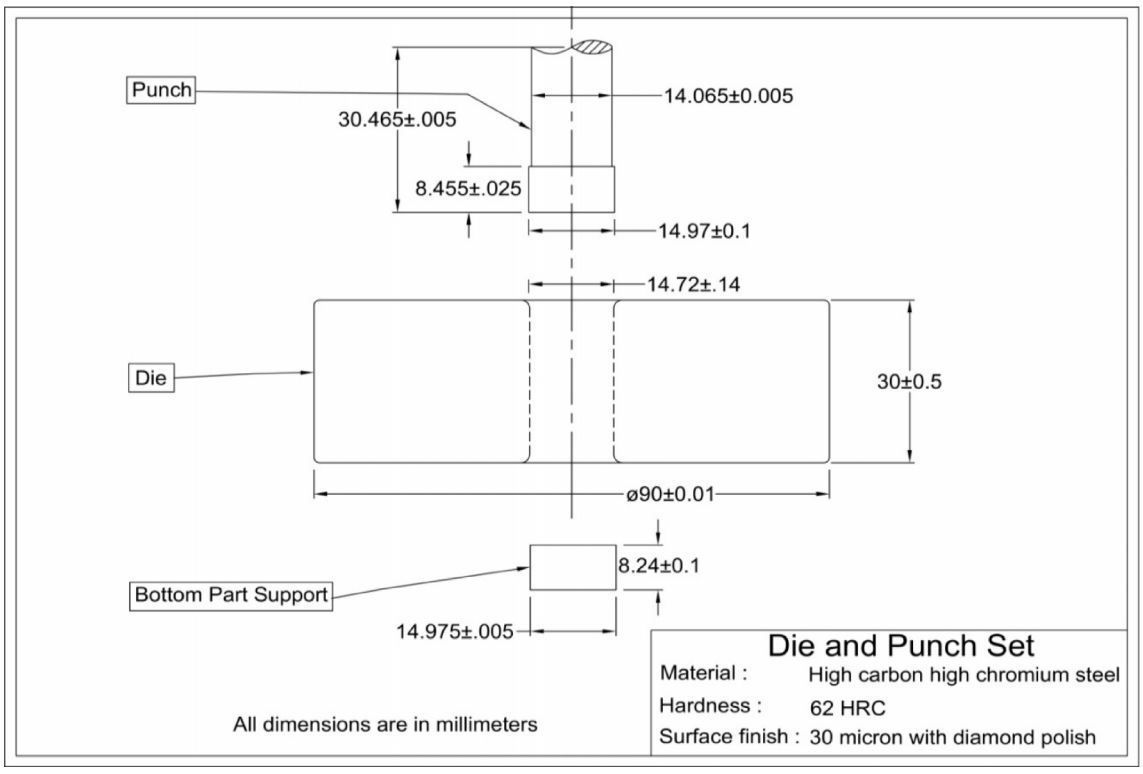

Figure 3.1 Sketch of the die and punch set used to fabricate cylindrical preform

The powder blend was subsequently squeezed at a pressure of 840 MPa in a Universal testing machine (of 400 kN capacity, Model No. KUT-40, Sl. No. 2K7/85) (Specification given in Annexure), for 5 minutes, to get multiple PM titanium green compact samples.

Figure 3.2 Universal testing machine [Courtesy: ARCI, Hyderabad]

Afterwards, the green compacts were preheated at 400˚C in Nitrogen environment to eliminate the binder ACRAWAX in quartz made cylindrical tube heater (hot zone measurement 75 mm diameter, length 150 mm and greatest temperature 1000˚C) (Specification given in Annexure). The samples were preheated to 400˚C at a rate of 5˚C/min, consequently holding at 400˚C for 2 hours and after that the samples were furnace cooled under nitrogen environment to expel the ACRAWAX totally from them.

Figure 3.3 Floor-stand quartz made tubular furnace [Courtesy: ARCI, Hyderabad]

The ACRAWAX free green compacts were later sintered in a Batch-type Electric Resistance Vacuum Furnace (working space measurements: width-100 mm, length-300 mm and height-100 mm; Sl. No. CHB3-1.3.1/ 20H2) (Specification given in Annexure) as appeared in Figure 3.4, upto a temperature of 1450˚C in 0.001mbar (7.6x10-4 Torr) absolute pressure (in vacuum) to evade oxidation. The sintering parameters are presented Table 3.1. [Technical specification of all the equipment used in this research are given in Annexure 2.]

Figure 3.4 Electric Resistance Batch-type Vacuum Furnace [Courtesy: ARCI, Hyderabad]

Table 3.1 Sintering parameters

Operation	**Initial temperature**	**Final temperature**	**Duration**
Heating	Ambient 30˚C	550˚C	55 min
Soaking	550˚C	550˚C	60 min
Heating	550˚C	1350˚C	80 min
Soaking	1350˚C	1350˚C	30 min
Furnace cooling	1350˚C	Ambient 30˚C	120 min

3.2 Microstructural Examination

The samples were at first prepared and afterwards tested in a Scanning Electron Microscope (JEOL make, Sl. No. JSM - 6360) (Specification given in Annexure). Tests for metallographic evaluation have been set up by grinding with 320, 400, 600, 800, 1200 and 1500 grit size abrasive papers pursued by cleaning with 6 μm precious diamond paste. At that point the samples were scratched with an etchant (2.5 ml Nitric acid, 1.5 ml HCl, 1 ml HF and 95 ml distilled water). The etched samples were dried and their microstructure seen by utilizing SEM at various magnifications. Figure 3.5 demonstrate the porous microstructure of the sintered compacts.

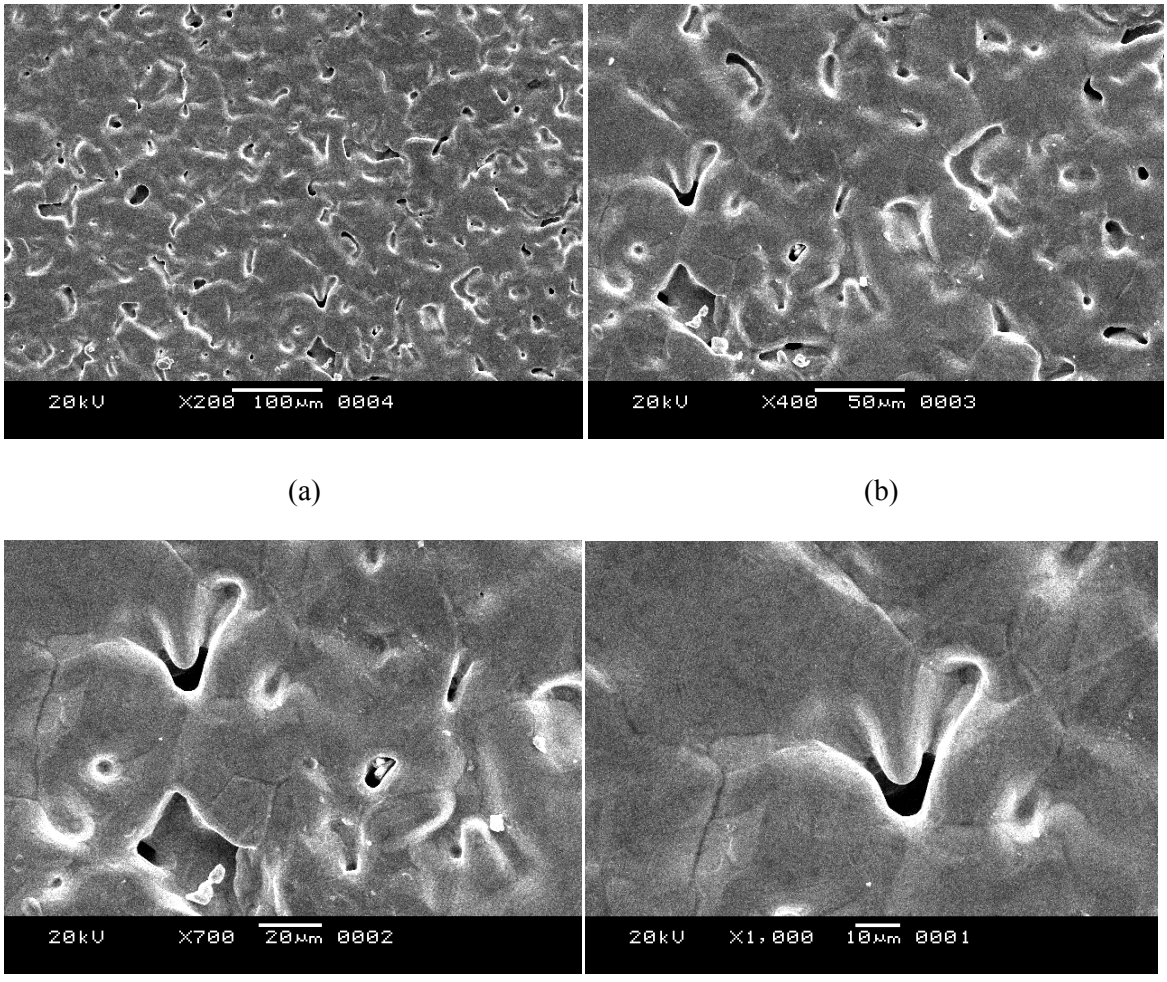

(a) (b)

(c) (d)

Figure 3.5(a-d): SEM micrographs of the sintered Ti-samples at different magnifications

From micro-structural examinations, it is clear that, P/M titanium has bonded very well during sintering, with the structure consisting uniform porosities. The maximum size of void is found to be ~10 μm. These porosities help in tissue growth inside the bio-implants.

3.3 Mechanical Properties

3.3.1 Density Measurement

The densities of the green and sintered samples were measured by Archimedes principle. The average relative density of the green compacts was about 77.5 %, whereas the average relative density of sintered compacts was approximately 92.5 %. The plots of density vs sintering temperature & compaction load is shown in Figure 3.6.

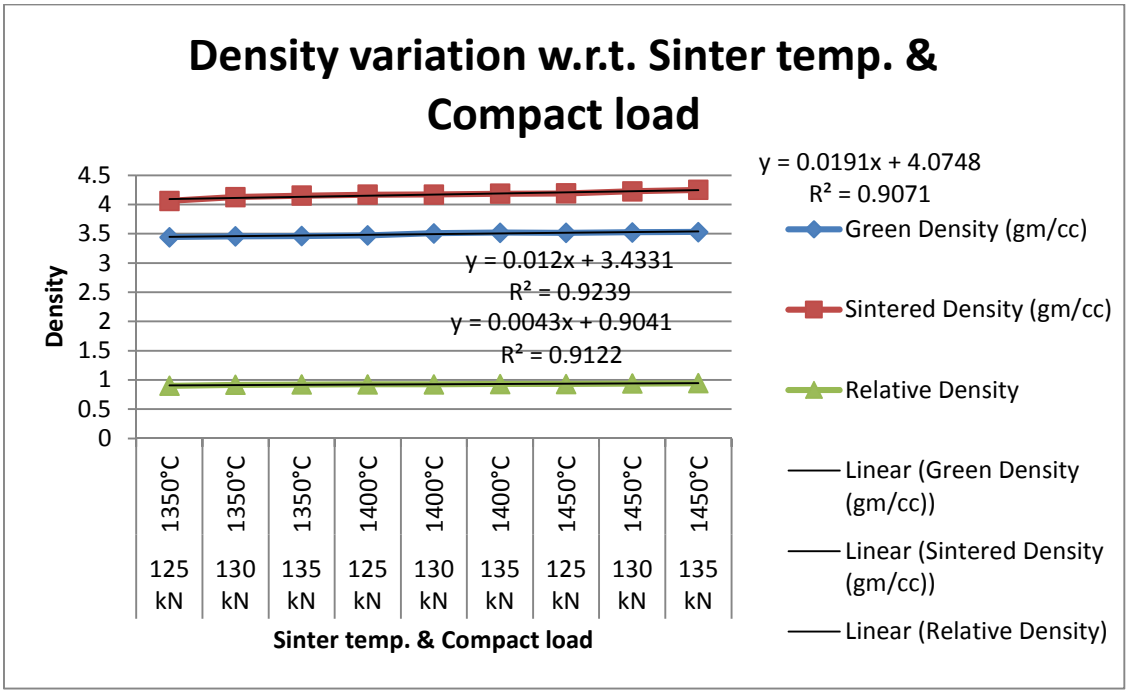

Figure 3.6 Density variation of with respect to Sinter temperature and Compact load

The best-fit curve (straight line) of green density (blue legend), sintered density (maroon legend) and relative density (green legend) are shown on the graph itself. The plot also shows R-squared values of the best-fit curves, which are close to 100%. It means that the density variation data fits well with the model of the best-fit curves.

3.3.2 Micro-hardness

The micro-hardness of the sintered samples was measured in Matsuzawa make AMT Series MMT-X micro-hardness tester with maximum load capacity of 2 kg. The micro-hardness of the samples (sintered at 1350°C) increases with increasing compacting load. It is also observed that micro-hardness of the samples increases with increasing sintering temperature at same compacting load and explained in Figures 3.7 and 3.8.

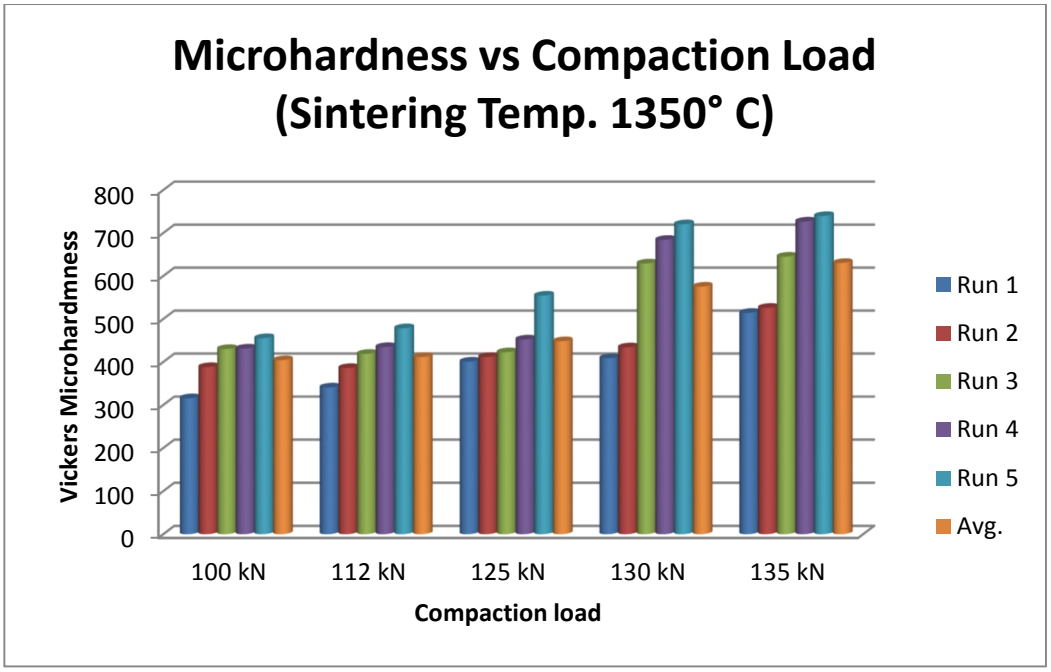

Figure 3.7 Variation of micro-hardness with respect to compaction load (at const. sintering temperature)

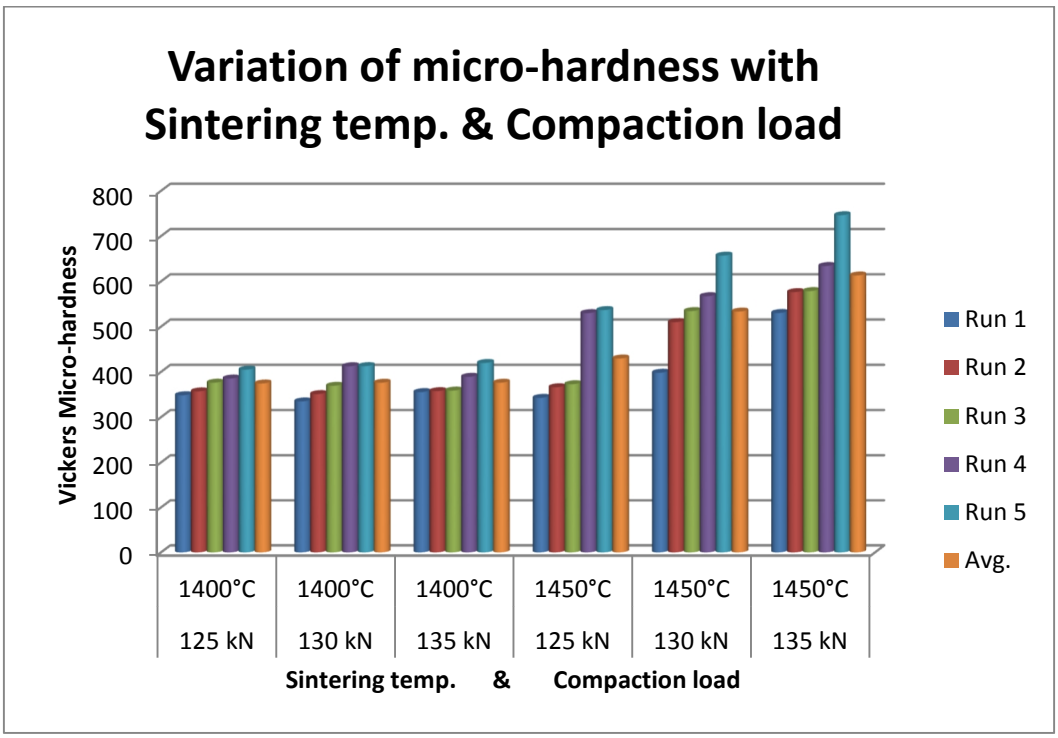

Figure 3.8 Variation of micro-hardness with respect to compaction load and sintering temperature

The different colour bars in figure 3.7 and 3.8 indicate five different runs in micro-hardness measurement on each sample, while the last bar (yellow) indicates average of the five runs.

3.3.3 Formability

Formability is the ability of a given metal work-piece to undergo plastic deformation without being damaged. The plastic deformation capacity of metallic materials is, however, limited to a certain extent, at which point, the material would experience fracture / tearing / breakage. Formability is measured with the help of 'Formability limit diagram' or 'forming limit curve'. The formability characteristics of the sintered samples were tested in an Instron (5500R) tensile compression tester at CGCRI, Kolkata and the load vs deformation curves were obtained electronically from the machine. Detailed discussions regarding load vs deformation characteristics are given in Chapter 4.

Figure 3.9 Instron 5500R Tensile Compression Tester [Courtesy: CGCRI, Kolkata]

3.3.4 Machining Analysis

The machining of the sintered PM samples was carried out on JOEMARS CNC Wire-cut EDM machine at MSME Tool Room Kolkata (Model: WT 355, Sl. No. 1050594) as shown in

Figure 3.10. The surface roughness properties and metal removal rate of each Ti-samples has been measured and detailed analysis of the same is presented in Chapter 5. The image of a sample before and after machining is shown in Figure 3.11. [Technical specification of all the equipment used in this research are given in Annexure 2.]

Figure 3.10 CNC Wire-cut EDM [Courtesy: MSME Tool Room, Kolkata]

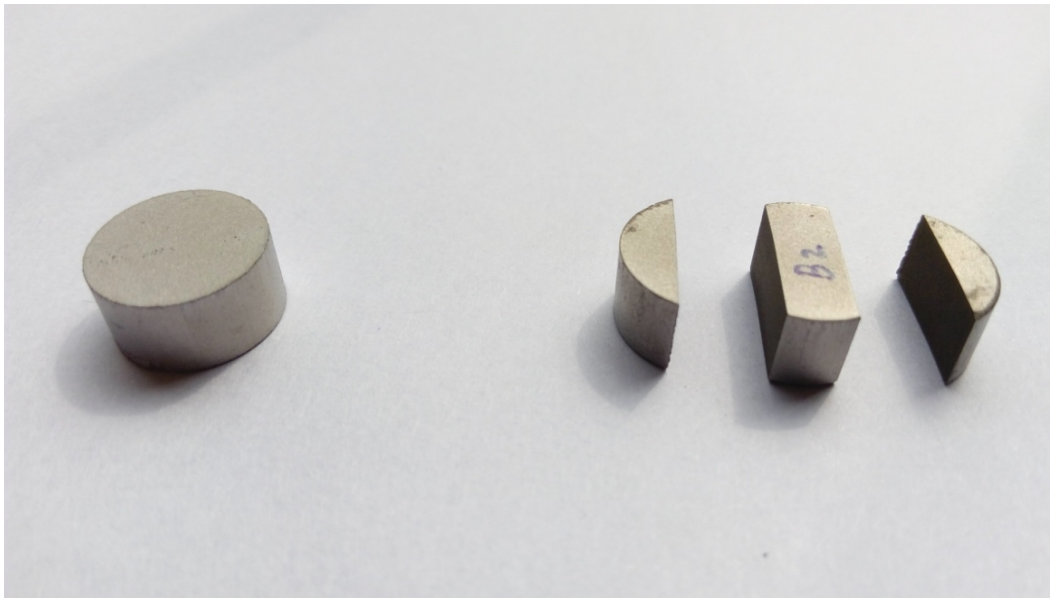

Figure 3.11 Sintered and Wire-cut EDM sample

While operating Wire-cut EDM, some machining fixed as well as variable parameters are required to be set. These parameters are illustrated in Table 3.2.

Table 3.2 Machining fixed and variable parameters at WEDM

Fixed Parameters	Value	Variable Parameters	Working Range	Value
Wire Electrode material	Brass wire of 0.25 mm dia.	Open Circuit Voltage	0-15 V	8 V
Spark gap	0.05 mm	Arc On Voltage	1-19 V	5 V
Wire feed	9 m/min	Arc Off Voltage	8-50 V	8 V
Di-electric fluid	De-ionized water	Wire Tension	0-15 kg	10 kg
Workpiece material	CP-Ti P/M components	Water Pressure	0-7 kg / cm^2	6 kg / cm^2
Workpiece dia.	14 mm	Feed sensitivity	0-99 V	50 V
Workpiece thickness	7 mm	Servo Voltage	25-150 V	60V

3.3.5 Surface Roughness

Figure 3.12 shows the stylus-type profilometer Talysurf (Taylor Hobson Surtronic 3+) surface roughness tester at the Metrology laboratory, ME Dept., JU, through which, the surface roughness (R_a values) of the samples were measured.

Figure 3.12 Taylor Hobson Surface Roughness Tester [Courtesy: Metrology Lab, JU]

3.4 Closure

This chapter presents the experimental procedure for preparing the sintered titanium powder metallurgy components. The machines used for preparation of the samples were discussed. Microstructural evaluation of the samples is presented and different characterization methods viz. relative density, micro-hardness, etc. are discussed. The equipment used for formability study and machining analysis are presented.

CHAPTER 4

FORMABILITY STUDY OF SINTERED TITANIUM SAMPLES DURING COLD FORGING

Outline of the Chapter: *4.1 Introduction, 4.2 Upper Bound Method, 4.3 Theoretical results for deformation, 4.4 Experimental validation of deformation, 4.5 Closure*

4.1 Introduction

Metal powder innovation is at present stirring interests in numerous parts of the world since creation of parts from metal powders is a viable option. Sinter forming of powder metallurgy components is creating near net shape large scale manufacturing innovation, by which compacted metal powder performs are shaped inside a couple of dies to deliver exact, high performing and financially viable designed parts. This procedure is alluring engineers because of the fact that it wipes out some significant number activities like casting, machining, welding etc. The density of such sinter shaped items compares positively with that of cast parts [96-98]. This innovation has colossal applications in the field of car industry, aviation innovation, defence and other familiar items, e.g., crankshafts, connecting rods and so on [99].

This part relates the distribution of pressure (at the work piece interface) and die load at the time of manufacturing of sintered cylindrical samples at slow speed. During examination, a fitting interfacial friction law and yield criteria for porous and permeable metal was utilized. The press and sinter shaping innovation is entirely dissimilar from the conventional cast metal forming, as qualities of porous materials amid pressure must be taken into contemplation. The densification (compaction or shutting of pores) and deformation (change of shape) of sintered preforms happen all the while amid sinter forming process and subsequently volumetric consistency guideline is not substantial here, as density of preform changes because of shutting of inter molecular pores. Consequently, the affectability of yielding because of hydrostatic stress part requires the utilization of appropriate yield criterion, which is reliant upon the relative density of the preform [100, 101]. The interfacial pressure applied for deformation breaks the die-work piece interfacial oil film and makes the conditions; that are modeled as composite friction including both sliding and sticking zone friction [102, 103].

To examine the deformation characteristics of the sintered preforms, which chooses different procedural parameters in actual work and for manufacturing purpose 'Upper bound theory' approach is by all accounts the best proper system, as this technique yields preferable outcome over the equilibrium method, when contrasted with experimental analysis [104]. The outcomes so acquired, are discussed fundamentally to demarcate the association of different parameters involved and exhibited graphically.

Interfacial friction condition between deforming die and work piece in metal working are of most noteworthy significance concerning various factors, for example, the force and the method of deformation, properties of the deformed sample and surface irregularity. The relative speed between the work piece material and the die-surface together with high interfacial load and/or deforming modes will make the conditions basic for an adhesion and sliding phenomenon. For such a component of composite friction, which more often than not happens in plastic deformation of metal powder preforms, the shear equation [98] is given as:

$$\tau = \mu[p + \rho_0 \phi_0] \qquad \ldots (4.1)$$

where, the first term ‘μp’ on the right hand side is the sliding friction and the second term ‘$\rho_0\varphi_0$’ is the friction because of adhesion, which is due to change in relative density of the perform. The adjustment in relative density relies on the deforming conditions, for example, speed and surface conditions. The equation 4.1 is used to analyze the deformation characteristics of metal powder preforms and used by several researchers.

Amid the deformation of a metal powder preform, the compressive force continuously increases the relative density, which later is directly proportional to the actual area of contact. The actual area of contact grows and approaches the apparent area as the force increases, which consequently increases the relative density. The pattern of metal flow amid the deformation of a metal powder perform is such that there exists two zones, an inward one where no relative movement between work piece and the die happens (namely the sticking zone) and an external zone where sliding happens. In this manner, the proper interfacial friction laws for various conditions given by Rooks [105] are:

$$\tau = \mu[p + \rho_0 \phi_0 \{1 - (\frac{r_m - r}{n r_0})\}] \qquad \ldots (4.2)$$

Figure 4.1 illustrates the forces acting on a cylindrical test specimen, considering an annular elementary strip of width ‘dr’ at a radius ‘r’ from the center. The vertical die pressure is denoted by ‘p’ and stress developed within the strip are denoted in terms of ‘σ_{rr}’ and ‘$\sigma_{\theta\theta}$’.

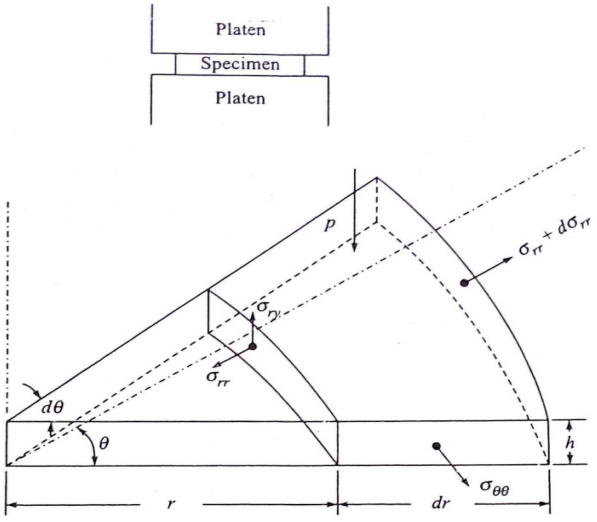

Figure 4.1 Force analysis of the cylindrical preform [104]

As we realize that amid plastic deformation of the metal powder preform, the volume changes and the yielding of metal powder preform is not insensitive totally to the hydrostatic stress imposed. Now, according to Tabata and Masaki [106], the yield criterion is:

$$\rho^k \sigma_0 = \sqrt{3J_2'} + 3\eta\sigma_m \quad \text{(where, } \eta \text{ is a constant, and function of } \rho \text{ only)} \qquad \ldots (4.3)$$

Or, $$\rho^k \sigma_0 = \sqrt{[\{(\sigma_1 - \sigma_2)^2 + (\sigma_2 - \sigma_3)^2 + (\sigma_3 - \sigma_1)^2\}/2]} \qquad \ldots (4.4)$$

$$= \eta(\sigma_1 + \sigma_2 + \sigma_3)$$

As, $\sigma_1 = \sigma_3 = \sigma_{rr} = \sigma_{\theta\theta}$ and $\sigma_2 = -p$, hence:

$(\sigma_1 - \sigma_2) \mp (2\sigma_1 + \sigma_2) + (\sigma_3 - \sigma_1) = \rho^k \sigma_0$ and for the positive sign we can write:

$$\sigma_1 = \frac{\rho^k \sigma_0}{(2\eta + 1)} - \frac{\eta - 1}{(2\eta + 1)}\sigma_2 \qquad \ldots (4.5)$$

4.2 Upper Bound Method

When a body is undergoing plastic deformation, its various particles move with respect to each other under the action of external forces. Hence a velocity field is created while deforming the body, though this actual velocity field is unknown to us. Generally, we assume a suitable velocity field, which satisfies the boundary conditions and the incompressibility condition. But, according to upper bound theorem, the rate of energy dissipation calculated from the assumed velocity field is always higher than that of the actual velocity field. As a

result, the die load calculated from the assumed velocity field is also higher than that due to the actual velocity field. The statement of upper bound theorem is stated below:

'Of all the kinematically admissible velocity fields the actual one minimizes the function J where'

$$J' = \int F_i U_i ds = \frac{2}{\sqrt{3}}\sigma_0 \int_v \sqrt{(\frac{1}{2}\varepsilon'_{ij}\varepsilon'_{ij})}dV + \int_s \tau|\Delta v|ds + \int_v \rho a_i U_i dV - \int_{st} T_i v_i ds \ldots (4.6)$$

where, the term *kinematically admissible* means that the chosen velocity field should satisfy the incompressibility as well as boundary conditions. Other terms are as follows:

J' = rate of work being done in deforming the body

U_i = displacement rate field, which satisfies the given displacement boundary conditions and the equation of incompressibility

ε'_{ij} = strain rate in deforming body

V = volume of deforming body

a_i = associated acceleration field

Δv = relative velocity of the specimen over the surface of the die and is equal to the velocity component of the specimen in the tangential direction at the interface, i.e. magnitude of velocity discontinuity on the surface S_t

T_i = stress vector prescribed on surface S_t at the zone of plastic deformation

v_i = velocity components on surface S_t

In equation 4.6, the Right Hand Side denotes the sum of different components of rate of work being done. The first term denotes the rate of internal energy dissipation *Wi* due to plastic strain rate, the second term denotes the frictional shear energy consumed W_f, the third term denotes energy dissipation due to inertia forces W_a and the last term signifies the rate of work being done against the external applied tractions W_t.

(a) Velocity fields:

$$U_r = \frac{(1-2\eta)U}{2(1+\eta)h}r$$

$$U_z = \frac{-zU}{h}$$

$$U_\theta = 0 \ldots (4.7)$$

(b) Strain rates:

$$\varepsilon_r' = \frac{\delta U_r'}{\delta r} = \frac{(1-2\eta)U}{2(1+\eta)h}$$

$$\varepsilon_\theta' = \frac{U}{r} + \frac{\delta U_\theta'}{\delta \theta} = \frac{(1-2\eta)U}{2(1+\eta)h} = \varepsilon_r'$$

$$\varepsilon_z' = \frac{\delta U_z'}{\delta z} = \frac{-U}{h} \ldots (4.8)$$

The aforesaid normal-strain components satisfy the compressibility equation for porous materials, so we can write:

$$\varepsilon_r' + \frac{(1-2\eta)}{2(1\pm\eta)}\varepsilon_z' = 0 \ldots (4.9)$$

Again from upper bound theorem, for plastic deformation of a metal powder preform, the external power *J'* supplied by the platens is given as:

$$J' = W_i + W_f + W_a + W_t \ldots (4.10)$$

In this case, the forces due to inertia are negligibly small and no external surface traction is stipulated, Therefore, $W_a = W_t = 0$.

Moreover, the external power *J'* supplied by the press through platen is:

$$J' = \int F_i U_i ds = PU \ldots (4.11)$$

(c) Internal power of deformation:

The plastic work done per unit volume is given by the following equation:

$$dW_i = \frac{\sqrt{2}}{3}\rho^k \lambda[(\varepsilon_r' - \varepsilon_\theta')^2 + (\varepsilon_\theta' - \varepsilon_z')^2 + (\varepsilon_z' - \varepsilon_r')^2]^{1/2} \ldots (4.12)$$

Therefore, we can write $$W_i = \frac{\rho^k \lambda U}{(1+\eta)}\pi b^2 \qquad \ldots (4.13)$$

(d) Energy dissipation due to friction is written as:

$$W_f = \int_s \tau |\Delta v| ds \qquad \ldots (4.14)$$

Considering magnitude of relative velocity,

$$|\Delta v| = \frac{(1-2\eta)U}{2(1+\eta)h} r$$

$$ds = r d\theta dr$$

$$\tau = (\mu_1 + \mu_2)[p + \rho_0 \phi_0 \{1 - (\frac{r_m - r}{nr_0})\}]$$

When, $\rho_0 \phi_0 = x.p = x\frac{P}{\pi b^2}$, where *0 < x < 1* and putting all the values in equation 4.14 and after integration we get:

$$W_f = \frac{1}{3}\frac{\pi(\mu_1 + \mu_2)(1-2\eta)Ub^3}{(1+\eta)h}[p + \rho_0 \phi_0 \{1 + \frac{3}{4nb} - \frac{r_m}{nb}\}] \ldots (4.15)$$

If, $\mu_1 = \mu_2 = \mu$ we can write,

$W_f = \frac{2}{3}\frac{\pi\mu(1-2\eta)Ub^3}{(1+\eta)h}[p + \rho_0 \phi_0 \{1 + \frac{3}{4nb} - \frac{r_m}{nb}\}] \ldots$ (4.16) developed by G. Sutradhar et al. [98]

(e) Die load:

From equation 4.14 we can write that: $J' = W_i + W_f = PU$

$$P = \frac{\rho^k \lambda}{(1+\eta)}\pi b^2 + \frac{1}{3}\frac{\pi(\mu_1 + \mu_2)(1-2\eta)b^3}{(1+\eta)h}[p + \rho_0 \phi_0 \{1 + \frac{3}{4nb} - \frac{r_m}{nb}\}] \ \ldots (4.17)$$

Again, if $\mu_1 = \mu_2 = \mu$

$$P = \frac{\rho^k \lambda}{(1+\eta)}\pi b^2 + \frac{2}{3}\frac{\pi\mu(1-2\eta)b^3}{(1+\eta)h}[p + \rho_0 \phi_0 \{1 + \frac{3}{4nb} - \frac{r_m}{nb}\}] \ldots (4.18)$$

Now, $p = \frac{P}{\pi b^2}$ from $\rho_0 \phi_0 = x.p = x\frac{P}{\pi b^2}$

$$P = [1 - \frac{1}{3}\frac{b(\mu_1 + \mu_2)(1-2\eta)}{(1+\eta)h} - \frac{1}{3}\frac{b(\mu_1 + \mu_2)(1-2\eta)x}{(1+\eta)h}\{1 + \frac{3}{4nb} - \frac{r_m}{nb}\}]^{-1}[\frac{\rho^k \lambda}{(1+\eta)}\pi b^2] \ \ldots (4.19)$$

$$\frac{P}{\lambda} = [1 - \frac{1}{3}\frac{b(\mu_1 + \mu_2)(1-2\eta)}{(1+\eta)h} - \frac{1}{3}\frac{b(\mu_1 + \mu_2)(1-2\eta)x}{(1+\eta)h}\{1 + \frac{3}{4nb} - \frac{r_m}{nb}\}]^{-1}[\frac{\rho^k}{(1+\eta)}\pi b^2] \ldots (4.20)$$

Again, for $\mu_1 = \mu_2 = \mu$

$$P = [1 - \frac{2}{3}\frac{b\mu(1-2\eta)}{(1+\eta)h} - \frac{2}{3}\frac{b\mu(1-2\eta)x}{(1+\eta)h}\{1 + \frac{3}{4nb} - \frac{r_m}{nb}\}]^{-1}[\frac{\rho^k \lambda}{(1+\eta)}\pi b^2] \ldots (4.21)$$

$$\frac{P}{\lambda} = [1 - \frac{2}{3}\frac{b\mu(1-2\eta)}{(1+\eta)h} - \frac{2}{3}\frac{b\mu(1-2\eta)x}{(1+\eta)h}\{1 + \frac{3}{4nb} - \frac{r_m}{nb}\}]^{-1}[\frac{\rho^k}{(1+\eta)}\pi b^2] \ldots (4.22)$$

developed by G. Sutradhar et al. [98]

4.3 Theoretical results for deformation

In metal powder forming operation, there are two procedures that happen at the same time i.e., compaction (densification) and deformation. At first compaction rules; so relative average pressure curve increments gradually. After compaction, phase deformation rules and a steep slope is noticed. Material flows mainly in the direction of punch movement, with little lateral flow in the starting. As the density increases, lateral flow increases. In the last stage of deformation, the lateral flow approaches the spreading behavior of pore free material. Lateral spreading increases with increasing initial density of perform.

Based on upper bound theorem and the aforesaid equation 4.21, calculations were carried out in MATLAB, taking 0.5 mm reductions in each step, from 0 to 40% deformation.

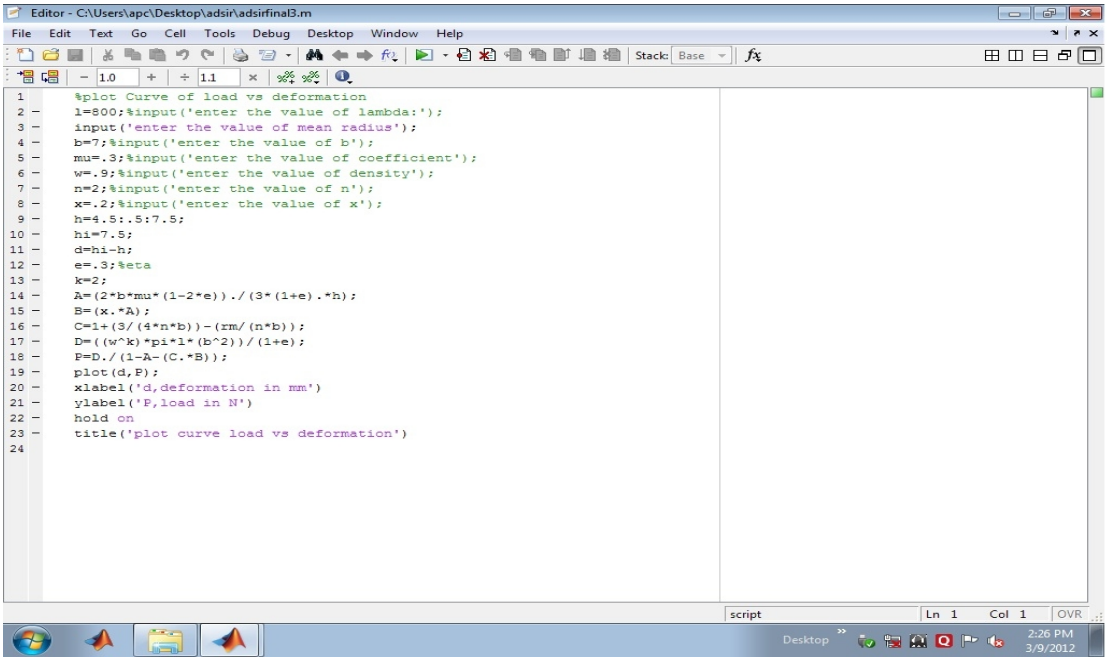

Figure 4.2 MATLAB programme to calculate theoretical load vs deformation plots

For the parametric analysis of deformation behavior of sinter metal perform during open die forging, let us assume following set of data for various processing parameters:

n = 1, 2, 3, 4

ρ = 0.7, 0.75, 0.8, 0.85, 0.9, 0.95

μ = 0.25, 0.3, 0.35, 0.4, 0.45

r_m = 2.5, 3, 3.5, 4, 4.5

λ = 650, 700, 750, 800, 850, 900

$_x$ = 0, 0.5, 1, 1.5, 2, 2.5, 3

The curves express the hypothetical results at 40% reduction of the circular preform for different values of the co-efficient of friction at the upper and bottom surfaces. As relative density of the sintered preform increases, the required amount of relative forging pressure increases. It is additionally observed that, the experimental values of the relative forging pressure are nearly in close concurrence with theoretical values obtained from equation 4.21 by upper bound theory.

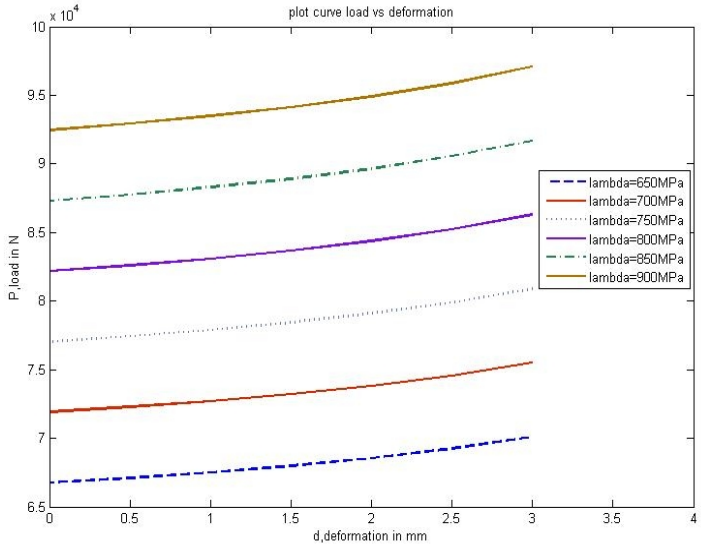

Figure 4.3 Theoretical variation of load vs deformation for different flow stresses (λ)

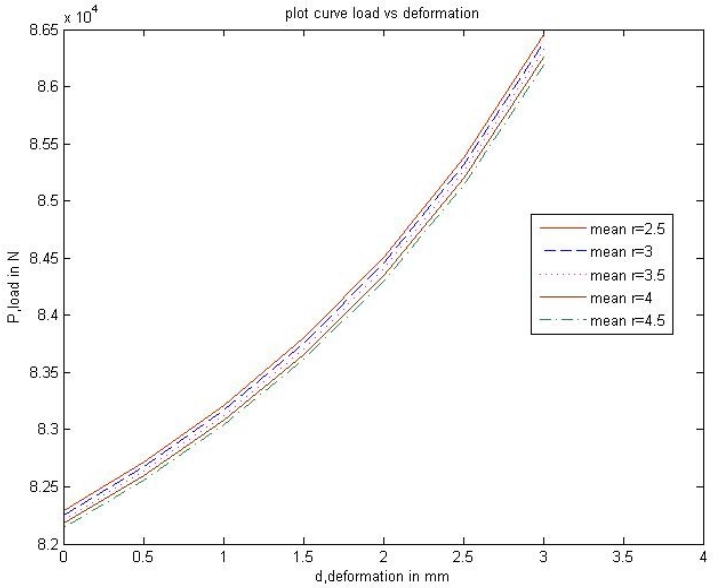

Figure 4.4 Theoretical variation of load vs deformation for different sticking zone radii (r_m)

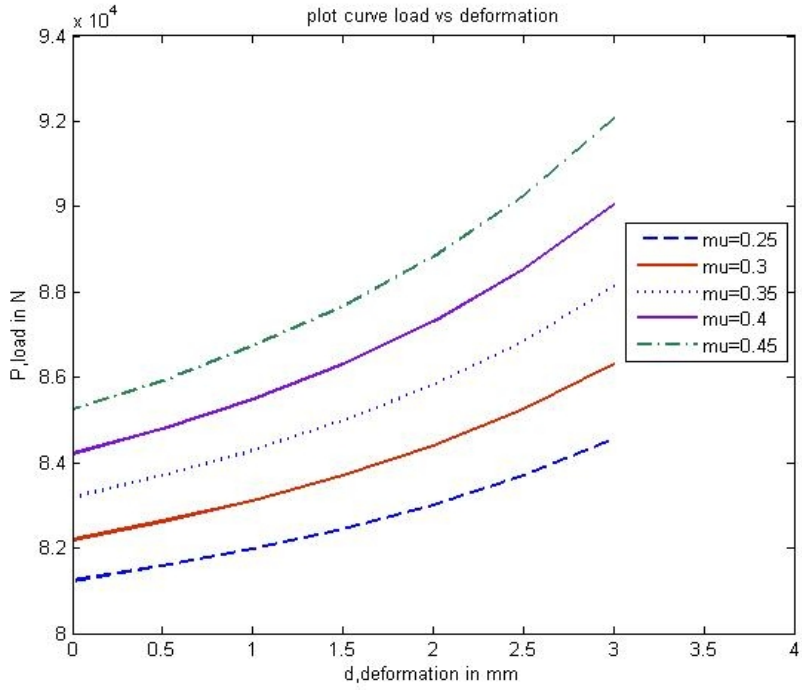

Figure 4.5 Theoretical variation of load vs deformation for different friction co-efficient (μ)

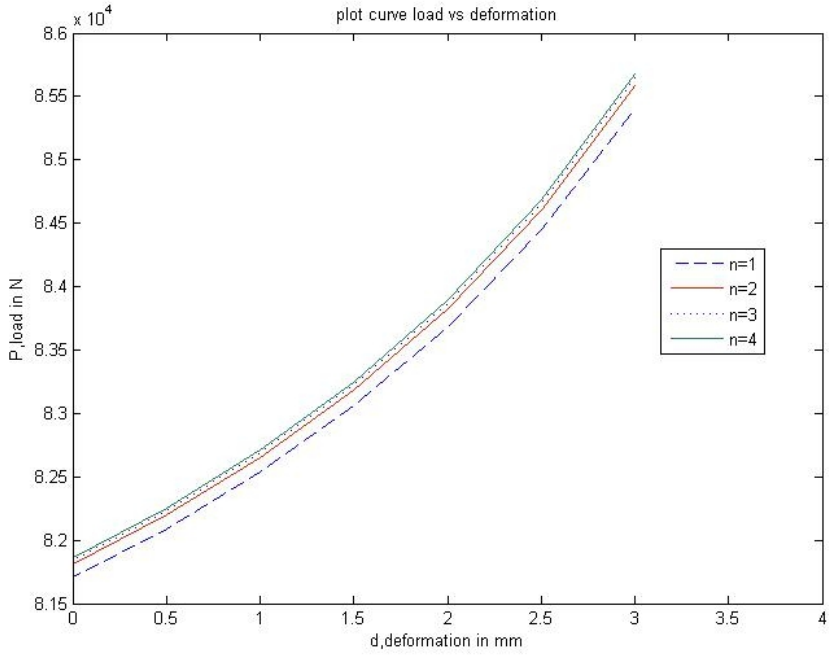

Figure 4.6 Theoretical variation of load vs deformation for different '$_n$' (a constant, whose value varies as 1,2,3& 4)

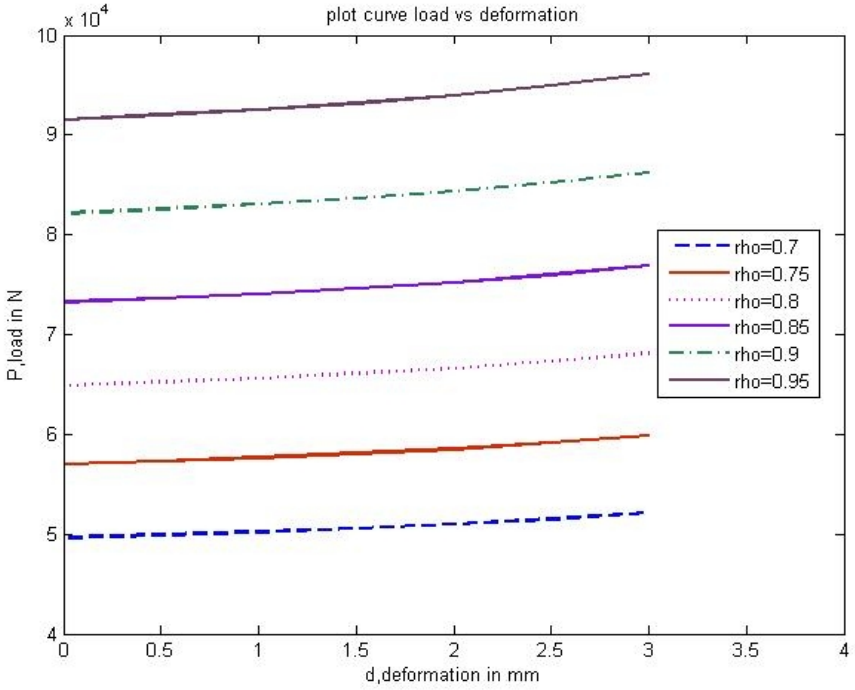

Figure 4.7 Theoretical variation of load vs deformation for different relative density (ρ)

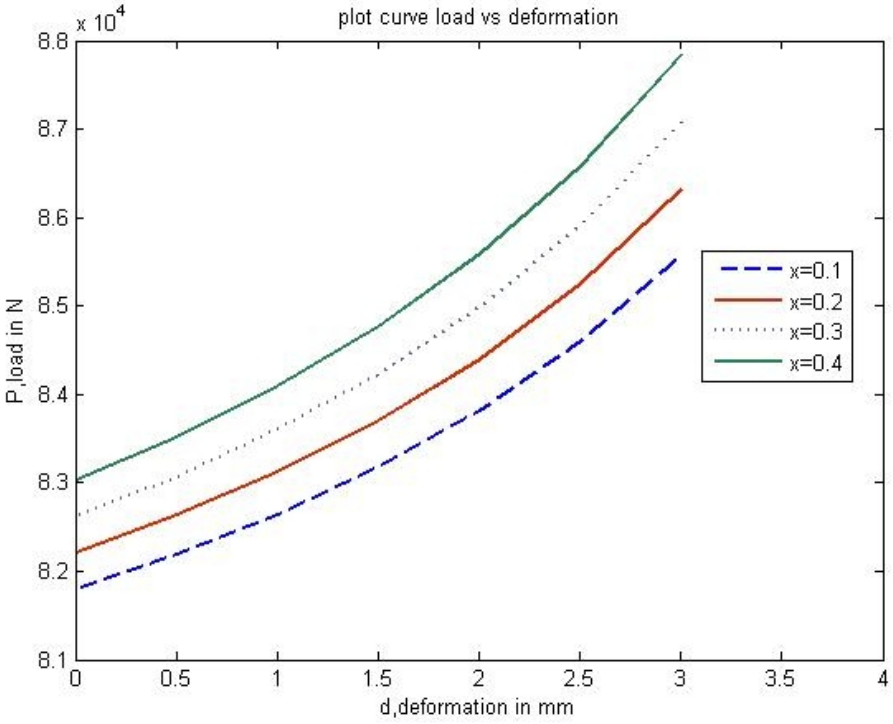

Figure 4.8 Theoretical variation of load vs deformation for different '$_x$', where x = 0, 0.5, 1, 1.5, 2, 2.5, 3

4.4 Experimental validation of deformation

The formability characteristics of the sintered samples were tested in an Instron-5500R at CGCRI, Kolkata and load vs deformation curves were obtained as shown in figures 4.9, 4.10 and 4.11 and Tables 4.1, 4.2 & 4.3 respectively.

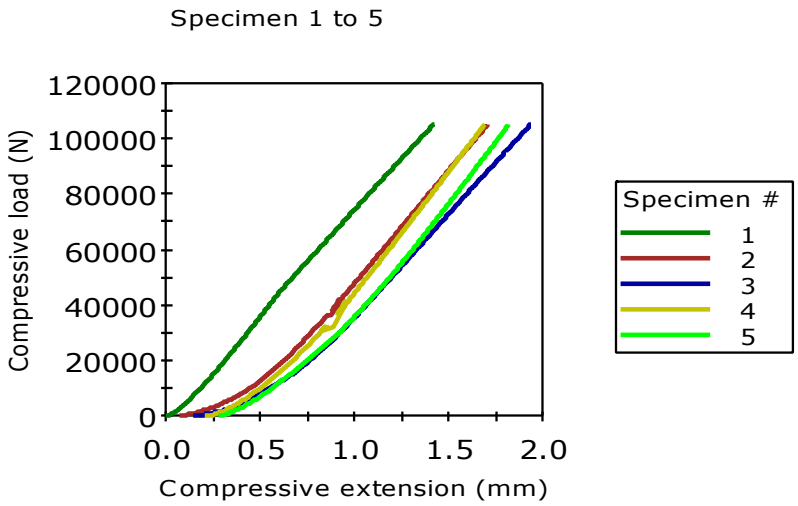

Figure 4.9 Actual compressive load – deformation characteristics for 1350°C sinter temperature

Table 4.1 Compressibility test data for 1350°C sinter temperature samples

	Spec. label	Diameter (mm)	Max. Comp. load (N)	Max. Comp. Stress (MPa)	Compressive extension at Maximum Comp. load (mm)
1	A-10	14.10	105,000.305	672.45	1.421
2	B-10	14.10	105,000.781	672.46	1.639
3	A-1	14.10	105,002.344	672.47	1.793
4	A-2	14.10	105,000.922	672.46	1.480
5	A-3	14.10	105,001.094	672.46	1.536
Mean		14.10	105,001.089	672.46	1.574
S. D.		0.00	0.76	0.00	0.15
C.V.(%)		0.00	0.00	0.00	9.31

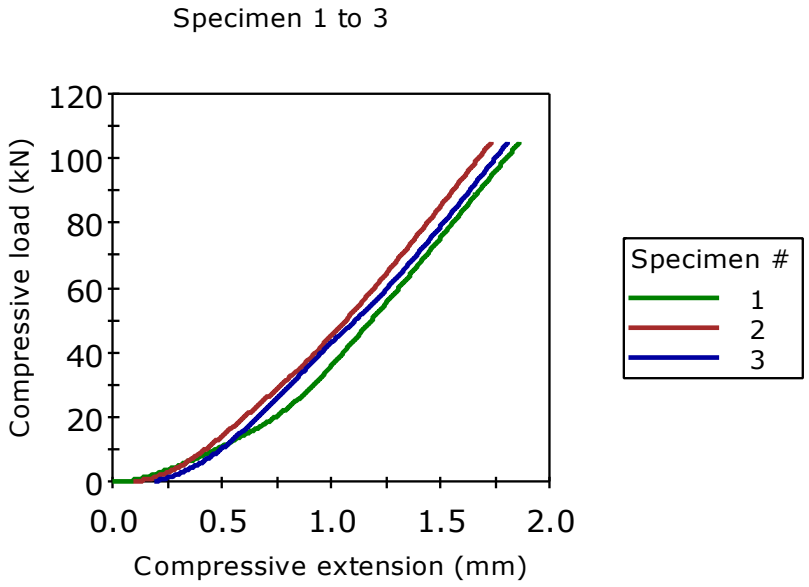

Figure 4.10 Actual compressive load – deformation characteristics for 1400°C sinter temperature

Table 4.2 Compressibility test data for 1400°C sinter temperature samples

	Spec. label	Diameter (mm)	Max. Comp. load (kN)	Max. Comp. Stress (MPa)	Compressive extension at Maximum Comp. load (mm)
1	A-4	14.10	105.001	672.46	1.865
2	A-5	14.10	105.003	672.47	1.641
3	A-6	14.10	105.003	672.47	1.622
Mean		14.10	105.002	672.47	1.709
S. D.		0.00	0.00	0.01	0.13
C.V.(%)		0.00	0.00	0.00	7.89

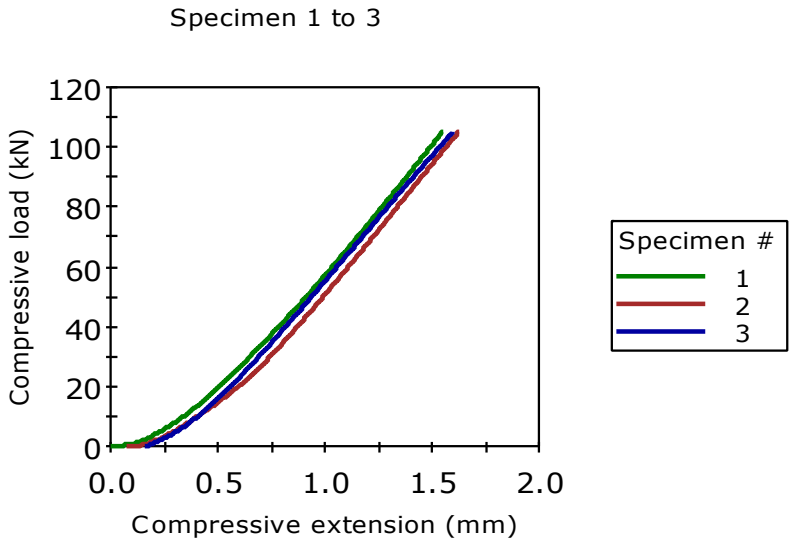

Figure 4.11 Actual compressive load – deformation characteristics for 1450°C sinter temperature

Table 4.3 Compressibility test data for 1450°C sinter temperature samples

	Spec. label	Diameter (mm)	Max. Comp. load (kN)	Max. Comp. Stress (MPa)	Compressive extension at Maximum Comp. load (mm)
1	A-7	14.10	105.000	672.45	1.549
2	A-8	14.10	105.001	672.46	1.546
3	A-9	14.10	105.002	672.46	1.444
Mean		14.10	105.001	672.46	1.513
S. D.		0.00	0.00	0.00	0.06
C.V. (%)		0.00	0.00	0.00	3.97

4.5 Closure

In the formability study of sintered titanium powder metal preforms, it is found that the theoretical analysis of the deformation characteristics through *upper bound theorem* matches well with the experimental results. The detailed comparative analysis is given in Annexure 3.

CHAPTER 5

EXPERIMENTAL DESIGN METHODOLOGY AND ANALYSIS FOR MACHINING OF SINTERED TITANIUM SAMPLES

Outline of the Chapter: *5.1 Design of experiments (DOE), 5.1.1 Components of Experimental Design, 5.2 Response Surface Methodology, 5.3 Box–Behnken design, 5.4 Results and Discussion, 5.4.1 Surface Roughness (Ra-value), 5.4.2 Sensitivity analysis (R_a-value) 5.4.3 Metal Removal Rate (MRR), 5.4.4 Sensitivity analysis (MRR), 5.4.5 Grey Relational Analysis, 5.4.5.1 Confirmatory Tests, 5.5 Microstructural examination and XRD analysis of the machined surface, 5.6 FESEM analysis, 5.7 Atomic Force Microscopy, 5.8 Energy Dispersive X-Ray (EDAX) Analysis, 5.9 Closure*

5.1 Design of experiments (DOE)

The term experiment is characterized as a systematic process carried under a controlled environment so as to find an unidentified outcome, to test or build up a theory, or to delineate a known output. While examining a procedure, tests are frequently used to assess which process parameters significantly affect the procedural yield, and what the objective level of those input parameters ought to be so as to accomplish an ideal yield or result. DOE is defined as Experimental Design as well.

5.1.1 Components of Experimental Design

Experimental Design has three components:

- ***Factors,*** which can be termed as either controlled or uncontrolled variables
- ***Levels***, or stages of each factor in the study
- ***Response***, or output of the experiment

5.2 Response Surface Methodology

Response surface methodology or RSM is a blend of numerical and statistical methods, which is useful for modeling and analysis of problems, by which a response output of interest is influenced by several input variables and its objective is to optimize the response output [37]. In this case we wish to find the levels of sintering temperature (x_1), pulse-on time (x_2)

and pulse-off time(x_3) that optimize the surface roughness and metal removal rate of the WEDM process and which can be expressed as:

$$y = f(x_1, x_2, x_3) + \varepsilon \quad \ldots (5.1)$$

where, 'y' is the output or response and x_1, x_2, x_3 are the process or input variables influencing the output and 'ε' represents the noise or error in the response 'y'.

5.3 Box–Behnken Design

Box–Behnken Design is experimental design for response surface methodology, formulated by George Box and Donald Behnken in the year 1960. For this situation, each factor (or autonomous variable), is set to one of the three similarly dispersed values, generally coded as -1, 0, +1. Box-behnken design has lesser design points, for this reason, they are more affordable to run than Central Composite Design with same number of factors. The design is adequate to fit a quadratic model, i.e., one containing squared terms and products of two factors. Usually a second-order model is utilized in RSM. The equation may be given as:

$$y = \beta_0 + \sum_{i=1}^{k} \beta_i x_i + \sum_{i=1}^{k} \beta_{ii} x_i^2 + \sum_{i<j} \beta_{ij} x_i x_j + \varepsilon \quad \ldots (5.2)$$

where, x_1, x_2, x_3,…, x_k are the input variable factors which impact the reaction output 'y'; β_0, β_{ii},…..β_{ij}, in which (i=1, 2, …, k), and (j=1,2, …, k) are the unknown parameters and 'ε' is a random error, which is negligible for the present case. The different stages of the control factors, chosen for Box-Behnken Design have been delineated in Table 5.1.

Based on the proposed 2nd order polynomial model, the impacts of the procedure variables on the Surface Roughness (Ra-value) and Metal Removal Rate (MRR) were determined and tabulated using MINITAB-16 software and shown in Table 5.2.

Table 5.1 Levels of variables chosen for Box-Behnken Design

Parameters	Unit	Symbol	Level		
			Low	Medium	High
			-1	0	1
WEDM Pulse on time	µs	N	6	8	10
WEDM Pulse off time	µs	F	9	11	13
Sintering temperature	°C	T	1350	1400	1450

Table 5.2 Box-Behnken Design lay-out and experimental results of Metal Removal Rate and Surface Roughness

	Coded Factors			Actual Factors			Actual Response	Actual Response
Run Order	*N*	*F*	*T*	Pulse-on time (*N*)	Pulse-off time (*F*)	Sintering Temp. (*T*)	MRR (mm^3/s)	Surface Roughness (Ra in μm)
1	-1	-1	0	6	9	1400	5.76	2.41
2	0	0	0	8	11	1400	7.996	2.64
3	1	0	1	10	11	1450	8.55	2.85
4	0	-1	1	8	9	1450	6.969	2.72
5	-1	1	0	6	13	1400	6.774	2.72
6	0	0	0	8	11	1400	7.15	2.75
7	-1	0	-1	6	11	1350	6.169	2.77
8	-1	0	1	6	11	1450	5.986	2.49
9	0	1	1	8	13	1450	7.551	2.36
10	0	1	-1	8	13	1350	9.049	2.7
11	1	-1	0	10	9	1400	7.674	3.03
12	0	-1	-1	8	9	1350	6.948	2.76
13	1	1	0	10	13	1400	9.903	2.72
14	1	0	-1	10	11	1350	7.688	3.04
15	0	0	0	8	11	1400	7.13	2.59

5.4 Results and Discussion

5.4.1 Surface Roughness (Ra-value)

Mathematical model developed for R_a-value and optimization of the process parameters

The mathematical relationship co-relating the surface roughness (R_a) and the procedural input factors under consideration, in particular sintering temperature (T), pulse-on time (N) and pulse-off time (F), is obtained as follows:

$$R_a = 2.66 + 0.156N - 0.053F - 0.106T + 0.106N^2 - 0.046F^2 + 0.021T^2 + 0.155NF + 0.023NT - 0.075FT \quad \ldots (5.3)$$

The regression model has been inspected using the analysis of variance (ANOVA) and F-ratio test and these results are presented in Tables 5.3 and 5.4 respectively. From Table 5.3 it might be seen that R^2 value for response is 92.97% and R-Square (adjusted) value is 80.30%, which recommends that the regression model provides an extremely decent connection between the independent variables and the response output (Ra). In Table 5.4 the calculated

values of F-ratio for lack of fit are contrasted with the standard values of F-ratio corresponding to the degrees of freedom.

Impacts of sintering temperature (while formation of the P/M product) and pulse-on time & pulse-off time while machining at Wire-cut EDM on the surface roughness (R_a) is shown graphically in Figures 5.4, 5.6 and 5.8 as surface plots. Figure 5.4 demonstrates that surface roughness increases as pulse-on time increases and pulse-off time diminishes. In addition, for a fixed value of pulse-off time, surface roughness diminishes as sintering temperature increases and pulse-on time diminishes, as represented in Figure 5.6. Notwithstanding that, for a given value of pulse-on time; an expanding pulse-off time and expanding sintering temperature, diminishes the surface roughness, which is certain from Figure 5.8. Hence, the best surface finish was found to be related with greatest sintering temperature, greatest pulse-off time and least pulse-on time.

Physical interpretation: Pulse-on time is required for discharge energy and spark intensity. Pulse-off time is required for de-ionization of di-electric medium and re-establishment of insulation at the working gap. Other parameters such as – feed rate, peak current, peak voltage remains constant. At fixed and relatively low value of pulse-off time (9 μs), as pulse-on time increases, Ra-value also increases, as there is more metal removal. Also at lower value of constant pulse-on time (6 μs), as the pulse-off time increases, Ra-value increases. But, at higher value of pulse-on time (10 μs), keeping it constant, as pulse-off time increases Ra-value diminishes. Reason is – at high pulse-on time, though pulse-off time is increasing, the di-electric medium is not capable of accommodating the metal removal at that pulse-off time.

Table 5.3 Regression analysis for Surface Roughness

Term	Co-efficient	P-Value
Constant	2.66	0
N	0.156	0.004
F	-0.053	0.143
T	-0.106	0.017
N^2	0.106	0.062
F^2	-0.046	0.346
T^2	0.021	0.653
NF	-0.155	0.015
NT	0.023	0.621
FT	-0.075	0.139
	R-Sq = 92.97%	R-Sq(adj) = 80.30%

Table 5.4 Analysis of variance for Surface Roughness

Source	DOF	Sum of Squares	Adj. Mean Square	F-Value	P-Value
Regression	9	0.4821	0.0536	7.34	0.02
Linear	3	0.3077	0.1026	14.06	0.007
Square	3	0.0538	0.0179	2.46	0.178
Interaction	3	0.1206	0.0402	5.51	0.048
Residual Error	5	0.0365	0.0073		
Lack-of-fit	3	0.0231	0.0077	1.15	0.497
Pure Error	2	0.0134	0.0067		
Total	14	0.5185			

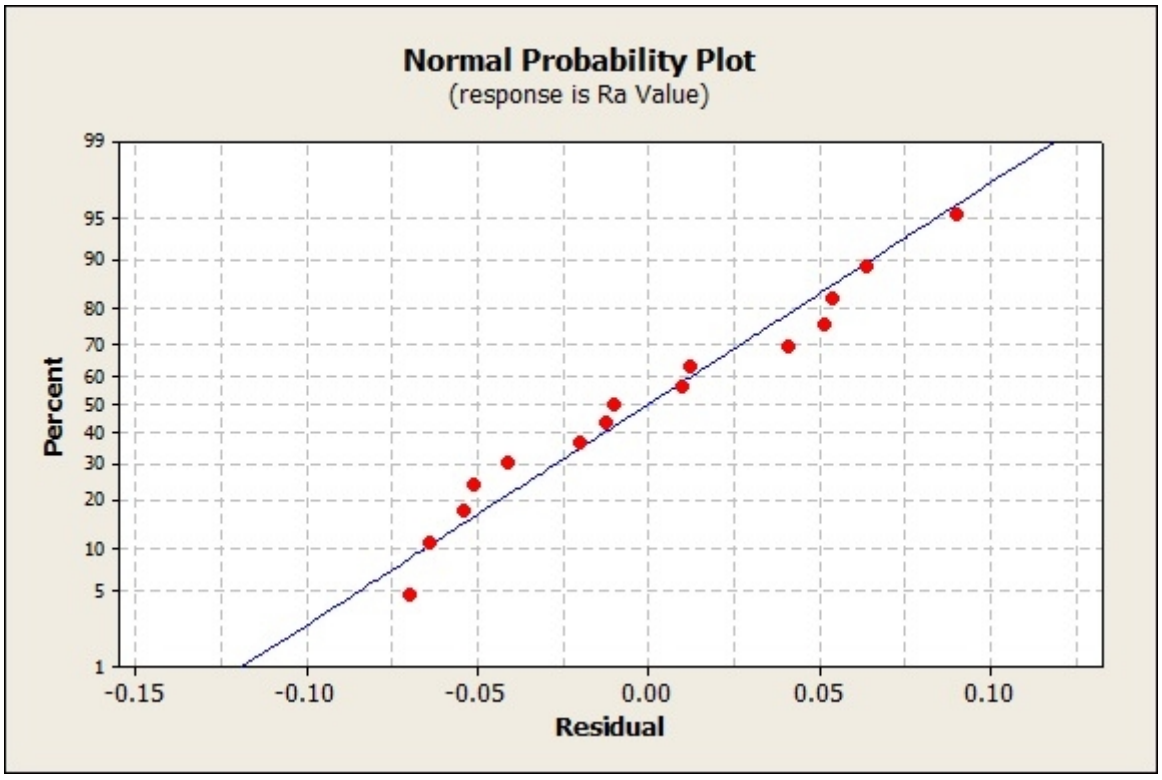

Figure 5.1 Normal probability plot of residuals for surface roughness

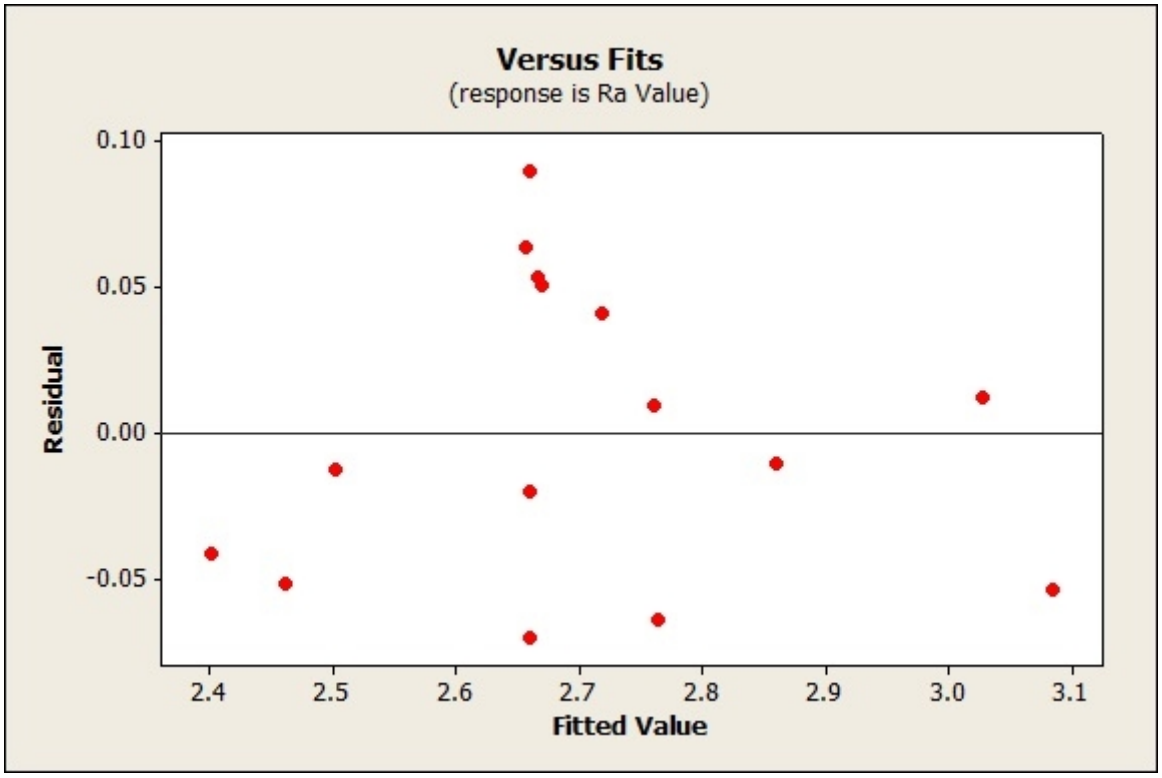

Figure 5.2 Plot of residuals versus the fitted value for surface roughness

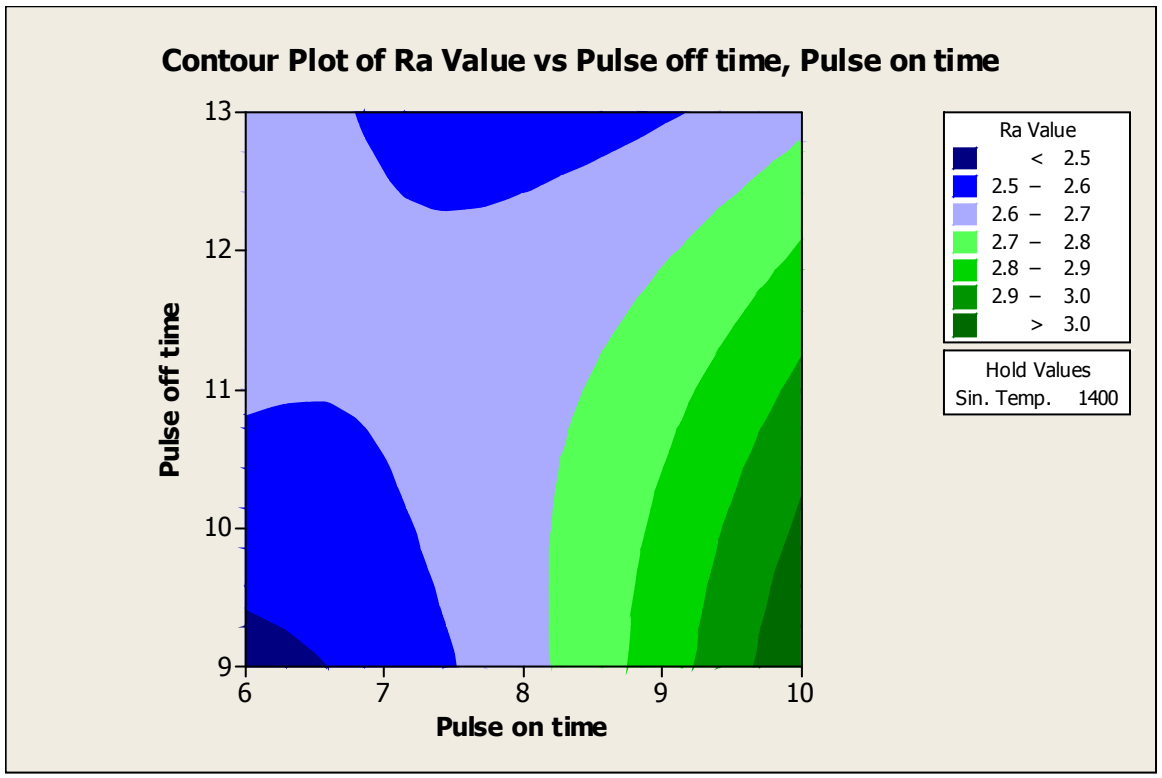

Figure 5.3 Surface roughness contour plot for pulse off time and pulse on time

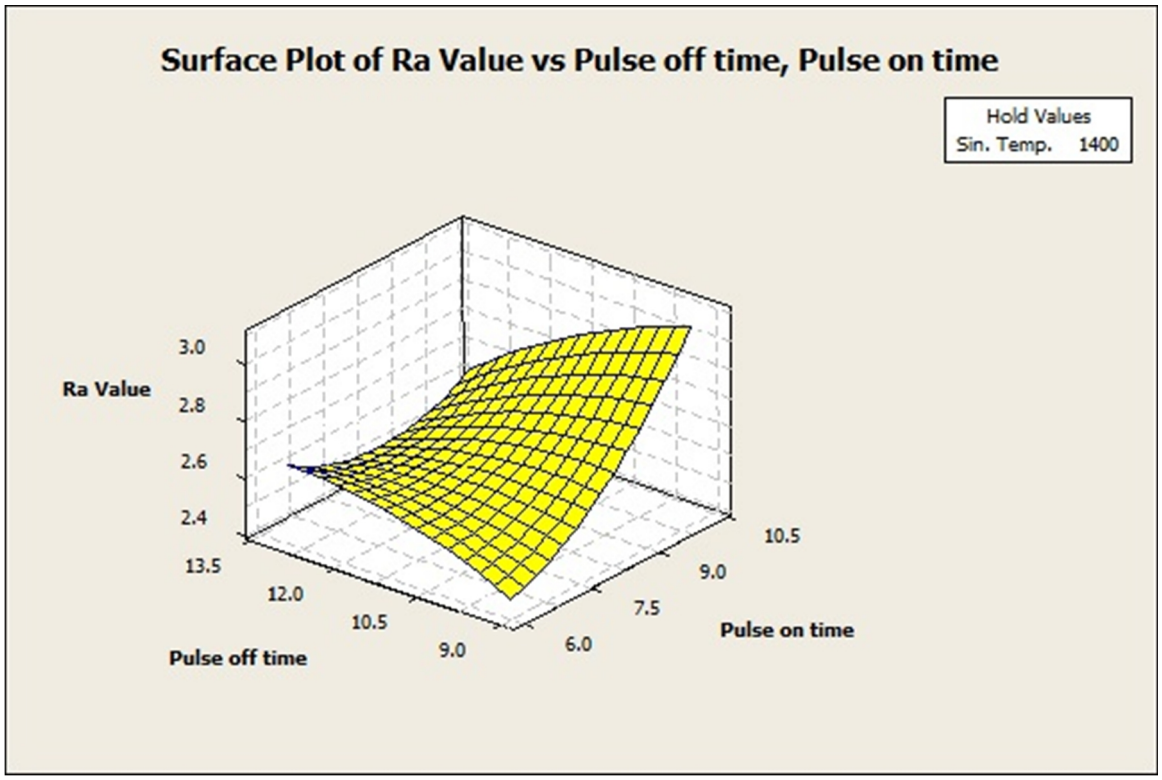

Figure 5.4 Surface roughness surface plot for pulse off time and pulse on time

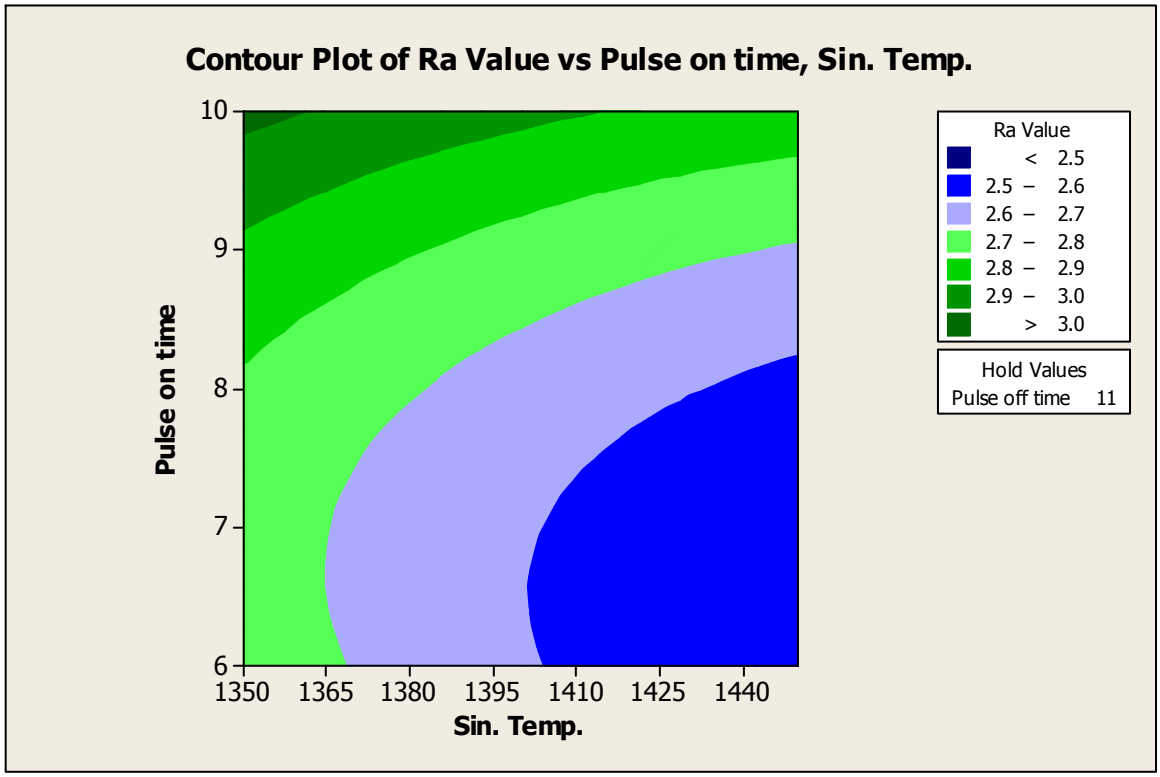

Figure 5.5 Surface roughness contour plot for sintering temperature and pulse on time

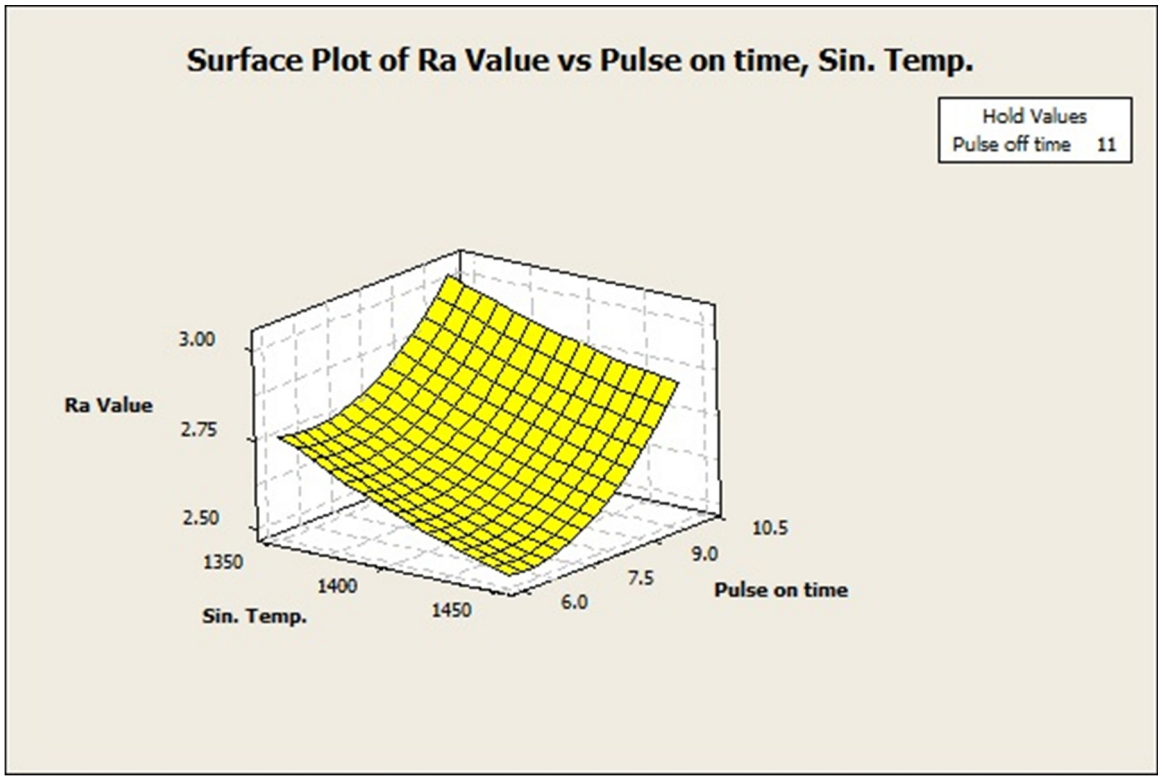

Figure 5.6 Surface roughness surface plot for sintering temperature and pulse on time

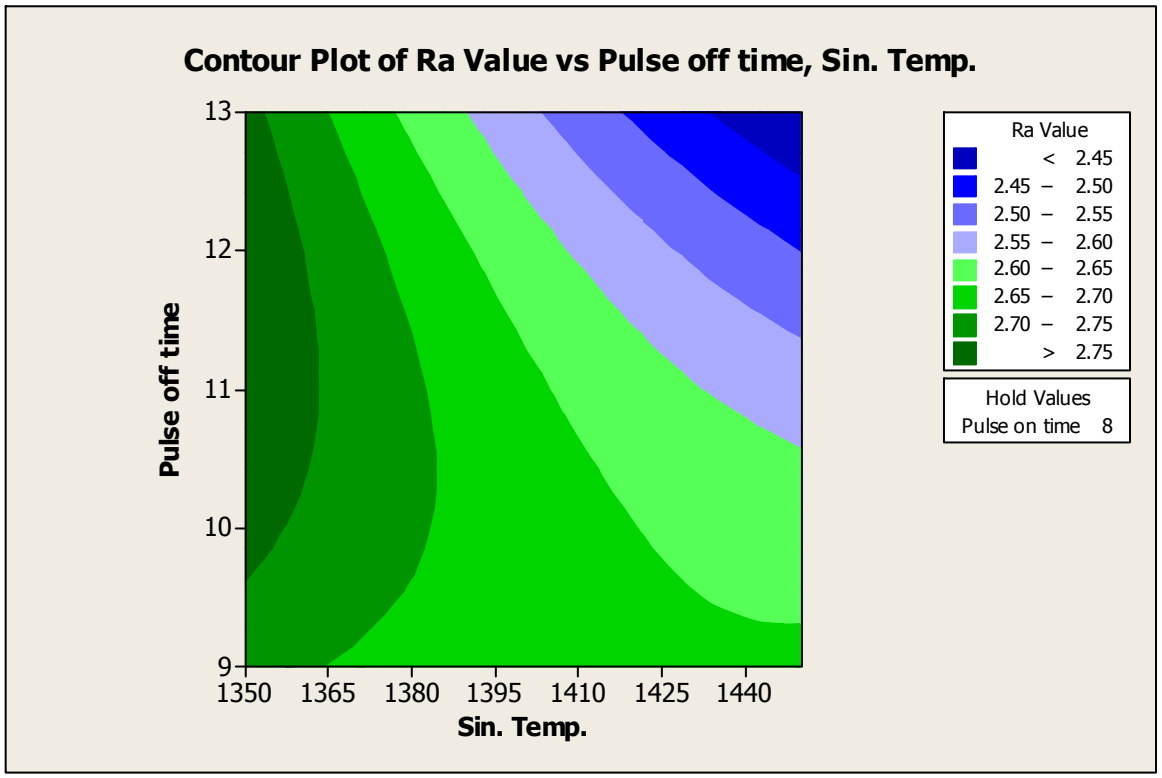

Figure 5.7 Surface roughness contour plot for pulse off time and sintering temperature

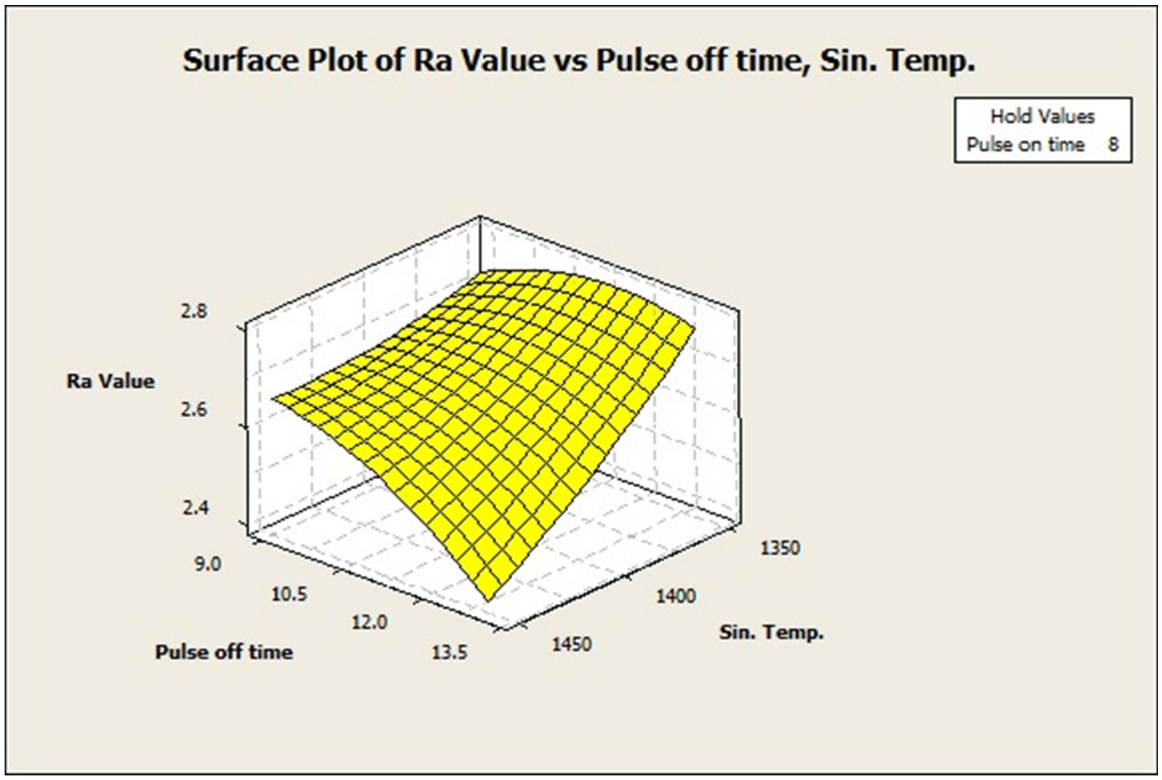

Figure 5.8 Surface roughness surface plot for pulse off time and sintering temperature

Table 5.5 Comparative study of predicted response versus actual response for Ra-value

Actual Factors				Actual Response	Predicted Response
Run Order	Pulse on time (N)	Pulse off time (F)	Sintering Temp. (T)	(R_a Value)	(R_a Value)
1	6	9	1400	2.41	2.5996
2	8	11	1400	2.64	2.7033
3	10	11	1450	2.85	2.7533
4	8	9	1450	2.72	2.6496
5	6	13	1400	2.72	2.4946
6	8	11	1400	2.75	2.7033
7	6	11	1350	2.77	2.6533
8	6	11	1450	2.49	2.4408
9	8	13	1450	2.36	2.5446
10	8	13	1350	2.7	2.7571
11	10	9	1400	3.03	2.9121
12	8	9	1350	2.76	2.8621
13	10	13	1400	2.72	2.8071
14	10	11	1350	3.04	2.9658
15	8	11	1400	2.59	2.7033

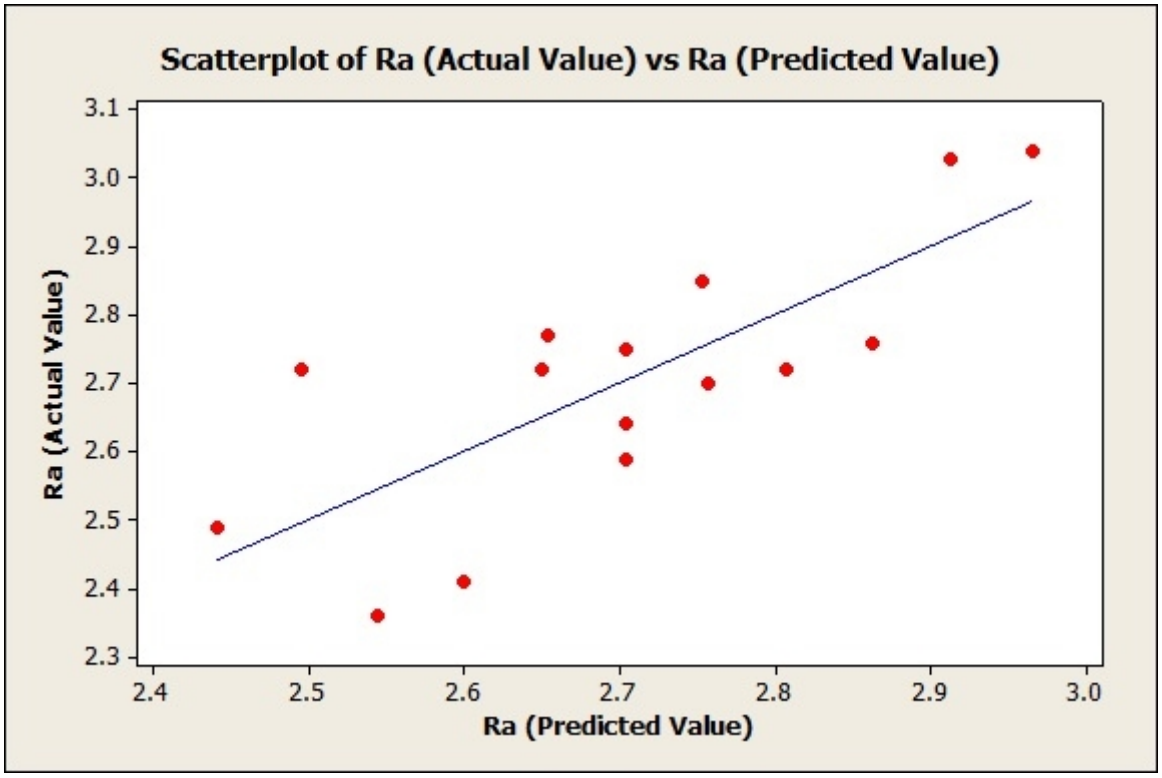

Figure 5.9 Scatter plot of actual response versus predicted response for surface roughness

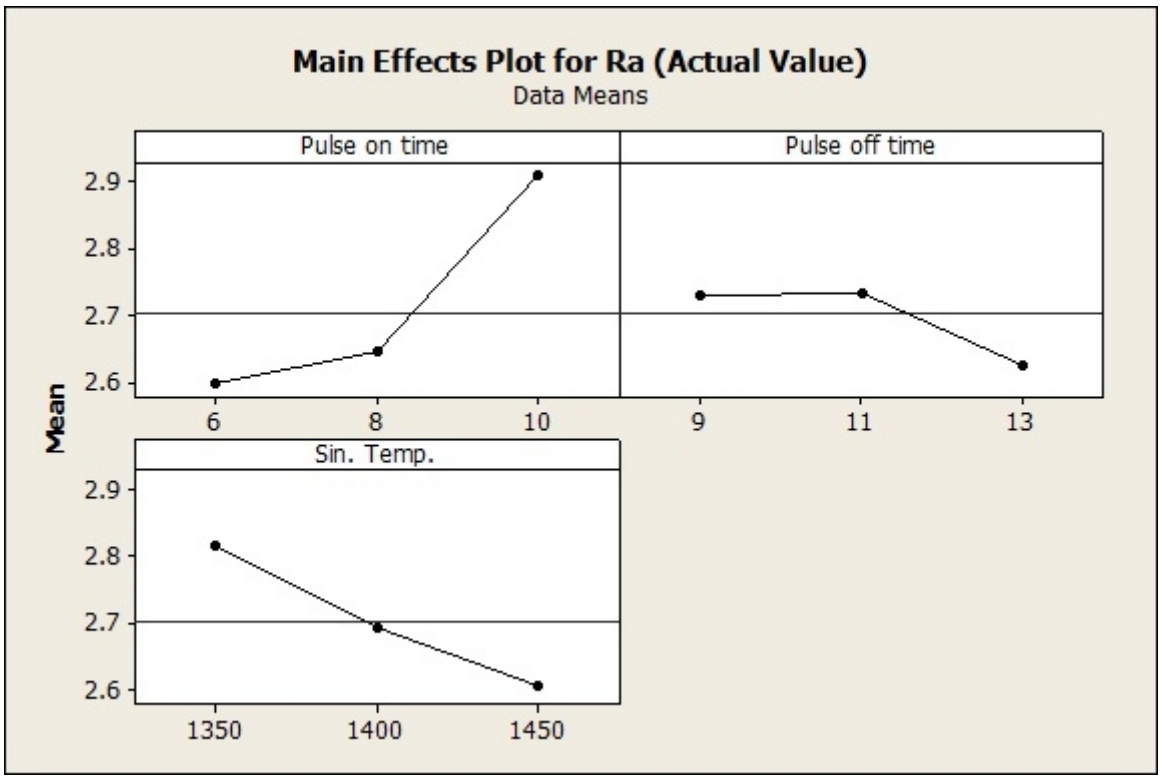

Figure 5.10 Main effects plot for roughness parameter (Ra-value)

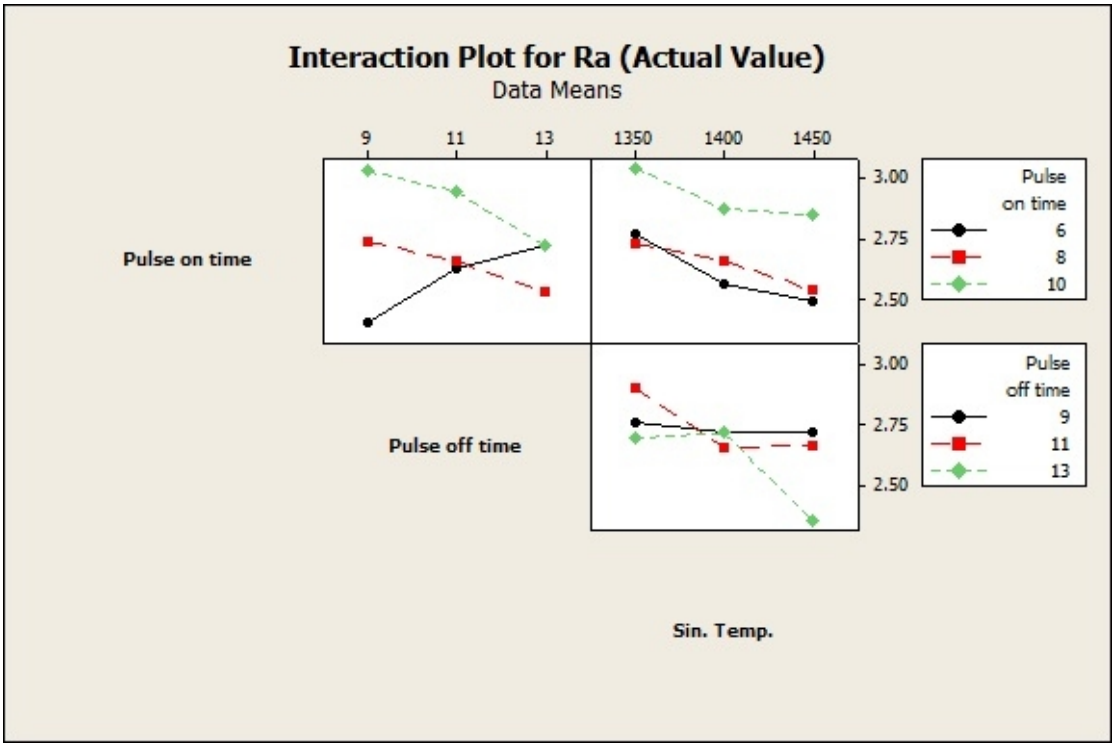

Figure 5.11 Interaction plot for roughness parameter (Ra-value)

5.4.2 Sensitivity analysis (R_a-value)

Sensitivity analysis is the most important step in optimization problem, since it gives information about the incremental or diminishing propensity of the reaction yield with respect to the process input parameters. Thus, sensitivity assumes a critical role in figuring out which process parameter ought to be altered for viable enhancement of the output yield. Numerically, sensitivity of a design output function with respect to the process factors is the partial derivative of that functional output with respect to its input variables.

$$\frac{\delta R_a}{\delta N} = 0.156 + 0.212N - 0.155F + 0.023T \qquad \ldots (5.4)$$

$$\frac{\delta R_a}{\delta F} = -0.053 - 0.092F - 0.155N - 0.075T \qquad \ldots (5.5)$$

$$\frac{\delta R_a}{\delta T} = -0.106 + 0.042T + 0.023N - 0.075F \qquad \ldots (5.6)$$

In this investigation, it is intended to envisage the tendency of surface roughness R_a value characteristics due to change in procedure parameters like: sintering temperature, pulse-on time and pulse-off time. In this situation, sensitivity equations from equation (5.3) have been derived for each process parameter. Thus the sensitivity equations (5.4) – (5.6) represent the sensitivity of R_a value for pulse-on time, pulse-off time and sintering temperature individually and are represented graphically in Figures 5.12, 5.13 and 5.14 separately. From

Figures 5.12, 5.13 and 5.14 it is apparent that, R_a-value is highly negatively sensitive to pulse-off time. For a little augmentation in pulse-off time, an immense decrement in R_a-value is watched. On the contrary, R_a-value is positively sensitive to pulse-on time and sintering temperature. In correlation between pulse-on time and sintering temperature, R_a-value is more sensitive to sintering temperature.

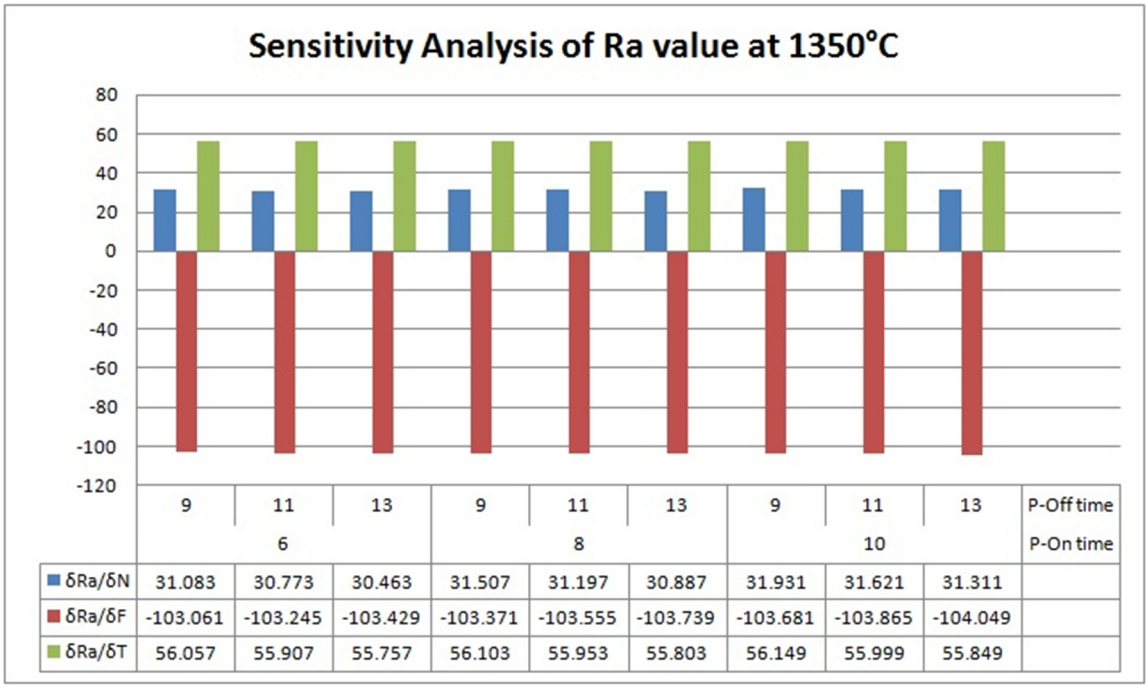

	9	11	13	9	11	13	9	11	13	P-Off time
		6			8			10		P-On time
δRa/δN	31.083	30.773	30.463	31.507	31.197	30.887	31.931	31.621	31.311	
δRa/δF	-103.061	-103.245	-103.429	-103.371	-103.555	-103.739	-103.681	-103.865	-104.049	
δRa/δT	56.057	55.907	55.757	56.103	55.953	55.803	56.149	55.999	55.849	

Figure 5.12 Sensitivity analysis for roughness parameter (Ra-value) at 1350°C

Sensitivity analysis is done to see the effects of independent variables on the output. Figure 5.12 to 5.14 shows the value of $\frac{\delta Ra}{\delta N}, \frac{\delta Ra}{\delta F}, \frac{\delta Ra}{\delta T}$ at different sintering temperatures (sintered at 1350°C, 1400 °C and 1450 °C respectively) at varying pulse-on time and pulse-off time.

It is found that, 'R_a' is positively sensitive to pulse-on time and sintering temperature and negatively sensitive to pulse-off time. Figure 5.12 to 5.14 shows that pulse-off time has more effect on Ra-value. From Figure 5.4, it is seen that at constant low value of pulse-on time Ra-value is increasing, whereas, at high value of pulse-on time R_a-value decreases. In between maximum and minimum value of pulse-off time, there is continuous change of R_a-behaviour with increasing pulse-off time. So it proves that, pulse-off time has got a remarkable effect on R_a-value. Physical reason for this behaviour may be explained in the manner – as pulse-on time increases the charge density also increases, which is capable of more metal removal of the sample. But at the same time effective removal of the material depends on preparation and deionization of dielectric medium and proper flushing out of debris from the gap between

wire and job, which is dictated by pulse-off time. So, at high value of pulse-on time, for more metal removal we need to provide sufficient pulse-off time for debris cleaning and deionization of dielectric medium which may not be sufficient in this case for high value of pulse-off time.

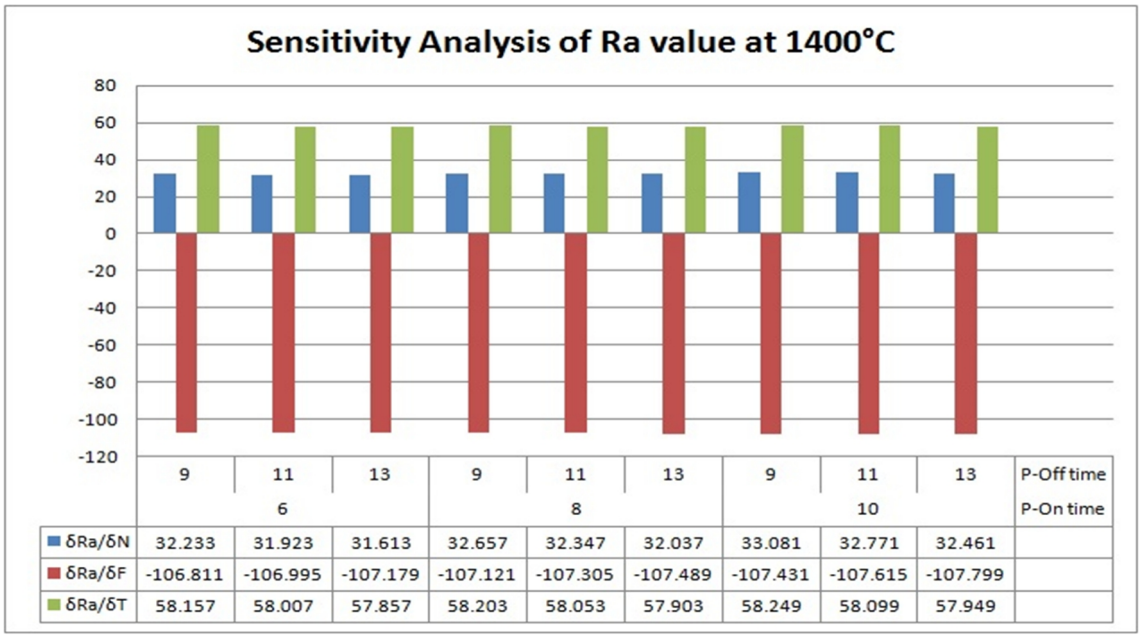

	9	11	13	9	11	13	9	11	13	P-Off time
		6			8			10		P-On time
δRa/δN	32.233	31.923	31.613	32.657	32.347	32.037	33.081	32.771	32.461	
δRa/δF	-106.811	-106.995	-107.179	-107.121	-107.305	-107.489	-107.431	-107.615	-107.799	
δRa/δT	58.157	58.007	57.857	58.203	58.053	57.903	58.249	58.099	57.949	

Figure 5.13 Sensitivity analysis for roughness parameter (Ra-value) at 1400°C

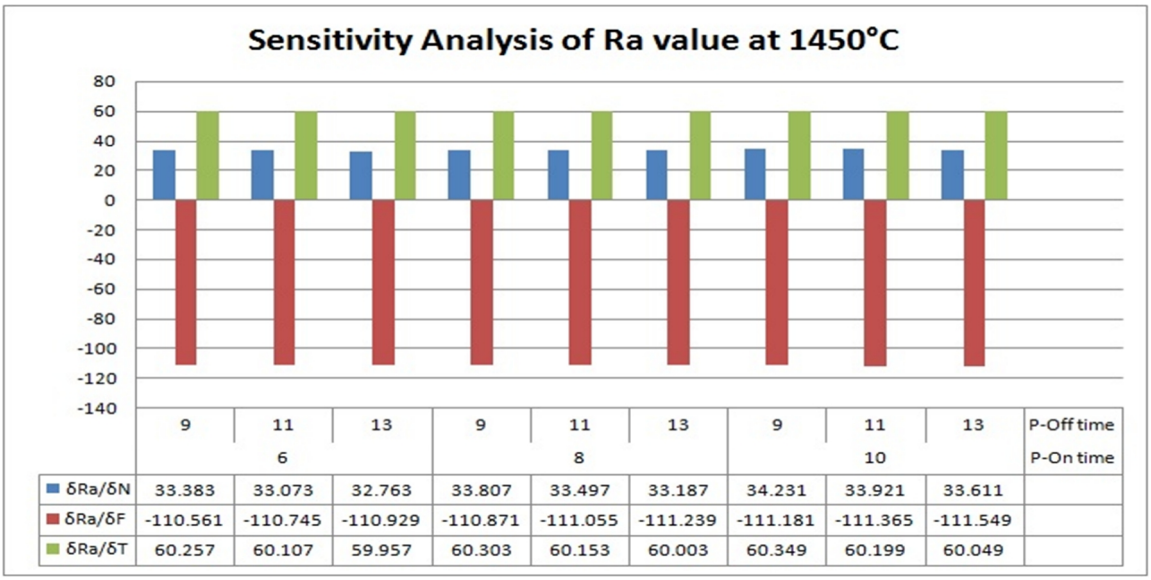

	9	11	13	9	11	13	9	11	13	P-Off time
		6			8			10		P-On time
δRa/δN	33.383	33.073	32.763	33.807	33.497	33.187	34.231	33.921	33.611	
δRa/δF	-110.561	-110.745	-110.929	-110.871	-111.055	-111.239	-111.181	-111.365	-111.549	
δRa/δT	60.257	60.107	59.957	60.303	60.153	60.003	60.349	60.199	60.049	

Figure 5.14 Sensitivity analysis for roughness parameter (Ra-value) at 1450°C

5.4.3 Metal Removal Rate (MRR)

Mathematical model developed for MRR and optimization of the process parameters. The numerical relationship co-relating the Metal Removal Rate (MRR) and the procedure

variables under consideration, namely sintering temperature (*T*), pulse-on time (*N*) and pulse-off time (*F*), is obtained as follows:

$$\begin{aligned} MRR = {} & 7.425 + 1.141N + 0.741F - 0.10T - 0.214N^2 + 0.317F^2 - 0.113T^2 \\ & + 0.304NF + 0.261NT - 0.38FT \end{aligned} \quad \ldots (5.7)$$

The regression model has been inspected utilizing the analysis of variance (ANOVA) and F-ratio test and these results are exhibited in Tables 5.6 and 5.7 individually. From Table 5.6 it might be seen that R^2 value for response is 93.18% and R-Square (adjusted) value is 80.91%, which reflects that the regression model provides a decent connection between the independent process variables and the response output (in this case MRR). In Table 5.7 the determined values of F-ratio for lack of fit are contrasted with the standard values of F-ratio corresponding to the degrees of freedom.

Impacts of sintering temperature (while formation of the P/M product) and pulse-on time & pulse-off time (while machining the samples at Wire-cut EDM) on the metal removal rate (MRR) is shown graphically in Figures 5.18, 5.20 and 5.22 as surface plots. Figure 5.18 demonstrates that metal removal rate (MRR) increments as pulse-on time and pulse-off time increments. For a fixed value of pulse-off time, as showed in Figure 5.20, metal removal rate (MRR) diminishes as pulse-on time diminishes & vice-versa and it remains more or less invariant with sintering temperature. From Figure 5.22, we can construe that, for a given value of pulse-on time, MRR increments with expanding pulse-off time, but it remains roughly unaltered with sintering temperature. Hence, the best metal removal rate (MRR) is observed to be connected with highest pulse-on time and pulse-off time.

Table 5.6 Regression Analysis for Metal Removal Rate

Term	Co-efficient	P-Value
Constant	7.425	0
N	1.141	0.001
F	0.741	0.008
T	-0.01	0.593
N^2	-0.214	0.443
F^2	0.317	0.273
T^2	-0.113	0.68
NF	0.304	0.274
NT	0.261	0.339
FT	-0.38	0.185
	R-Sq = 93.18%	R-Sq(adj) = 80.91%

Table 5.7 Analysis of Variance for Metal Removal Rate

Source	DOF	Sum of Squares	Adj. Mean Square	F-Value	P-Value
Regression	9	16.7344	1.8594	7.59	0.019
Linear	3	14.8798	4.9599	20.26	0.003
Square	3	0.6358	0.2119	0.87	0.517
Interaction	3	1.2189	0.4063	1.66	0.289
Residual Error	5	1.2241	0.2448		
Lack-of-fit	3	0.7354	0.2451	1.00	0.534
Pure Error	2	0.4887	0.2443		
Total	14	17.9586			

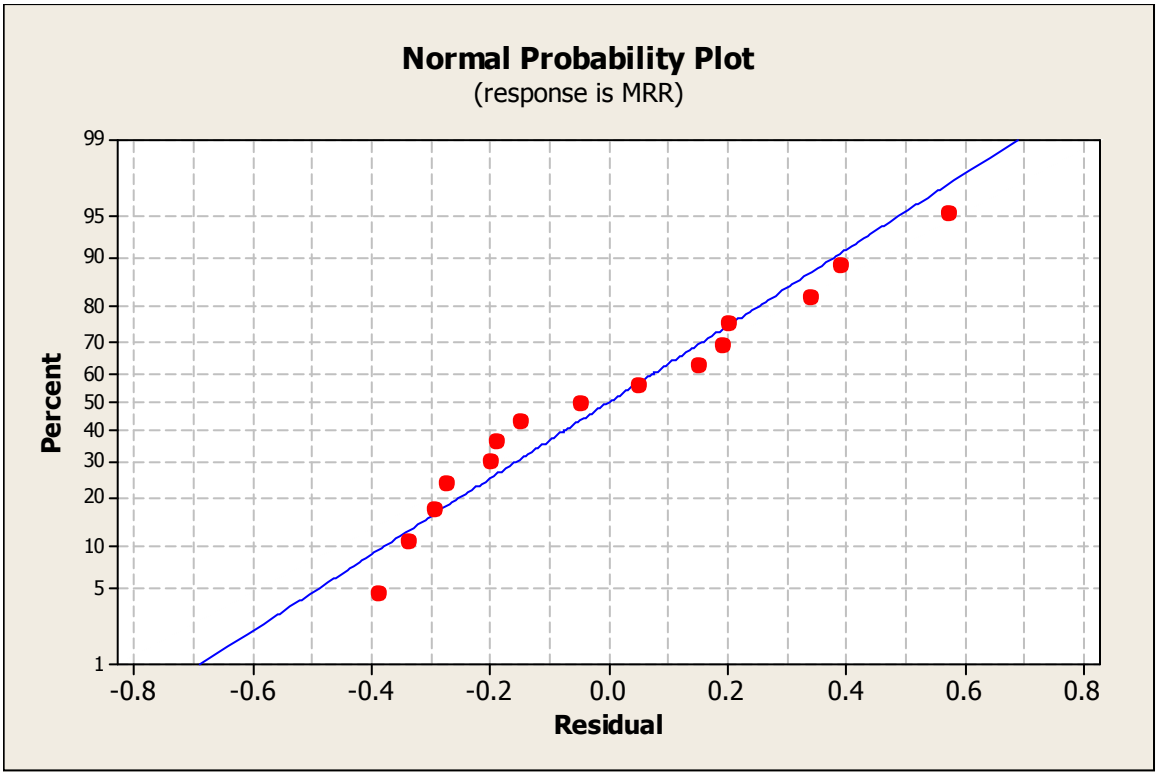

Figure 5.15 Normal probability plot of Residuals for MRR

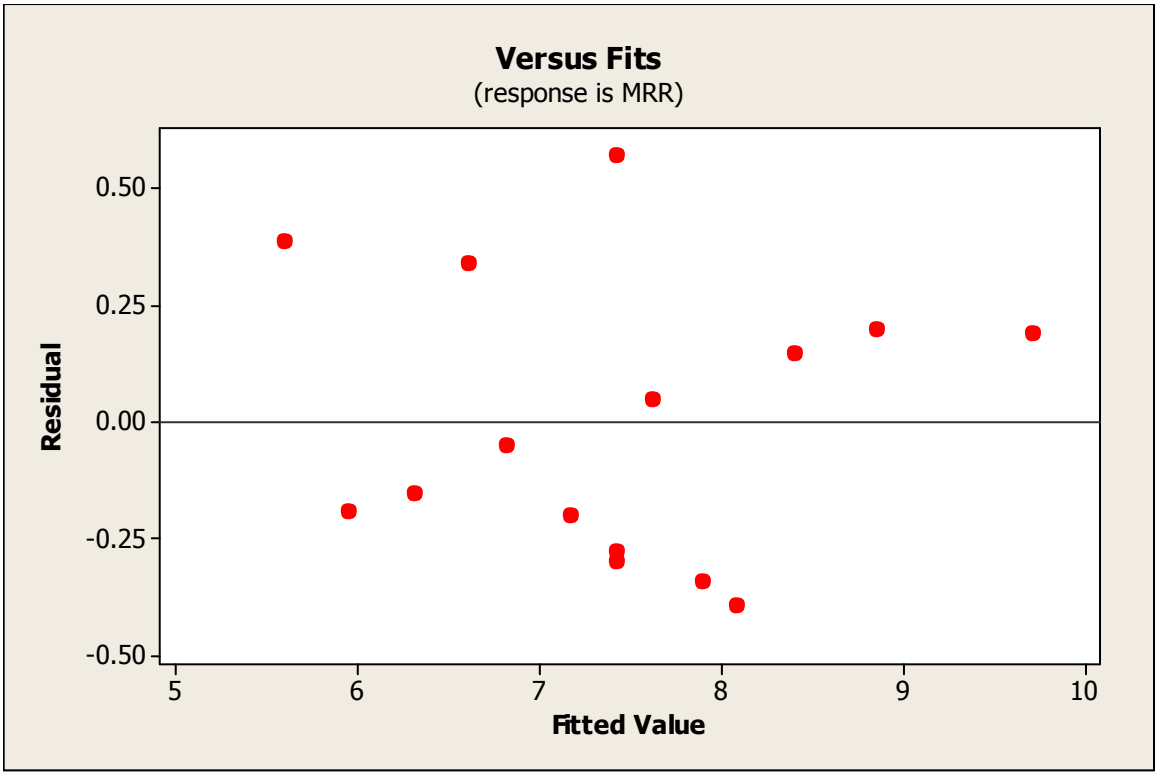

Figure 5.16 Plot of residuals versus the fitted value for MRR

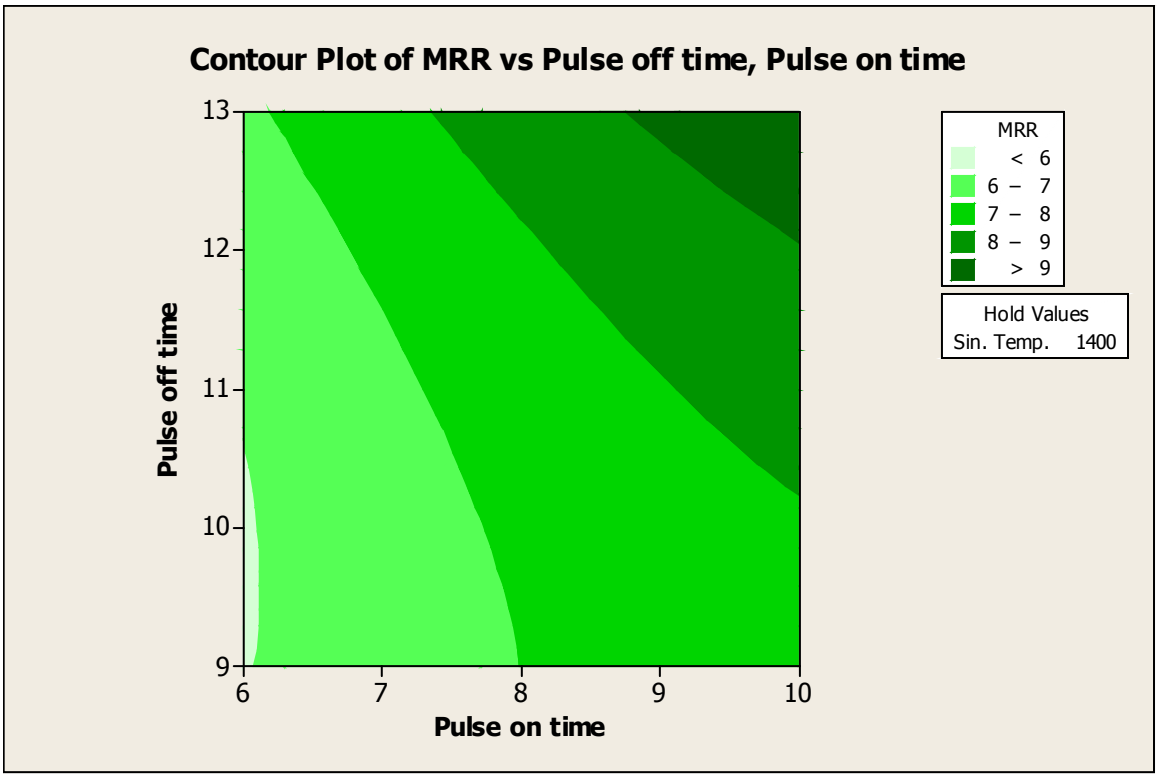

Figure 5.17 Contour plot for MRR with respect to pulse-off time and pulse-on time

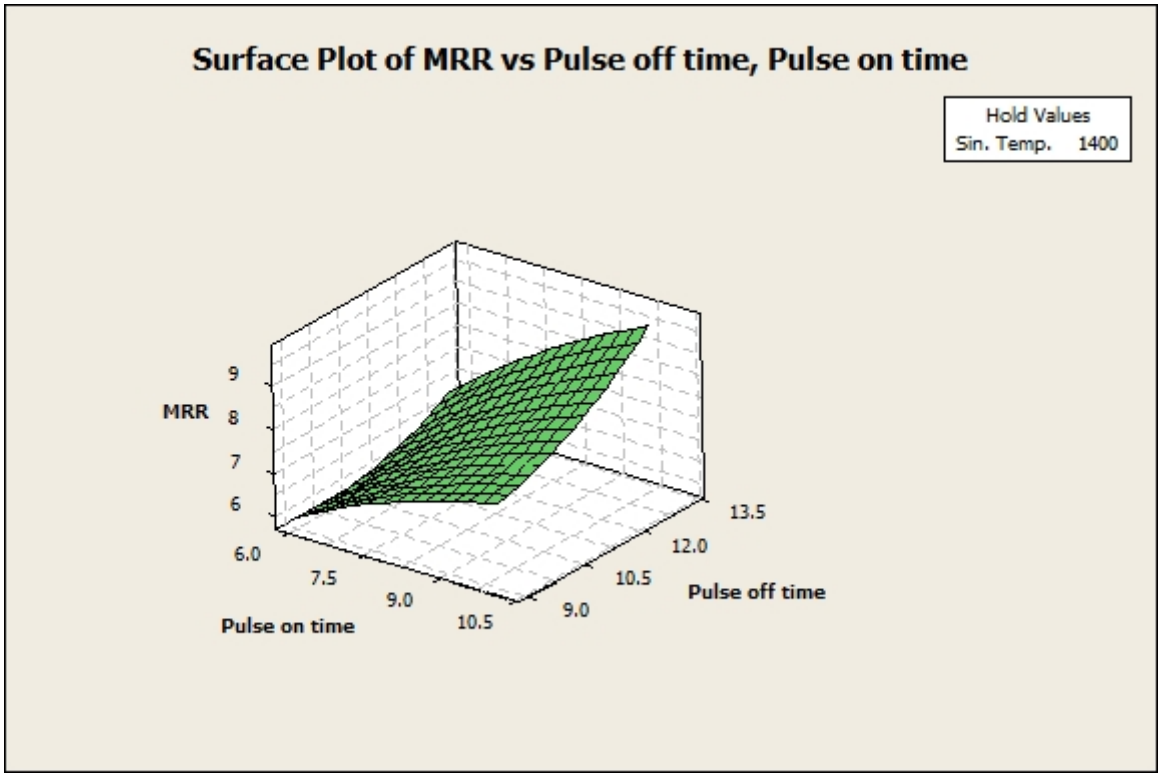

Figure 5.18 Surface plot for MRR with respect to pulse-off time and pulse-on time

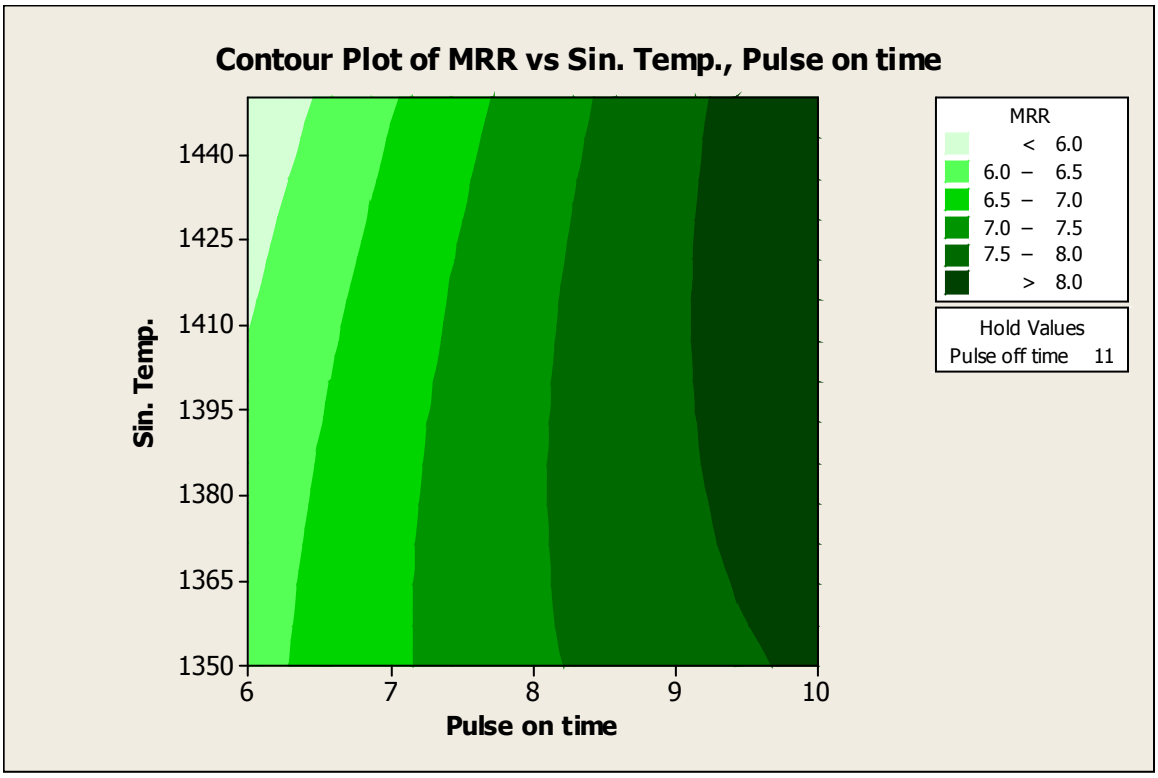

Figure 5.19 Contour plot for MRR with respect to sintering temperature and pulse-on time

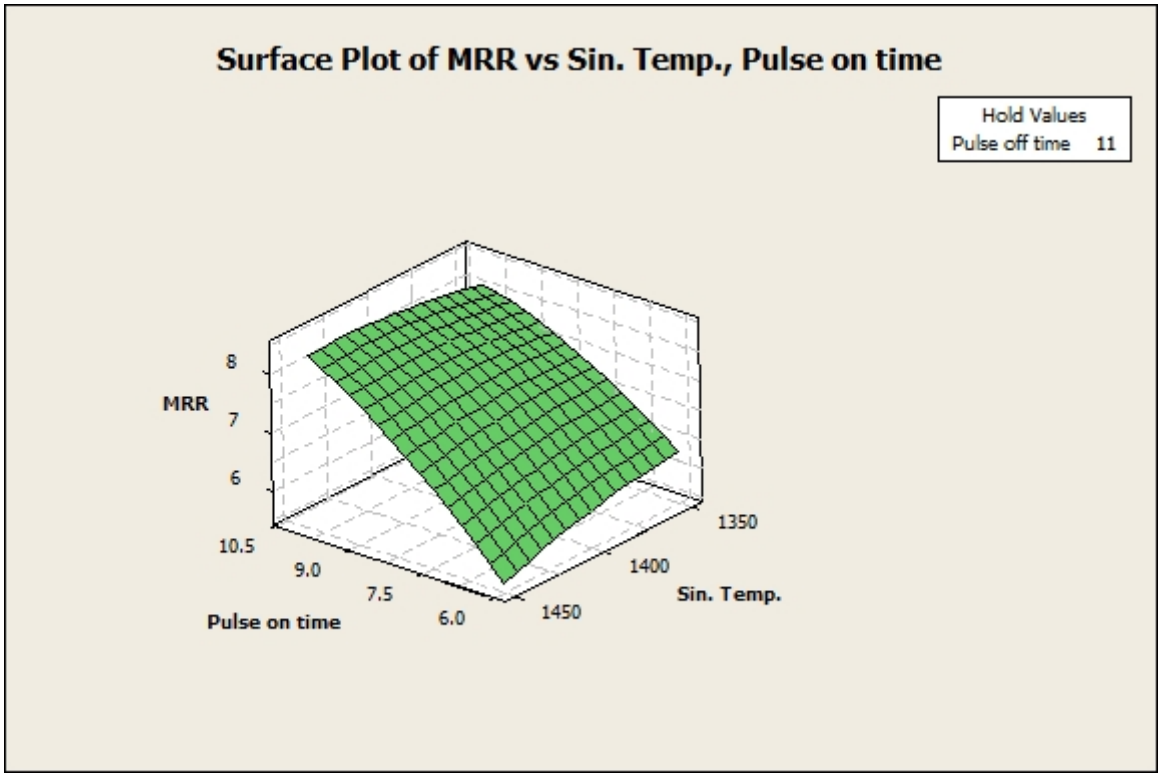

Figure 5.20 Surface plot for MRR with respect to sintering temperature and pulse-on time

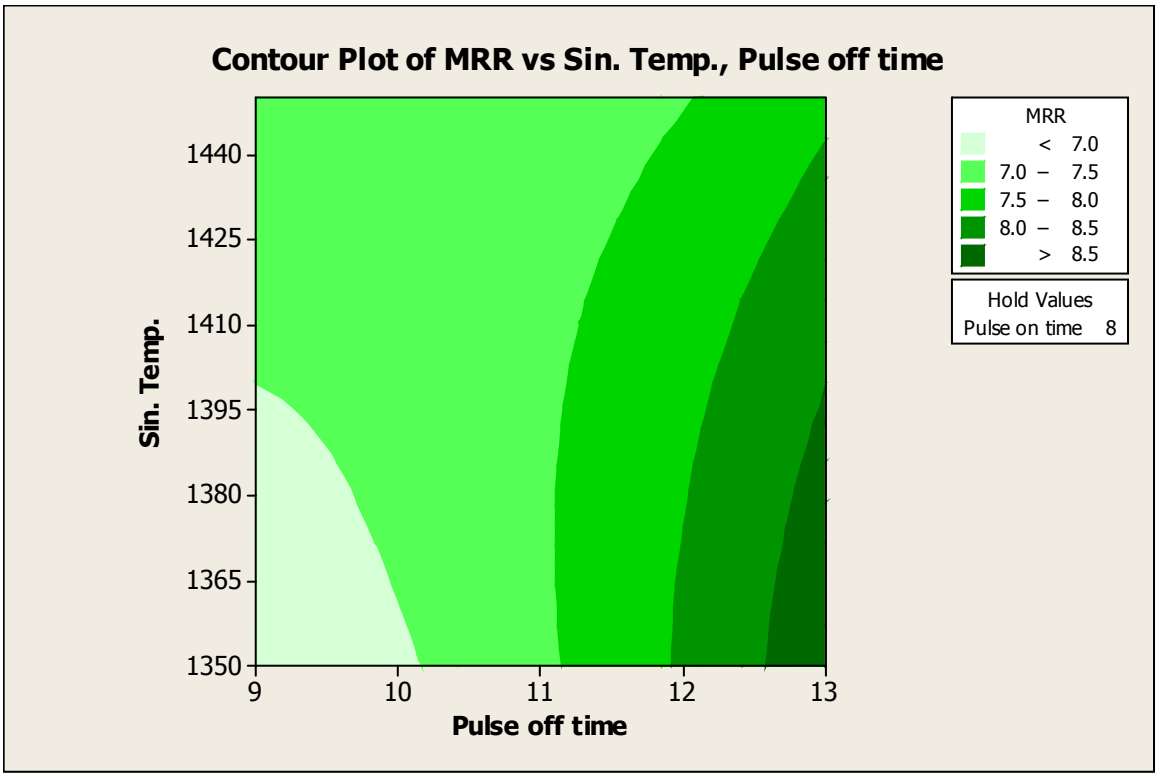

Figure 5.21 Contour plot for MRR with respect to sintering temperature and pulse-off time

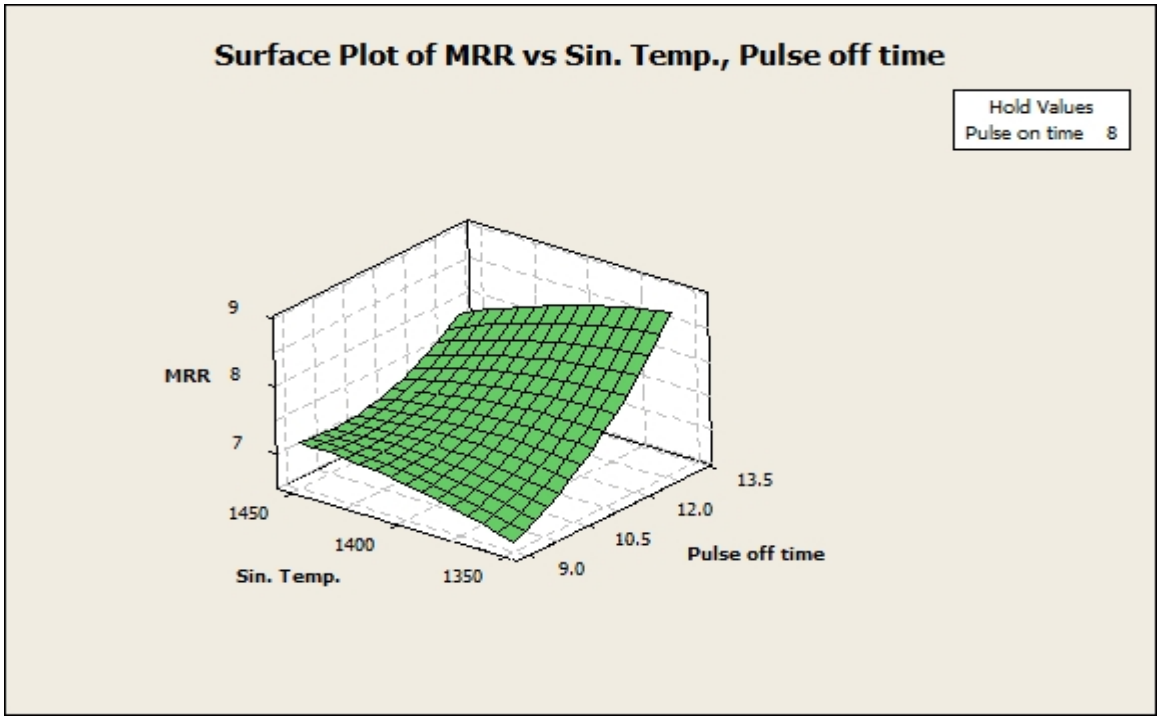

Figure 5.22 Surface plot for MRR with respect to sintering temperature and pulse-off time

Table 5.8 Box-Behnken Design lay-out and experimental results versus predicted results of Metal Removal Rate

	Coded Factors			Actual Factors			Actual Response	Predicted Response
Run Order	*N*	*F*	*T*	Pulse-on time (*N*)	Pulse-off time (*F*)	Sintering Temp. (*T*)	MRR (Actual) (mm^3/s)	MRR (Predicted) (mm^3/s)
1	-1	-1	0	6	9	1400	5.76	5.538
2	0	0	0	8	11	1400	7.996	7.42
3	1	0	1	10	11	1450	8.55	8.461
4	0	-1	1	8	9	1450	6.969	6.579
5	-1	1	0	6	13	1400	6.774	7.02
6	0	0	0	8	11	1400	7.15	7.42
7	-1	0	-1	6	11	1350	6.169	6.379
8	-1	0	1	6	11	1450	5.986	6.179

9	0	1	1	8	13	1450	7.551	8.061
10	0	1	-1	8	13	1350	9.049	8.26
11	1	-1	0	10	9	1400	7.674	7.82
12	0	-1	-1	8	9	1350	6.948	6.779
13	1	1	0	10	13	1400	9.903	9.301
14	1	0	-1	10	11	1350	7.688	8.66
15	0	0	0	8	11	1400	7.13	7.42

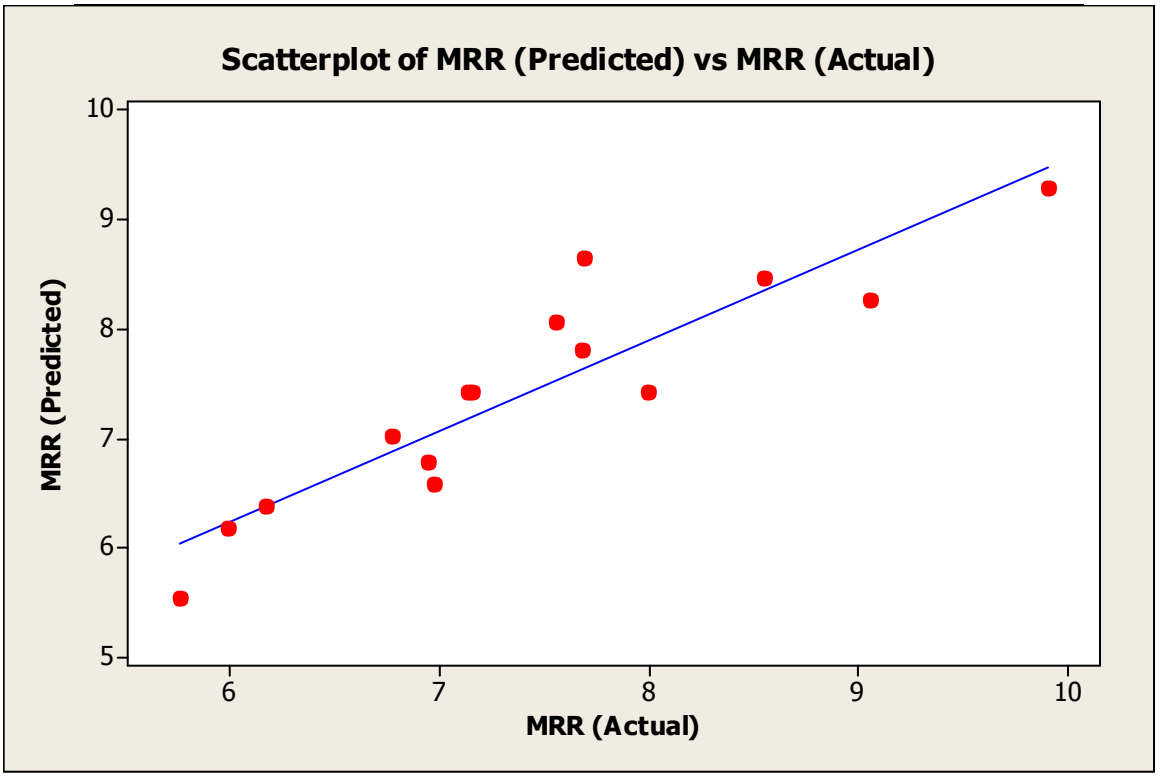

Figure 5.23 Scatter plot of actual response versus predicted response for MRR

The physical interpretation of the variation of MRR with respect to pulse-on time, pulse-off time and sinter temperature can be explained like this - as pulse-on time increases, MRR increases. This is because, higher the pulse-on time greater will be the dispersive energy and spark intensity leading to more amount of metal removal. The pulse-off time is the time required for re-establishment of insulation in the spark gap and deionization of the dielectric at the end of each discharging duration. At short pulse-off time MRR is less because, with short pulse-off time the probability of arcing is very high and the dielectric within the spark gap cannot be flushed away properly, so debris accumulate leading to less metal removal rate. On the contrary, sintering temperature does not have a significant effect on MRR.

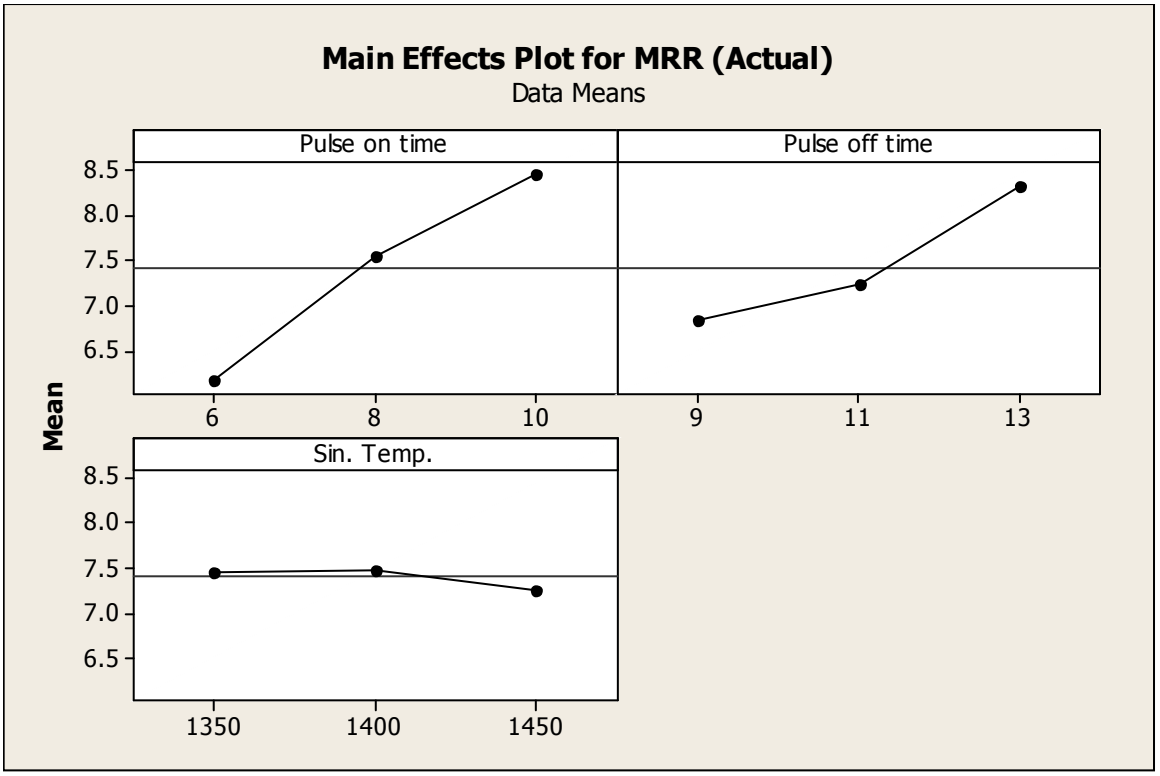

Figure 5.24 Main effects plot for Metal removal rate

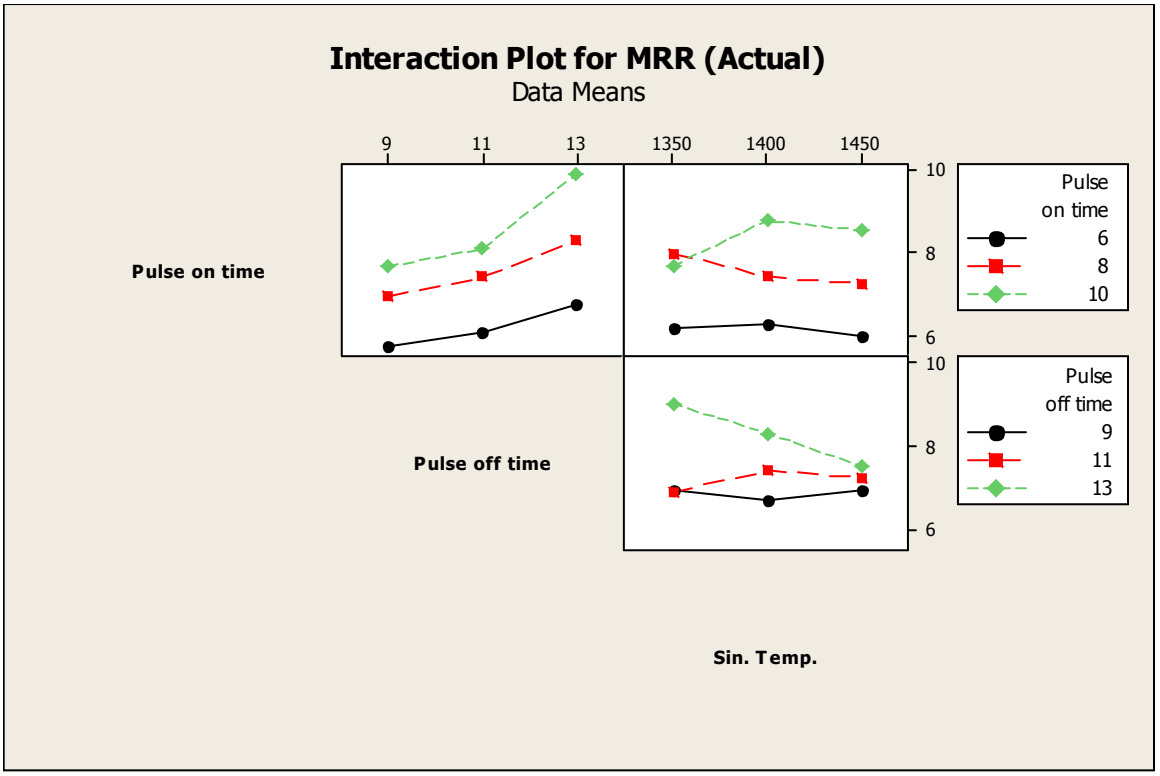

Figure 5.25 Interaction plot for metal removal rate

5.4.4 Sensitivity analysis (MRR)

In this study, it is aimed to predict the tendency of MRR characteristics due to change in process parameters like: sintering temperature, pulse-on time and pulse-off time. In this context, sensitivity equations from Equation (5.7) have been derived for each process parameter. Thus, the sensitivity Equations (5.8), (5.9) & (5.10) represent the sensitivity of MRR for pulse-on time, pulse-off time and sintering temperature respectively and are represented graphically in Figures 5.26, 5.27 and 5.28.

$$\frac{\delta MRR}{\delta N} = 1.141 - 0.428N + 0.304F + 0.261T \qquad \ldots (5.8)$$

$$\frac{\delta MRR}{\delta F} = 0.741 + 0.634F + 0.304N - 0.38T \qquad \ldots (5.9)$$

$$\frac{\delta MRR}{\delta T} = -0.10 - 0.226T + 0.261N - 0.38F \qquad \ldots (5.10)$$

From figures 5.26, 5.27 and 5.28, it is found that MRR is negatively sensitive to pulse-on time, i.e., for a small increment in pulse-on time, a slight decrement in MRR occurred. On the contrary, MRR is positively sensitive to pulse-off time, because, as pulse-off time increases, MRR decreases. In case of sintering temperature, MRR decreases, as sintering temperature increases. So, MRR is negatively sensitive to sintering temperature.

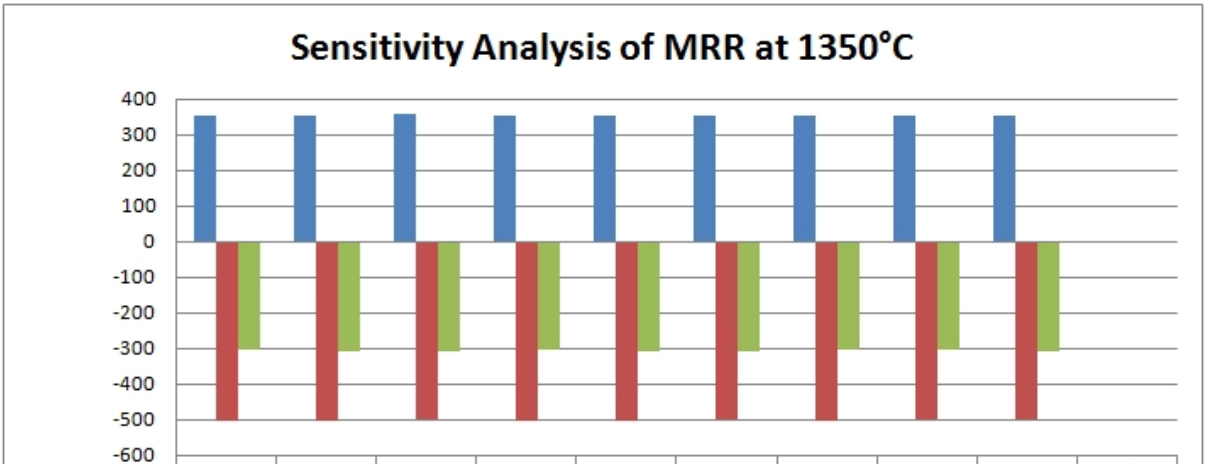

	9	11	13	9	11	13	9	11	13	P-Off time
	6			8			10			P-On time
δ(MRR)/δN	353.659	354.267	354.875	352.803	353.411	354.019	351.947	352.555	353.163	
δ(MRR)/δF	-504.729	-503.461	-502.193	-504.121	-502.853	-501.585	-503.513	-502.245	-500.977	
δ(MRR)/δT	-307.054	-307.814	-308.574	-306.532	-307.292	-308.052	-306.01	-306.77	-307.53	

Figure 5.26 Sensitivity analysis for metal removal rate at 1350°C

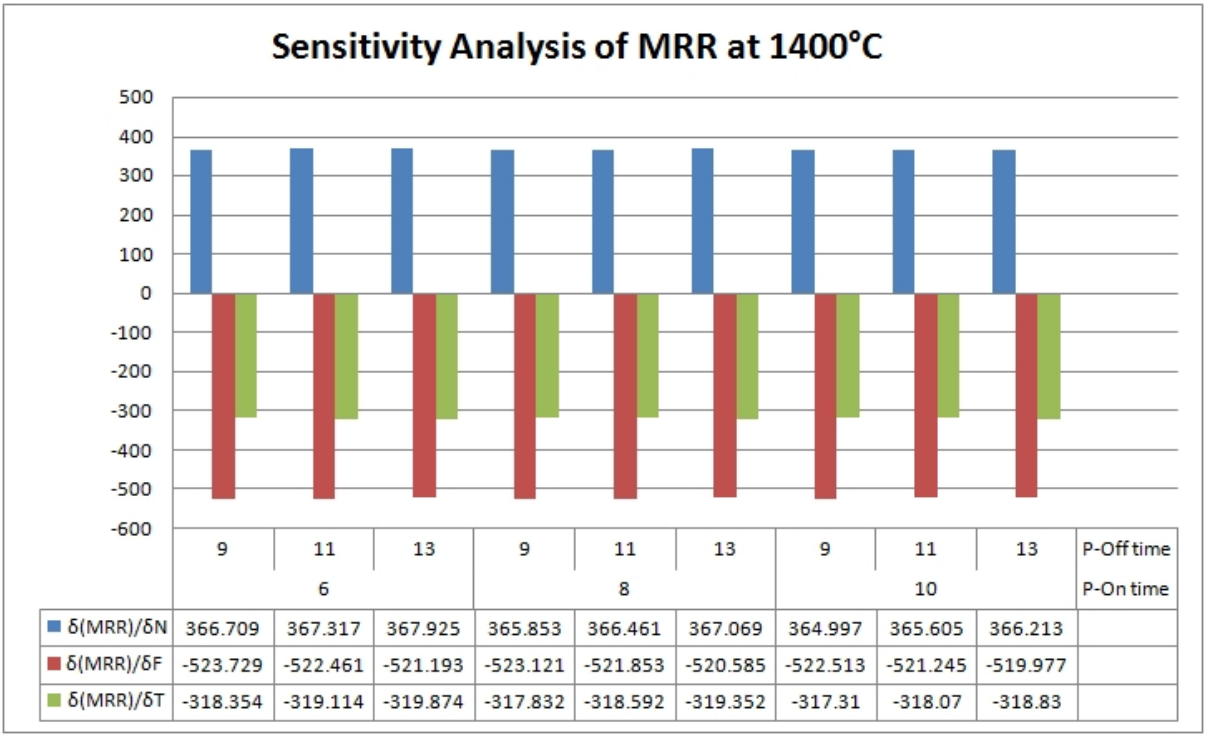

	9	11	13	9	11	13	9	11	13	P-Off time
	6			8			10			P-On time
δ(MRR)/δN	366.709	367.317	367.925	365.853	366.461	367.069	364.997	365.605	366.213	
δ(MRR)/δF	-523.729	-522.461	-521.193	-523.121	-521.853	-520.585	-522.513	-521.245	-519.977	
δ(MRR)/δT	-318.354	-319.114	-319.874	-317.832	-318.592	-319.352	-317.31	-318.07	-318.83	

Figure 5.27 Sensitivity analysis for metal removal rate at 1400°C

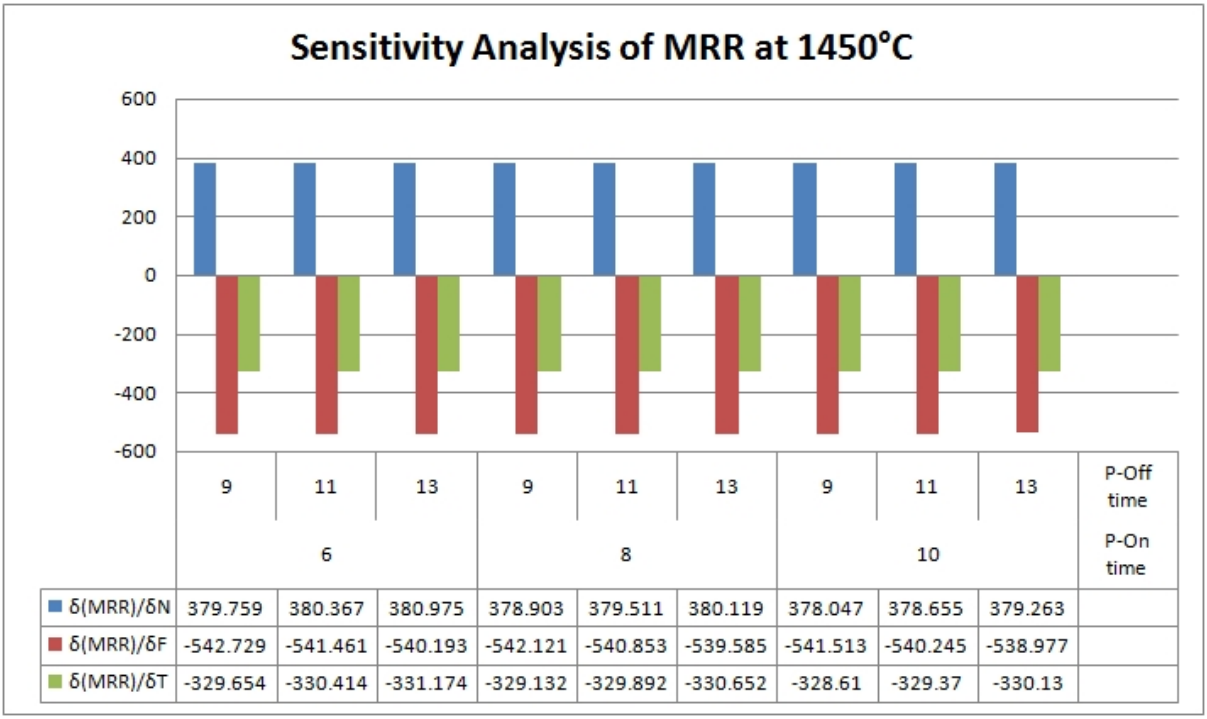

	9	11	13	9	11	13	9	11	13	P-Off time
	6			8			10			P-On time
δ(MRR)/δN	379.759	380.367	380.975	378.903	379.511	380.119	378.047	378.655	379.263	
δ(MRR)/δF	-542.729	-541.461	-540.193	-542.121	-540.853	-539.585	-541.513	-540.245	-538.977	
δ(MRR)/δT	-329.654	-330.414	-331.174	-329.132	-329.892	-330.652	-328.61	-329.37	-330.13	

Figure 5.28 Sensitivity analysis for metal removal rate at 1450°C

5.4.5 Grey Relational Analysis

Grey relational analysis (GRA) is an efficient tool for multiple response investigation. It was first proposed by J. L. Deng and it proved to be a proficient tool for solving inter-relationship among numerous response outputs. GRA utilizes a particular idea of data. It characterizes circumstances with no data as black, and those with ideal data as white. Be that as it may, neither of these idealized circumstances happens in actuality. Circumstances between these two boundaries are portrayed as being grey, fuzzy or hazy. Subsequently, grey system means – a system in which a piece of the information is known and a piece of it being obscure or unknown. Since improbability always exists, one is always somewhere in the middle, somewhere between the boundaries or extremities, somewhere in the grey area. This incompleteness of information is the basic characteristic and it serves as the fundamental starting point of the investigation of grey system. With this definition, information quantity and quality a continuum is formed in GRA, from a total absence of information to full information – from black to grey to white.

In GRA, the initial step is to perform the grey relational generation in which the consequences of the trials are standardized in the scope of 0 and 1. At that point, the second step is to compute the grey relational co-efficients from the standardized information to decide the relationship between the desired and actual experimental data. The overall grey relational grade is then processed by averaging the grey relational co-efficients, corresponding to each performance characteristics. Final evaluation of the multiple performance characteristics is based on the calculated grey relational grades. As a result, optimization of the complicated multiple performance characteristics is converted into optimization of a single grey relational grade. The optimal level of the process parameters is the level with the highest grey relational grade. Furthermore, a statistical analysis of variance (ANOVA) is performed to find out that, which process parameters are measurably significant. With GRA and statistical ANOVA, optimal combination of the process parameters can be predicted. Finally, a confirmation experiment is completed to confirm the ideal procedure parameters, obtained from the analysis.

The initial step in solving the grey relational analysis is the grey relational generation. In this method, the normalized data for Surface Roughness parameter (R_a-value), is processed corresponding to lower-the-better criterion (LB), and can be expressed as:

$$x_i(k) = \frac{\max y_i(k) - y_i(k)}{\max y_i(k) - \min y_i(k)} \qquad \ldots (5.11)$$

Similarly, the normalized data for Metal removal rate (MRR) is processed using higher-the-better characteristics, which is as follows:

$$x_i(k) = \frac{y_i(k) - \min y_i(k)}{\max y_i(k) - \min y_i(k)} \qquad \ldots (5.12)$$

where x_i (k) is the normalized grey relational value for the 'k' th response, max y_i (k) is the largest value of y_i (k) for the 'k' th response, min y_i (k) is the smallest value of y_i (k) for the kth response, y_i (k) is the experimental value for the 'k' th response and i = 1–15, which is experiment number, k = 1–3 depends on the number of factors.

The second step is to calculate the Grey Relational Coefficient (GRC) of the responses from the normalized values which represent the relationship between the desired and actual experimental data according to the following equation:

$$\xi_i(k) = \frac{\Delta_{min} + \zeta \Delta_{max}}{\Delta_{oi}(k) + \zeta \Delta_{max}} \qquad \ldots (5.13)$$

where, ξ_i (k) is the grey relational co-efficient, Δ_{min} and Δ_{max} is the minimum and maximum values of absolute differences (Δ_{oi}(k)) of all comparing sequences, Δ_{oi} = || X_o (k) – X_i (k) || is the difference of the absolute value between X_o (k) and X_i (k), X_o (k) is the reference sequence and 'ζ' is the distinguishing coefficient $0 \leq \zeta \leq 1$. The distinguishing coefficient 'ζ' depends on equal weightage of response outputs, in this case, Ra-value and metal removal rate. So 'ζ' is considered 0.5, to provide moderate distinguishing effects and good stability of the outcomes.

After calculating grey relational coefficients, the grey relational grade γ_i can be calculated by using the following equation. It is calculated by averaging the grey relational coefficient corresponding to each performance characteristics.

$$\gamma_i = \frac{1}{n} \sum_{k=1}^{n} \xi_i(k) \qquad \ldots (5.14)$$

where, n is the number of responses. The final grey relational grade gives the overall evaluation of multiple performances. As per the analysis, the optimal level of process parameter is the level with the highest grey relational grade. Since, design of experiments is orthogonal; the highest grey relational grade obtained from the analysis is independent.

Table 5.9 Experimental results of Ra-value and MRR along with normalised and grey relational co-efficient

Exp Run	Pulse-on time (N)	Pulse-off time (F)	Sintering Temp. (T)	Ra-Value	MRR	Normalized Ra-Value	Normalized MRR	Grey Co-efficient (Ra-Value)	Grey Co-efficient (MRR)
1	6	9	1400	2.41	5.76	0.9265	0	0.8718	0.3333
2	8	11	1400	2.64	7.996	0.5882	0.5397	0.5484	0.5207
3	10	11	1450	2.85	8.55	0.2794	0.6734	0.4096	0.6049
4	8	9	1450	2.72	6.969	0.4706	0.2918	0.4857	0.4138
5	6	13	1400	2.72	6.774	0.4706	0.2448	0.4857	0.3983
6	8	11	1400	2.75	7.15	0.4265	0.3355	0.4658	0.4294
7	6	11	1350	2.77	6.169	0.3971	0.0987	0.4534	0.3568
8	6	11	1450	2.49	5.986	0.8081	0.0545	0.7234	0.3459
9	8	13	1450	2.36	7.551	1	0.4323	1	0.4683
10	8	13	1350	2.7	9.049	0.5	0.7939	0.5	0.7081
11	10	9	1400	3.03	7.674	0.0147	0.462	0.3366	0.4817
12	8	9	1350	2.76	6.948	0.4118	0.2867	0.4595	0.4121
13	10	13	1400	2.72	9.903	0.4706	1	0.4857	1
14	10	11	1350	3.04	7.688	0	0.4654	0.3333	0.4833
15	8	11	1400	2.59	7.13	0.6618	0.3307	0.5965	0.4276

Table 5.10 Grey Relational Grade and its orders

Exp Run	Grey Relational Grade	Orders
1	0.6026	4
2	0.5346	6
3	0.5073	8

4	0.4498	9
5	0.4420	11
6	0.4476	10
7	0.4051	15
8	0.5347	5
9	0.7342	2
10	0.6041	3
11	0.4092	13
12	0.4358	12
13	0.7429	1
14	0.4086	14
15	0.5121	7

The largest Grey Relational Grade is chosen as optimal procedure parameter setting for the experiment, which corresponds to Run No. 13. From the performed GRA Table, the process parameters' setting of Experiment No. 13 has the highest Grey Relational Grade. Based on the Grey Relational Grade values, the optimal parameter for maximum MRR and minimum Ra-value was obtained at 1400°C sintering temperature (level 2), 10µs pulse-on time (level 3) and 13µs pulse-off time (level 3) combination.

Table 5.11 Response table for grey relational grade

Average grey relational grade for each factor level							
Process Parameters	Unit	Symbol	Level 1	Level 2	Level 3	Max - Min	Rank
WEDM Pulse on time	µs	N	0.4961	0.5312*	0.5170	0.0351	3
WEDM Pulse off time	µs	F	0.4744	0.4786	0.6308*	0.1564	1
Sintering temperature	°C	T	0.4634	0.5273	0.5565*	0.0931	2

Mean value of Grey relational grade: 0.5195 * Indicates optimum process level

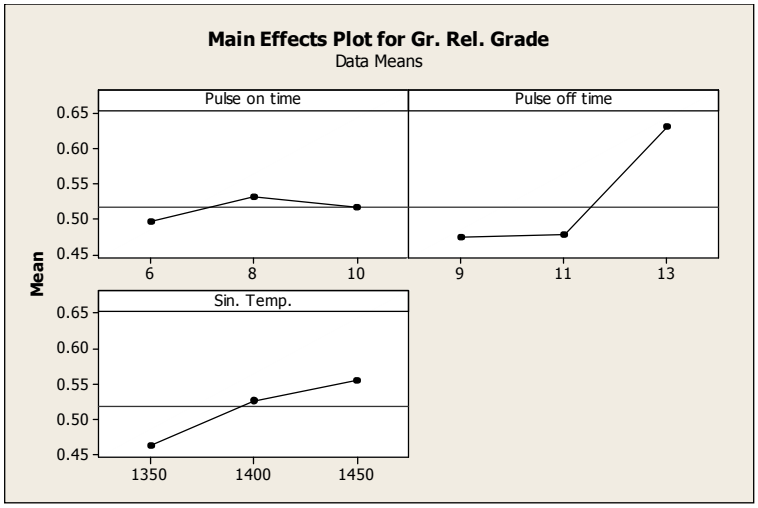

Figure 5.29 Main effects plot for grey relational grade

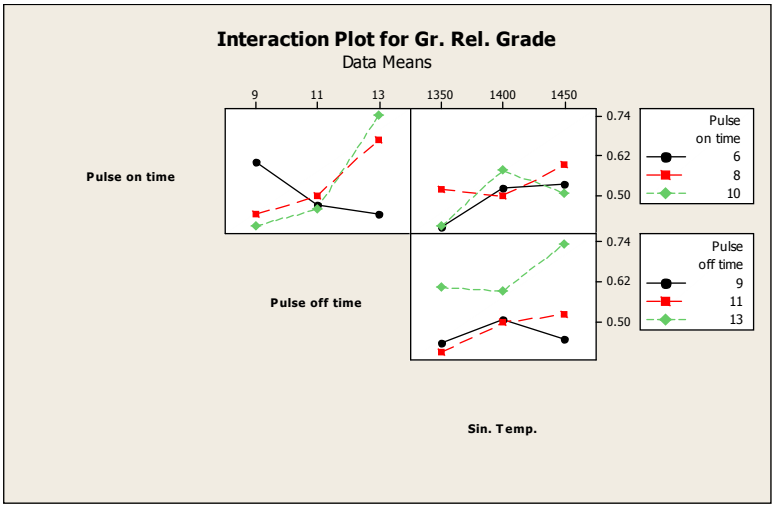

Figure 5.30 Interaction plot for grey relational grade

Table 5.12 ANOVA table for grey relational grade

Source	DOF	Sum of Squares	Adj. Mean Square	F-Value	P-Value
Regression	9	0.154394	0.017155	5.08	0.044
Linear	3	0.067162	0.022387	6.63	0.034
Square	3	0.02254	0.007513	2.22	0.203
Interaction	3	0.064692	0.021564	6.38	0.037
Residual Error	5	0.016895	0.003379		
Lack-of-fit	3	0.012816	0.004272	2.09	0.339
Pure Error	2	0.004078	0.002039		
Total	14	0.171289			

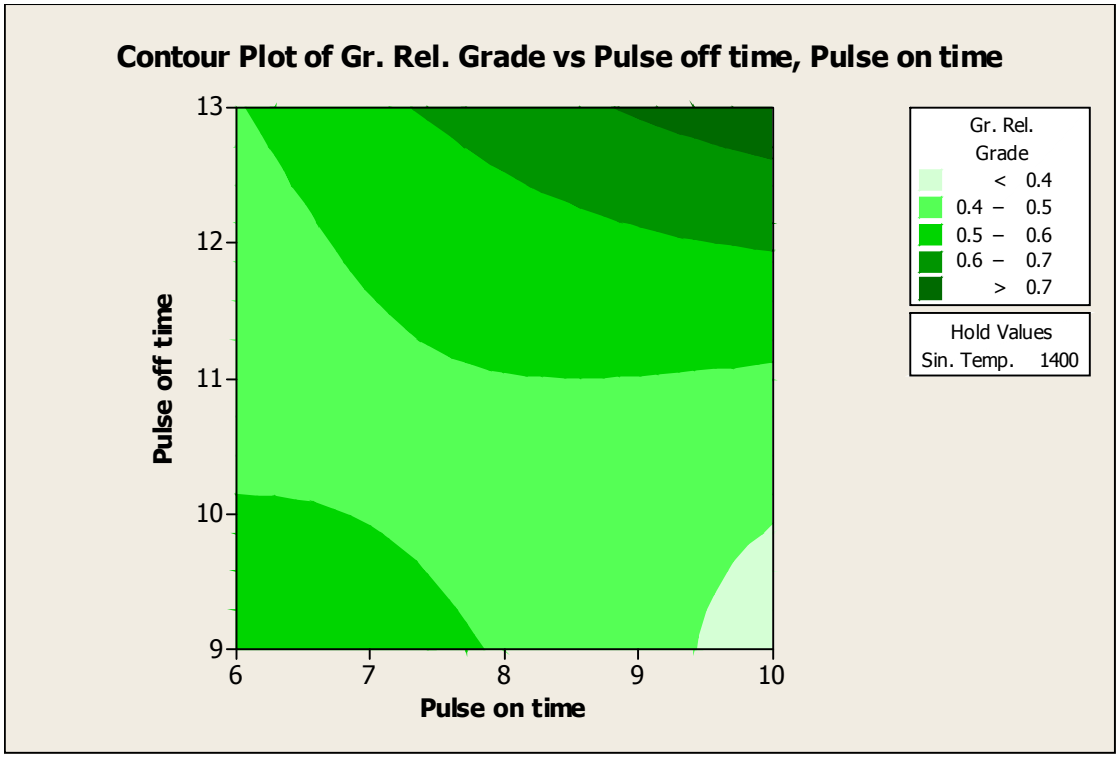

Figure 5.31 Contour plot for grey relational grade with respect to pulse-off time and pulse-on time

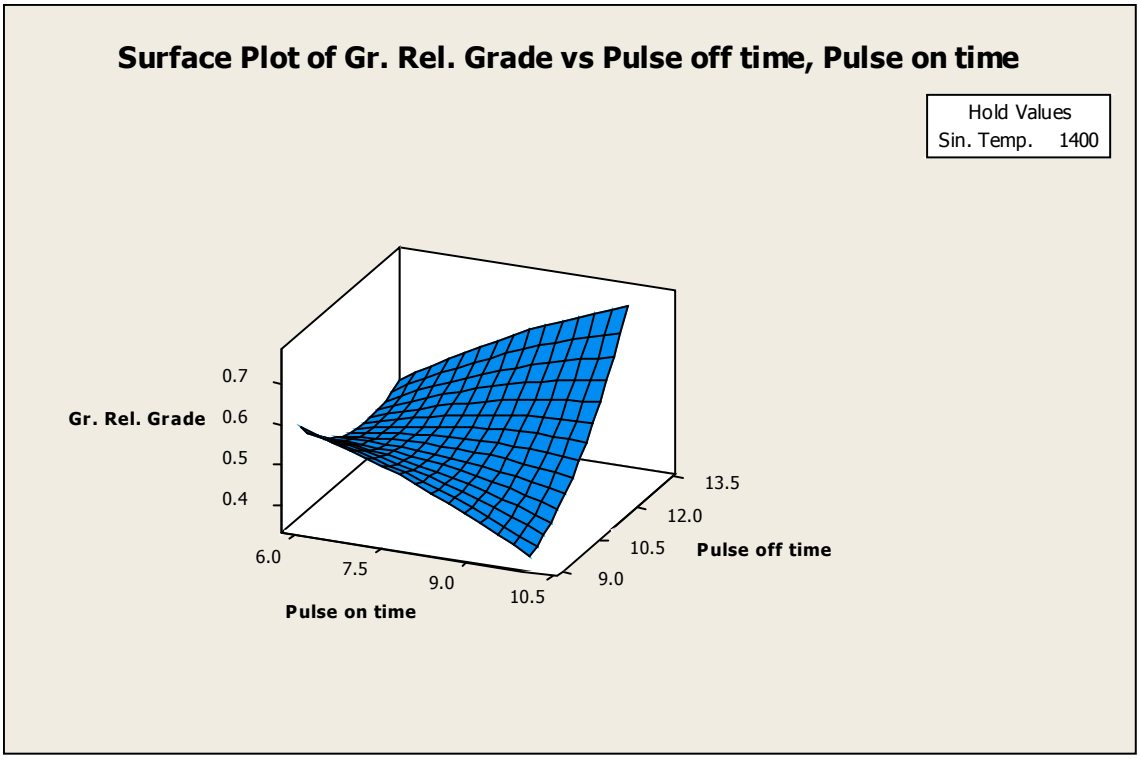

Figure 5.32 Surface plot for grey relational grade with respect to pulse-off time and pulse-on time

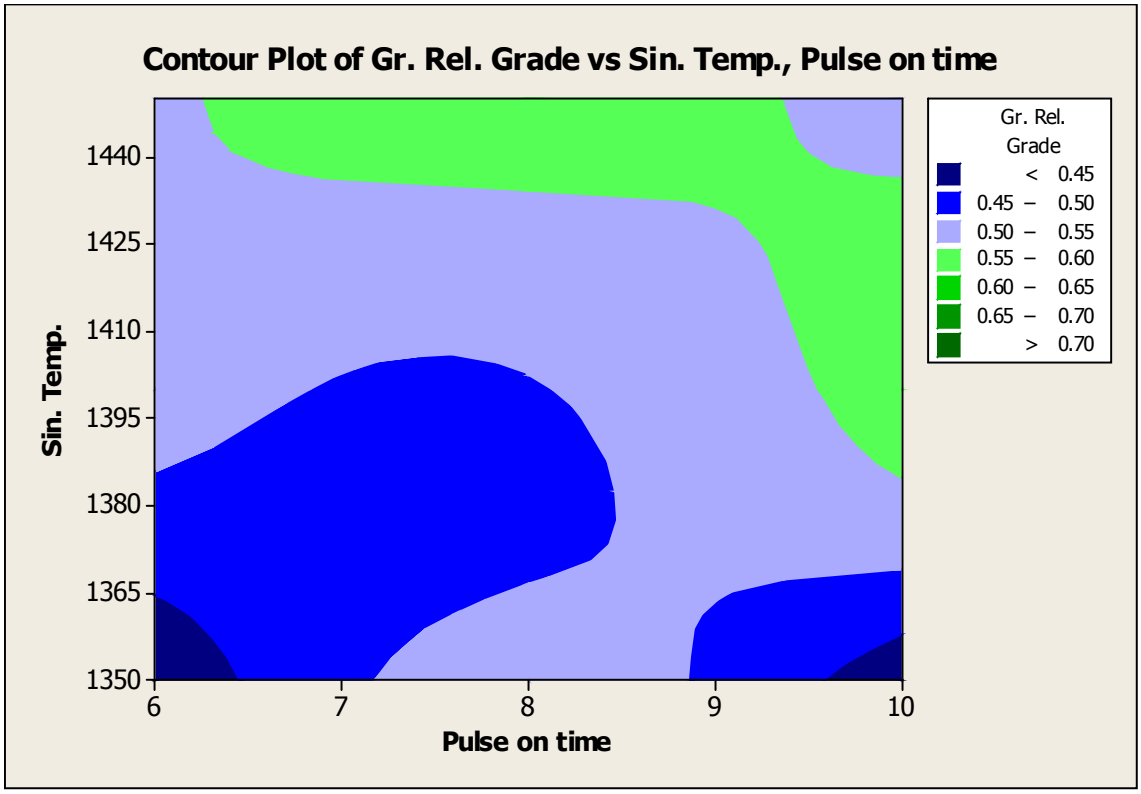

Figure 5.33 Contour plot for grey relational grade with respect to sintering temperature and pulse-on time

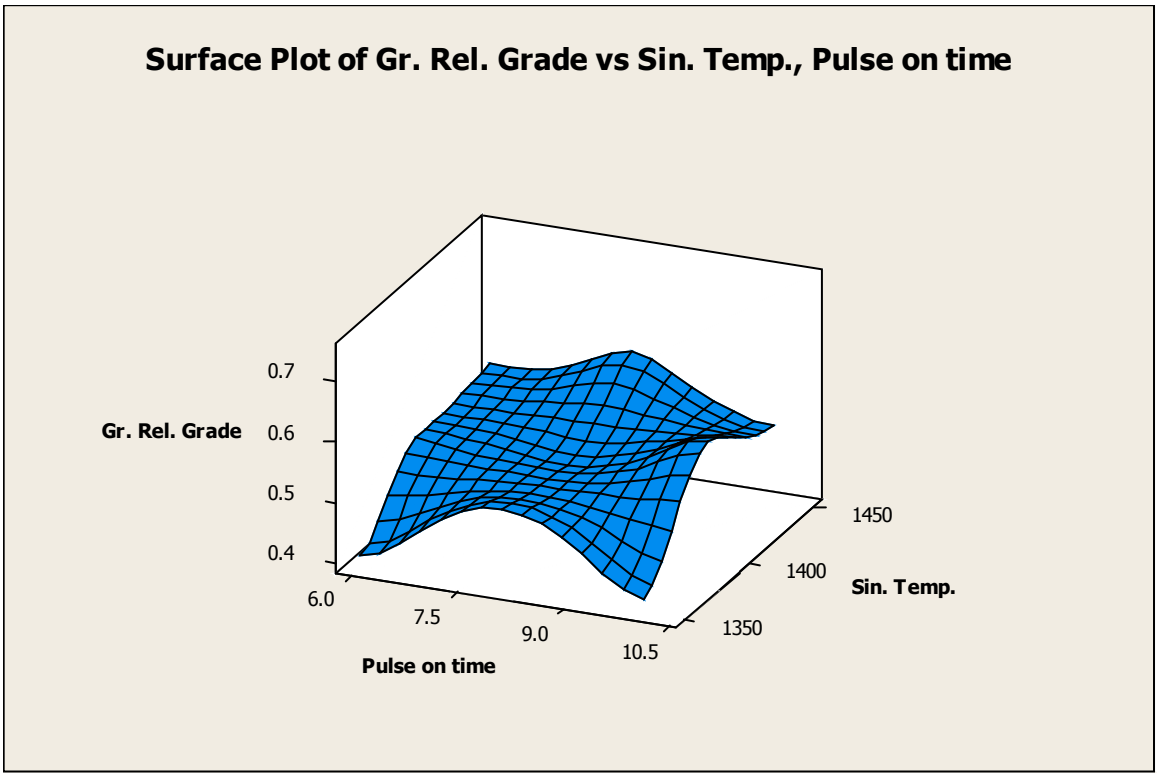

Figure 5.34 Surface plot for grey relational grade with respect to sintering temperature and pulse-on time

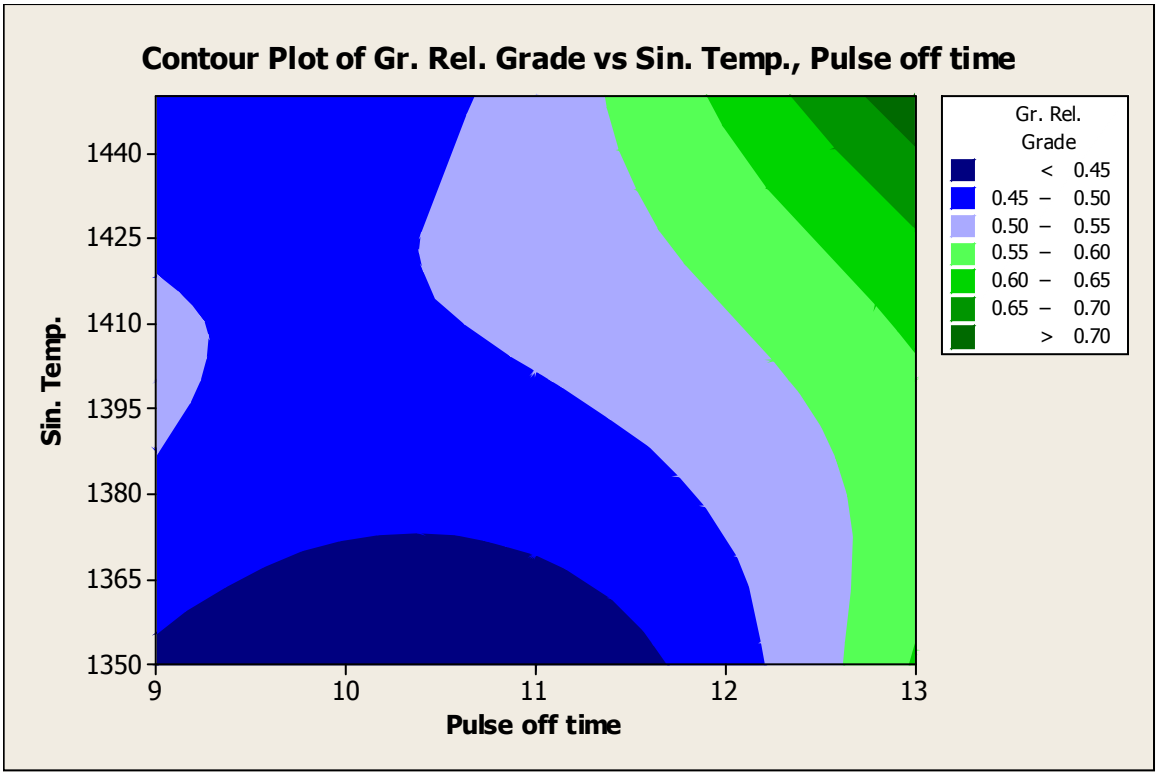

Figure 5.35 Contour plot for grey relational grade with respect to sintering temperature and pulse-off time

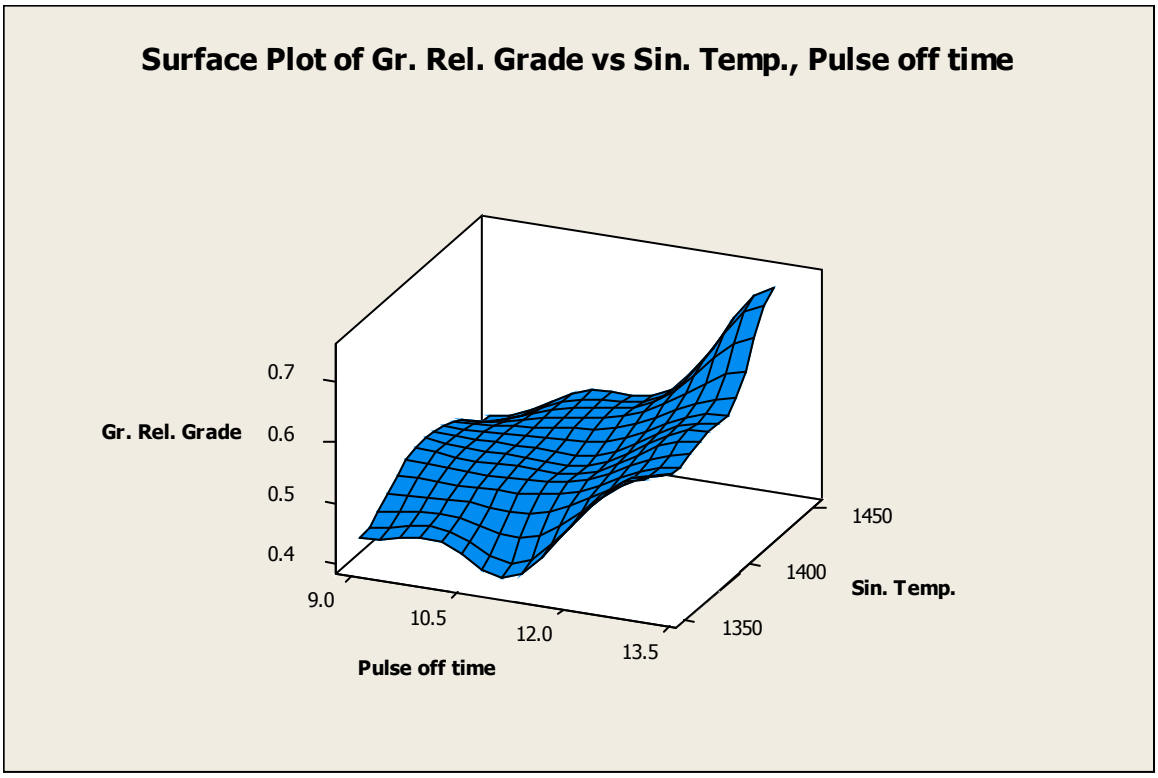

Figure 5.36 Surface plot for grey relational grade with respect to sintering temperature and pulse-off time

5.4.5.1 Confirmatory Test

After the optimal level of the parameters has been ascertained, a confirmation test needs to be carried out to check the correctness of the analysis. The estimated Grey Relational Grade, γ, using the optimal level of the process parameters can be evaluated as:

$$\gamma = \gamma_m + \sum_{i=1}^{o} (\bar{\gamma}_i - \gamma_m) \qquad \ldots (5.15)$$

where, 'γ_m' is the total mean grey relational grade, $\bar{\gamma}_i$ is the mean grey relational grade at the optimal level and 'o' is the number of the main design parameters that considerably affect the Ra-value and MRR during WEDM of CP-Ti P/M components.

Table 5.13 Results of confirmatory test

	Initial parameters	Optimal parameters	
		Theoretical	Experimental
Level	N2F2T2	N2F3T3	N2F3T3
Ra-value	2.59		2.36
MRR	7.13		7.551
Grey Grade	0.5121	0.6795	0.7342

Improvement of grey relational grade = 0.2221

5.5 Microstructural examination and XRD analysis of the machined surface

After Wire-cut EDM, the samples were analyzed in a Scanning Electron Microscope (JEOL make, Sl. No.JSM-6360) at 500X and 1000X magnifications respectively, as appeared in Figure 5.37 and 5.38. The SEM pictures demonstrate craters (stamped 1), pockmarks (stamped 2), voids (stamped 3) and micro-cracks (stamped 4). These craters, pockmarks and micro-cracks have been formed due to the variation of spark voltage and pulse duration, whereas voids were present since the initial formation of the sintered metal from Ti-powders. Voids are useful in bio-materials for tissue development inside the inserts.

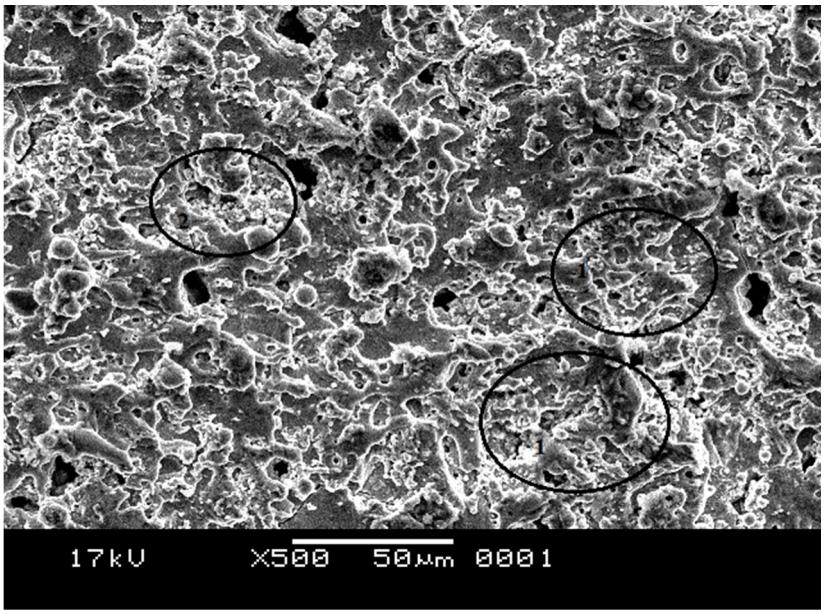

Figure 5.37 SEM micrograph at 500X of CP-Ti P/M sample after WEDM at conditions of Run No.4 (i.e., pulse-on time=8 µs, pulse-off time=9 µs and Sintering temperature=1450°C)

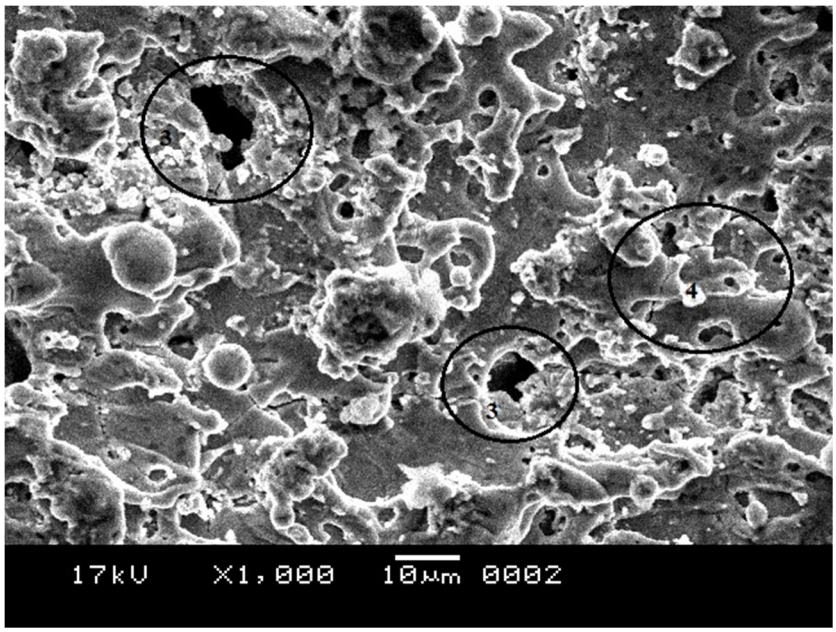

Figure 5.38 SEM micrograph at 1000X of CP-Ti P/M sample after WEDM at conditions of Run No.4 (i.e., pulse-on time=8 µs, pulse-off time=9 µs and Sintering temperature=1450°C)

X-Ray Diffraction analyzer (Rigaku, Ultima III) utilizing Cu (40 kV, 30 mA) radiation is utilized to study the phase change of titanium P/M test specimens during Wire-EDM. The XRD plots are appeared in Figure 5.39. The highest peak is at 2θ value 43.196°. In addition, due to machining by brass electrode wire, elemental Copper (Cu) is observed at 2θ value

75.253°. Some titanium oxide is additionally formed at the machined surface, which resulted amid machining at high temperature with a di-electric fluid like *de-ionised water*.

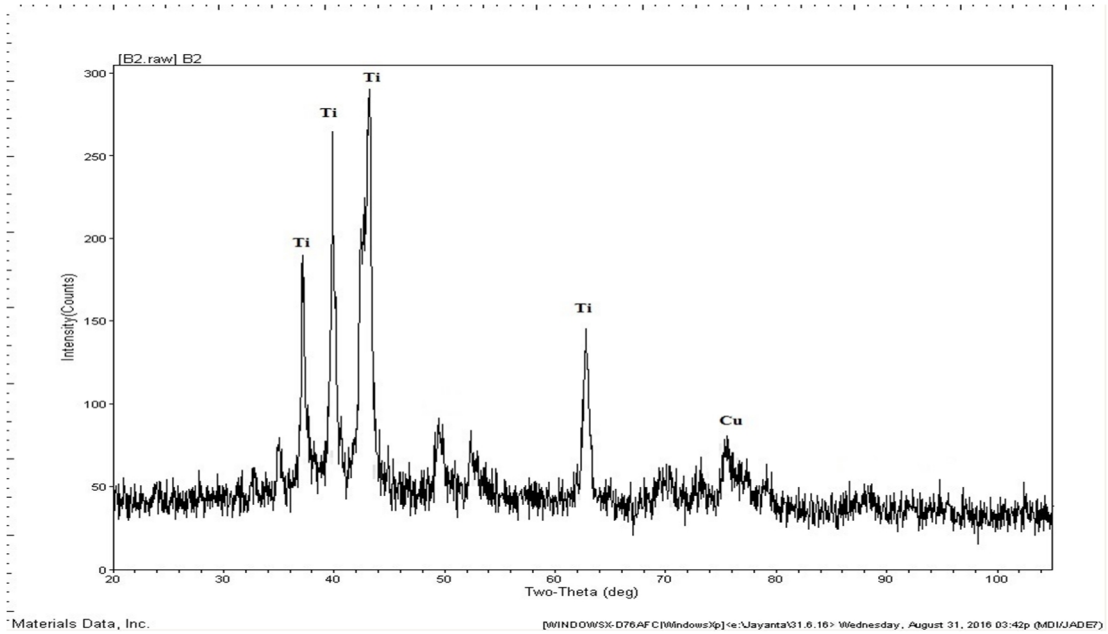

Figure 5.39 XRD analysis of CP-Ti P/M sample after WEDM at conditions of Run No.4 (i.e., pulse-on time=8 µs, pulse-off time=9 µs and Sintering temperature=1450°C)

5.6 FESEM analysis

After Wire-cut EDM, the samples were examined in a Field Emission Scanning Electron Microscope (FESEM - Quanta FEG 250) at approximately 2600X and 6000X magnifications, as shown in Figures 5.40 and 5.41.

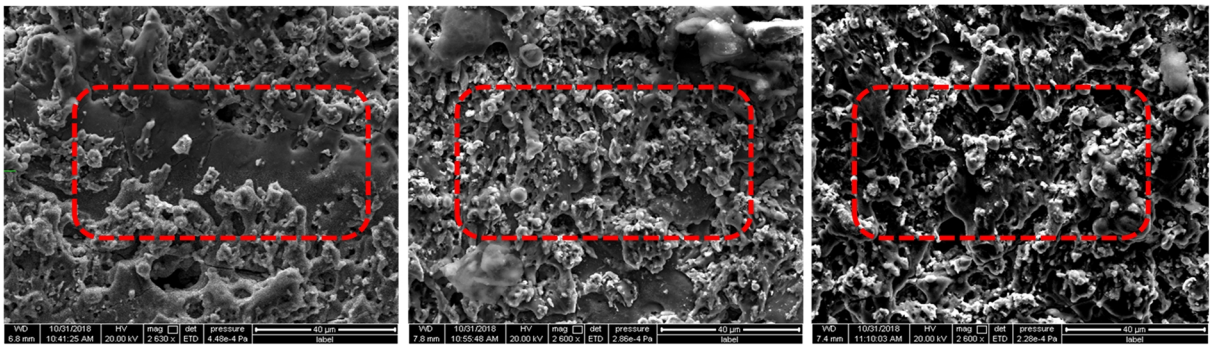

(a)1350°C (b) 1400°C (c) 1450°C

Figure 5.40 FESEM micrograph at 2600X of CP-Ti P/M samples after WEDM at different Sintering temperatures, Sample (a) at 1350°C, sample (b) at 1400°C, Sample (c) at 1450°C

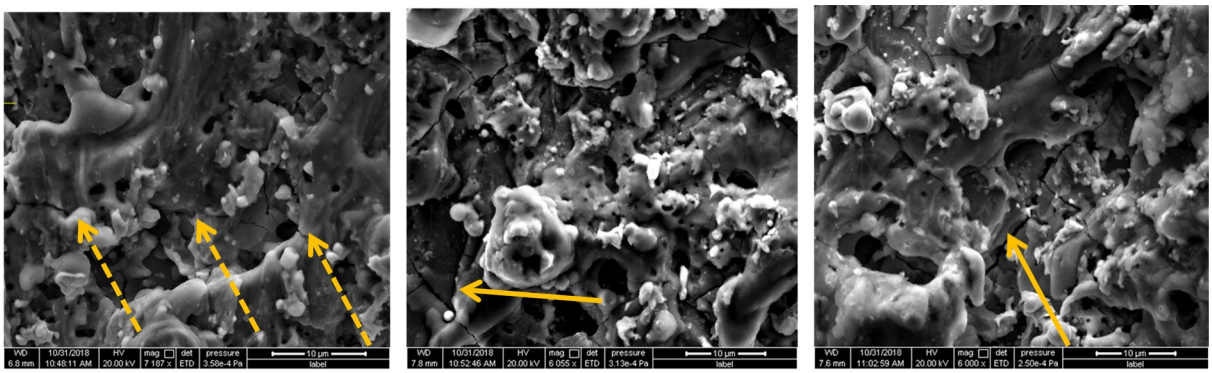

(a)1350°C (b) 1400°C (c) 1450°C

Figure 5.41 FESEM micrograph at approx. 6000X of CP-Ti P/M samples after WEDM at different Sintering temperatures, Sample (a) at 1350°C, Sample (b) at 1400°C, Sample (c) at 1450°C

The FESEM images indicate that particle coalescence increases due to diffusion with increasing sintering temperature from 1350°C to 1450°C. Probable crack growth inhibitions have been formed due to coalescence of the particles.

5.7 Atomic Force Microscopy

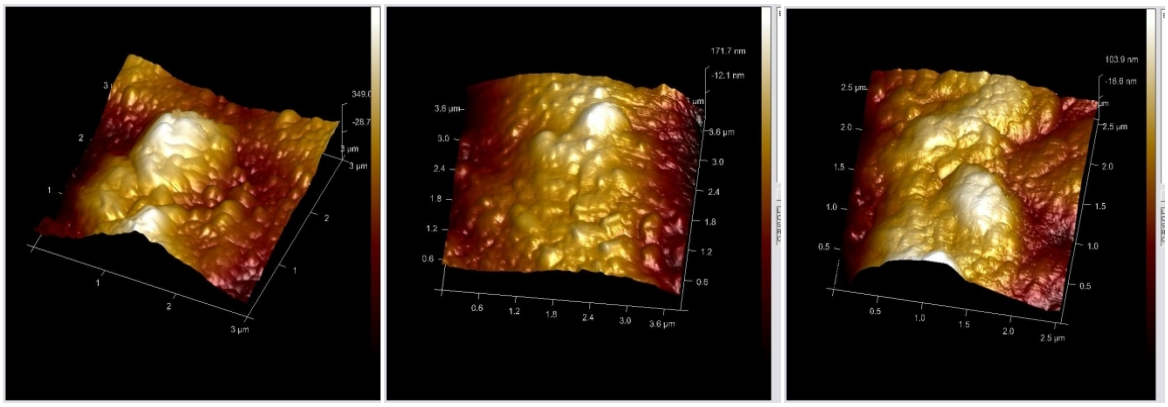

(a)1350°C (b) 1400°C (c) 1450°C

Figure 5.42 AFM of the samples after WEDM at different Sintering temperatures, Sample (a) at 1350°C, Sample (b) at 1400°C, Sample (c) at 1450°C

AFM images of the samples show that the sample surface sintered at 1350°C is more undulated then the samples sintered at 1400°C and 1450°C, whereas the sample sintered at 1400°C has smoother surface than others (as shown in Figure 5.42 a, b and c).

5.8 Energy Dispersive X-Ray (EDAX) Analysis

EDAX analysis (as shown in figure 5.43) reveal some copper and oxide at the machined surface. Surface smoothness can be co-related to better compaction and coalescence of the particles due to increase of diffusion at higher temperatures.

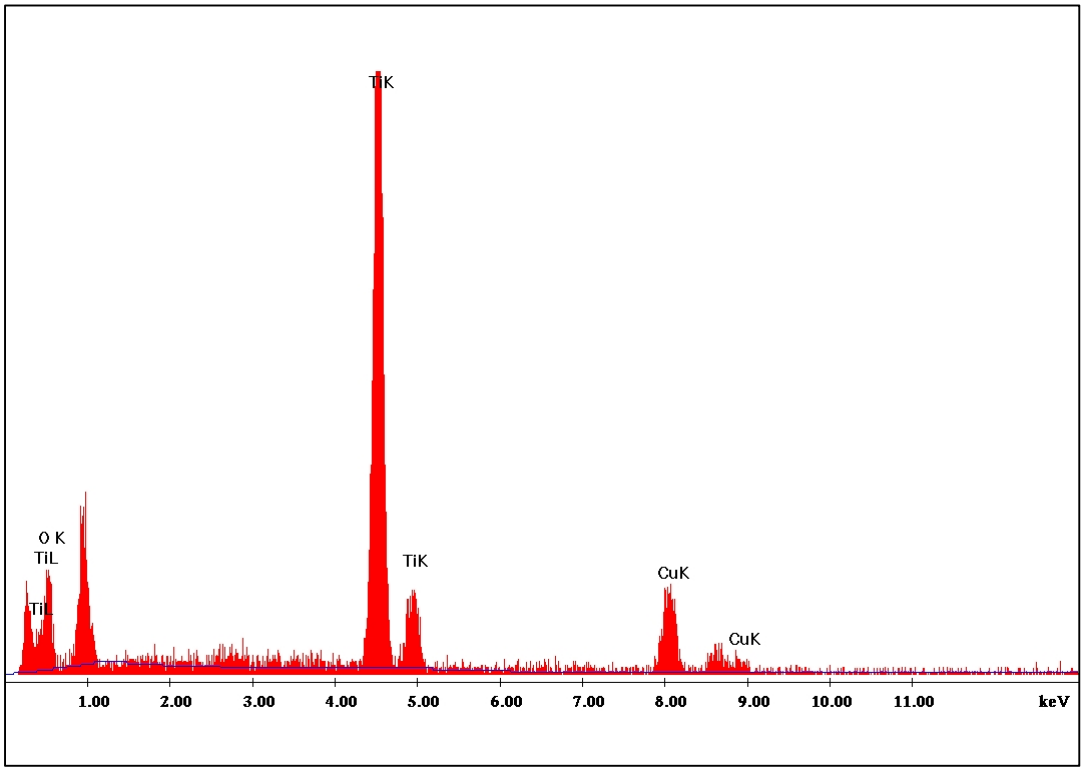

Figure 5.43 EDX analysis of CP-Ti P/M sample after WEDM

5.9 Closure

In the present work, a quadratic model for surface roughness and metal removal rate has been developed to connect the dominant parameters, for example, sintering temperature, pulse-on time and pulse-off time in the formation and WEDM procedure of commercially pure titanium powder metallurgy parts. Machining analysis of the Ti-parts were also being performed. In view of the above following conclusions can be drawn:

1. A useful connection between surface roughness parameter (R_a), sintering temperature, pulse-on time and pulse-off time is established through response surface methodology. Comparative relationship additionally exists between MRR, sintering temperature, pulse-on time and pulse-off time.

2. Wire-cut EDM is a satisfactory procedure to machine titanium, shaped through powder metallurgy route, which is generally hard to machine through the traditional machining processes.

3. The surface roughness (R_a) of pure titanium powder metallurgy components obtained lay in the scope of 2.36 μm to 3.04 μm by Wire-cut EDM process. The minimum surface roughness was achieved experimentally with the conditions of 6 μs pulse-on time, 13 μs pulse-off time and sintering temperature (used during the formation of CP-Titanium P/M components) of 1450°C.

4. Obtained range of metal removal rate (MRR) of pure titanium powder metallurgy components lay within the range of 5.76 mm^3/sec to 9.903 mm^3/sec by WEDM process. The maximum metal removal rate was accomplished under the conditions of 10 μs pulse-on time, 13 μs pulse-off time and at a sintering temperature of 1400 °C.

5. The sensitivity analysis of Surface Roughness (R_a) exposed that pulse-off time is the most significant negative factor influencing the response output. The most important positive response variables with respect to the output parameter are found to be pulse-on time and sintering temperature.

6. Similarly, sensitivity analysis of MRR disclosed that pulse-off time is the most important positive factor influencing the response output and the most noteworthy negative response variables with respect to the output parameter are found to be pulse-on time and sintering temperature.

7. Grey relational analysis reflected that 10 μs pulse-on time, 13 μs pulse-off time and 1400°C sintering temperature produces the optimum results, when surface roughness (Ra-value) and Metal removal rate (MRR) both are considered simultaneously.

8. FESEM, AFM and EDAX analysis reveal that the best surface properties were obtained for the samples sintered at 1400°C.

CHAPTER 6

CORROSION ANALYSIS OF SINTERED TITANIUM SAMPLES

Outline of the Chapter: *6.1 Introduction, 6.2 Experimental procedure for corrosion test, 6.2.1 Preparation of titanium samples – polishing, 6.2.2 Potentiostatic Polarization of titanium Samples, 6.3 Results and discussion, 6.3.1 Potentiodynamic Polarization Curves, 6.3.2 Electrochemical Impedance Spectroscopy (EIS), 6.3.2 Nyquist plots, 6.3.2 Optical images, 6.4 Closure*

6.1 Introduction

Corrosion is defined as the response of a material with its encompassing environment with a continuous deterioration in properties of the material. The response can be chemical, electrochemical, physical or their mix [107]. Three components are essential to study the corrosion phenomenon: the material, the environment and the material/environment interface. Titanium bio-inserts are placed in the close vicinity of body fluids, so it is vital to study the corrosion conduct of the inserts. In this chapter, nine samples sintered at different temperatures were placed into Hank solution to study the corrosion characteristics of PM titanium in detail.

6.2 Experimental procedure for corrosion test

6.2.1 Preparation of titanium samples - polishing

All samples of titanium (14 mm diameter x 7 mm height) were taken to carry out the corrosion test experiments. The process of polishing carried out was belt polishing followed by emery paper polishing. The papers used were 120,180, 1/0, 2/0 and 3/0 grades. Sample polishing was done up to 1/0 and further up to 3/0. The polished samples were then washed by sonicating in acetone solution for 20 min.

6.2.2 Potentiostatic polarization of titanium samples

Polished titanium samples were taken for creating passivated oxide layer on the surface of the samples using the solution, by Potentiosatic Polarization technique, with the help of Gamry Potentiostat (PC/750, USA), using standard three-electrode electrochemical cell comprising working electrode (test sample), reference electrode (saturated calomel electrode), and

auxiliary electrode (graphite electrode). The passivation potential for the titanium samples were selected from the initial potentiostatic polarization experiment carried out in the solution. Current transient experiments were carried out on titanium samples in the solution. Pre-selected polarization potentials were applied in the sample for fixed duration of time in order to achieve passive layer on the titanium surface. The corrosion data is given in Annexure 4.

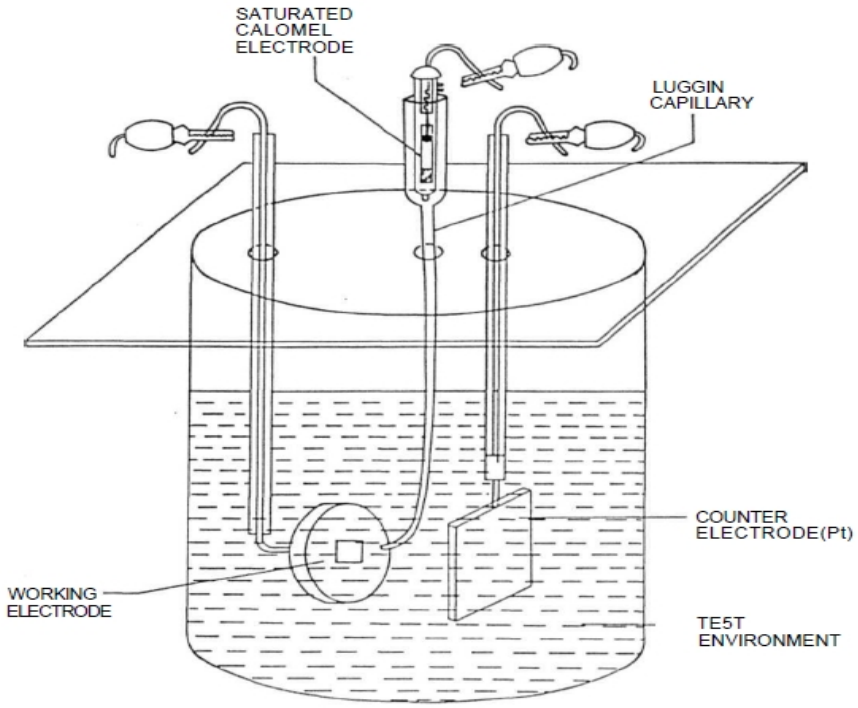

Figure 6.1 Experimental set up for corrosion test

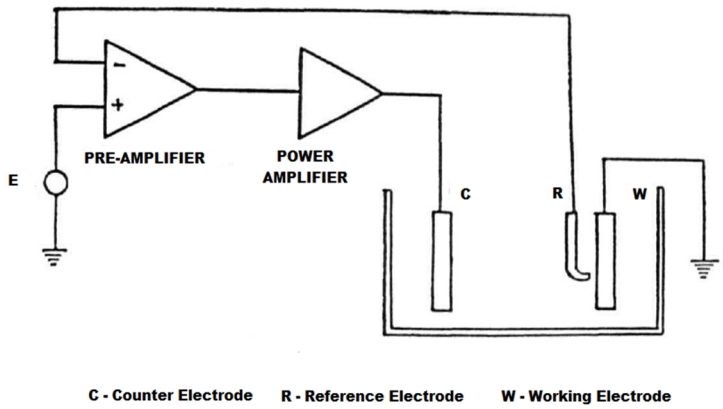

Figure 6.2 Schematic diagram of a potentiostat

6.3 Results and discussion

The various test results on corrosion of Ti-samples are illustrated in the following sections.

6.3.1 Potentiodynamic polarization Curves

'E_{corr}' and 'I_{corr}' of the samples were determined in Hank solution chosen for the present study by potentiodynamic polarization technique. The Polarization experiments with scan rate of 1mV/s were carried out as per ASTM ST72. The potentiostat is controlled by a computer, which stores all the polarization data. The polarization curve is obtained from a dedicated software. A tafel ruler is provided with the software to measure corrosion potential 'E_{corr}' and corrosion current density 'I_{corr}'. Tests were performed on the titanium samples sintered at different sintering temperatures. The samples were divided into groups of three. The potentiodynamic plots of sample 1 to 9 are showed in Figures 6.3 to 6.5 and the values of 'E_{corr}' and 'I_{corr}' are reported in the Table 6.1 to 6.3. The potentiodynamic study for a particular sample was repeated at least for three times.

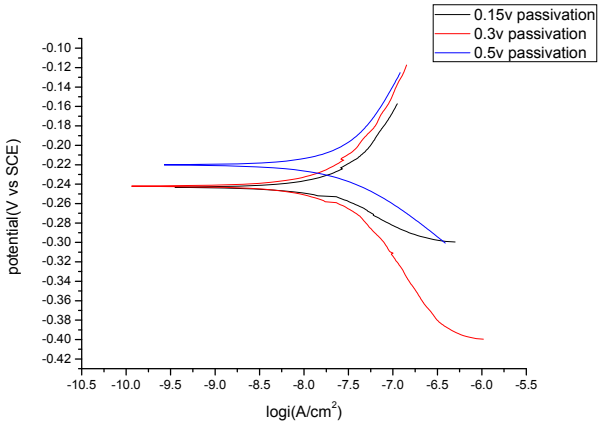

Figure 6.3 Potentiodynamic polarization curves for titanium samples sintered at 1350°C

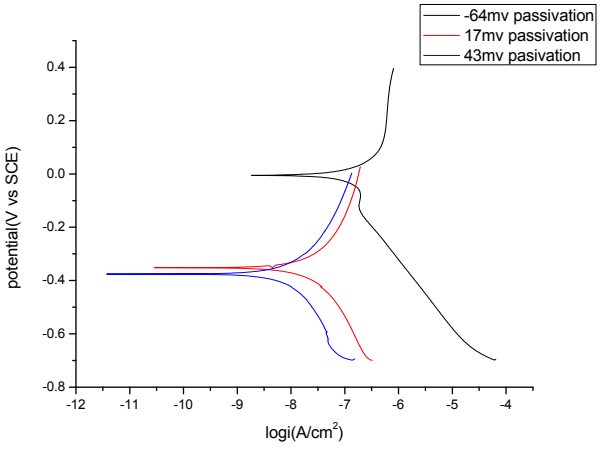

Figure 6.4 Potentiodynamic polarization curves for titanium samples sintered at 1400°C

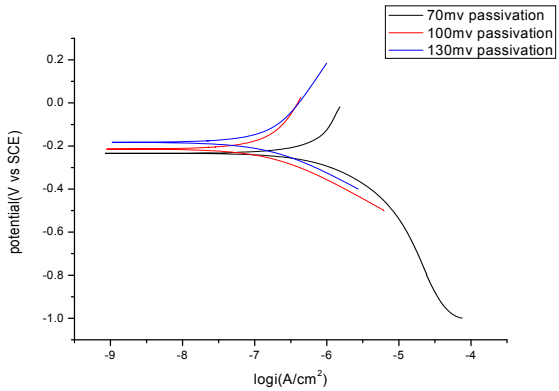

Figure 6.5 Potentiodynamic polarization curves for titanium samples sintered at 1450°C

Table 6.1 I_{corr} vs E_{corr} for Samples sintered at 1350°C

Samples	I_{corr}(nA/cm^2)	E_{corr}(V)
As received	488	.4
.15v passivation	16	.25
.3v passivation	10	.24
.5v passivation	7	.139

Table 6.2 I_{corr} vs E_{corr} Samples sintered at 1400°C

Samples	I_{corr}(nA/cm^2)	E_{corr}(mV)
As received	510	-312
-64 mv passivation	15	-6
17mv passivation	8	-350
43 mv passivation	5	-382

Table 6.3 I_{corr} vs E_{corr} Samples sintered at 1450°C

Samples	I_{corr}(nA/cm^2)	E_{corr}(mV)
As received	700	-275
70 mv passivation	80	-225
100mv passivation	50	-210
130 mv passivation	30	-170

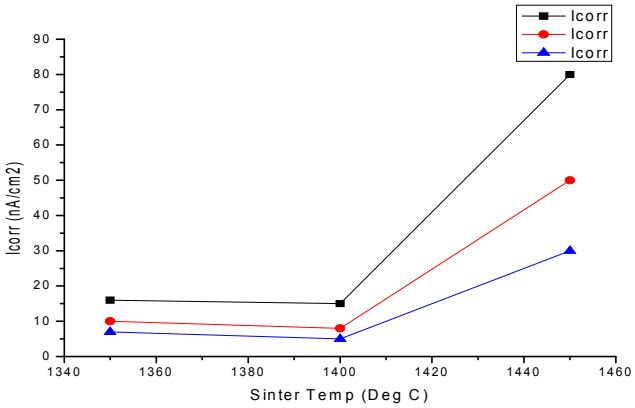

Figure 6.6 Variation of I_{corr} for titanium samples sintered at different temperatures

The Intersection of anodic process and cathodic process is known as corrosion potential or E_{corr}.. The current corresponding to E_{corr} is known as corrosion current or I_{corr}. Corrosion rate is proportional to corrosion current or I_{corr}, and corrosion is a steady state condition. Corrosion potential is not a property but a dynamic situation. Table 6.1, 6.2 and 6.3 shows the I_{corr} and E_{corr} values of Titanium samples sintered at three different sintering temperatures (i.e., 1350°C, 1400°C and 1450°C). The values of I_{corr} and E_{corr} has been taken for both as-received and passivated Ti-samples. From Table 6.1, 6.2 and 6.3, it is clear that, I_{corr} and E_{corr} values reduce significantly after passivation, that means after passivation corrosion reduces substantially. From Figure 6.6, it is also found that, for the Ti-samples sintered at 1350°C to 1400°C, there is minimal change in the corrosion current. However, for the CP-Ti samples sintered at 1450°C corrosion current (I_{corr}) increases drastically, leading to greater corrosion.

6.3.2 Electrochemical Impedance Spectroscopy (EIS)

Electrochemical Impedance spectroscopy (EIS) of the samples was carried out in the experimental solution. The impedance experiments were done using 100mV AC voltage (root-mean-square) and 1V DC voltage vs. SCE in the frequency ranged from 0.01 Hz to 300 kHz at 10 cycles per decade. The absolute impedance and phase angles were measured at each frequency. Nyquist plots were obtained. The impedance data were fit to appropriate equivalent electrical circuit using a simplex fit model, using both the real and imaginary components of the data. The impedance data were interpreted on the basis of equivalent electric circuit using simplex fit method. In this work most of the samples conformed to CPE (Constant Phase Element) model.

For CPE model the main results are Rp (polarization resistance), Ru (solution resistance), Y0 (capacitance) and α, an exponent that equals to 1 for a capacitor. For a constant phase

element α is less than one. As per the equation, resistance = 1 / 2πfC (capacitance C is inversely proportional with resistance). Corrosion rate is inversely proportional to Rp. The value of capacitance and resistance deliver the idea of surface and solution interface. The values of Rp, Ru, Y0 and α are illustrated in the Table 6.4 to 6.6.

Table 6.4 Potentiodynamic polarization data for samples sintered at 1350°C

Samples	R_p(ohm/cm^2)	R_u(ohm/cm^2)	α
.15v passivation	393	5.6	.78
.3v passivation	918	2.1	.80
.5v passivation	1200	3	.82

Table 6.5 Potentiodynamic polarization data for samples sintered at 1400°C

Samples	R_p(ohm/cm^2)	R_u(ohm/cm^2)	α
-64 mv passivation	480	7	.85
17mv passivation	940	11	.89
43 mv passivation	1240	19	.92

Table 6.6 Potentiodynamic polarization data for samples sintered at 1450°C

Samples	R_p(ohm/cm^2)	R_u(ohm/cm^2)	α
70 mv passivation	180	17	.74
100mv passivation	250	21	.79
130 mv passivation	300	26	.82

6.3.3 Nyquist plots

The impedance, Z(ω) may be expressed in terms of real, Z'(ω) and imaginary, Z''(ω). Components, $Z(\omega) = Z'(\omega) + Z''(\omega)$. This particular behavior of an electrode may be expressed in Nyquist plot of EIS. At very high frequency, the imaginary component, Z'', disappears, leaving only the solution resistance, Ru. At very low frequency, Z'' again disappears, leaving a sum of Ru and faradic resistance or polarization resistance, Rp. The graphical representation of Nyquist plot of nine samples were also divided into group of three, showed in Figures 6.7 to 6.9 in the following section.

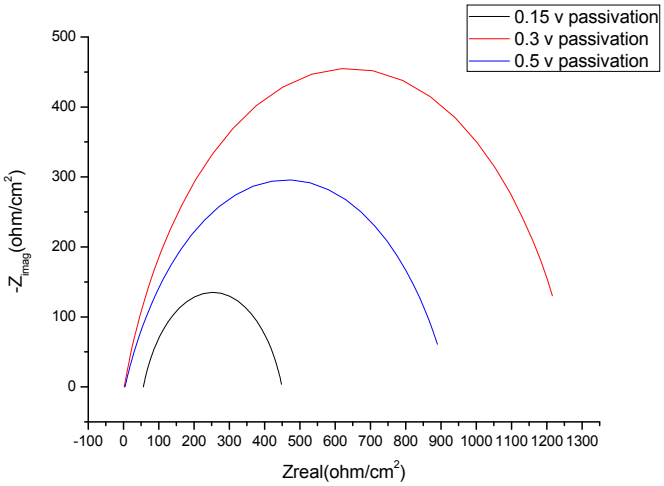

Figure 6.7 Nyquist plots of titanium samples sintered at 1350°C

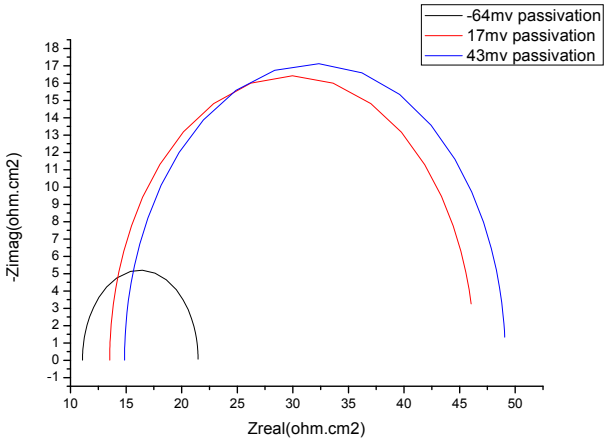

Figure 6.8 Nyquist plots of titanium samples sintered at 1400°C

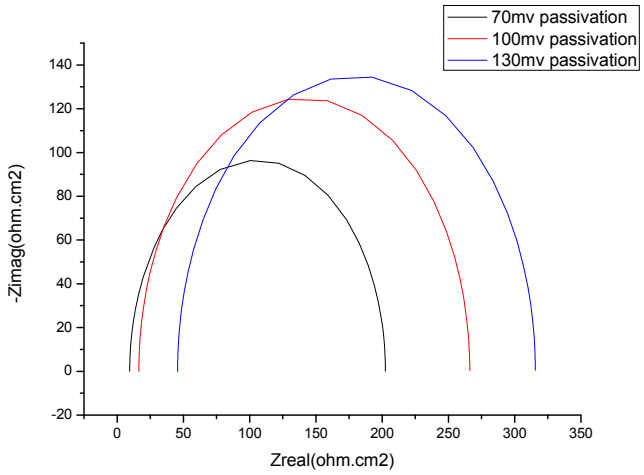

Figure 6.9 Nyquist plots of titanium samples sintered at 1450°C

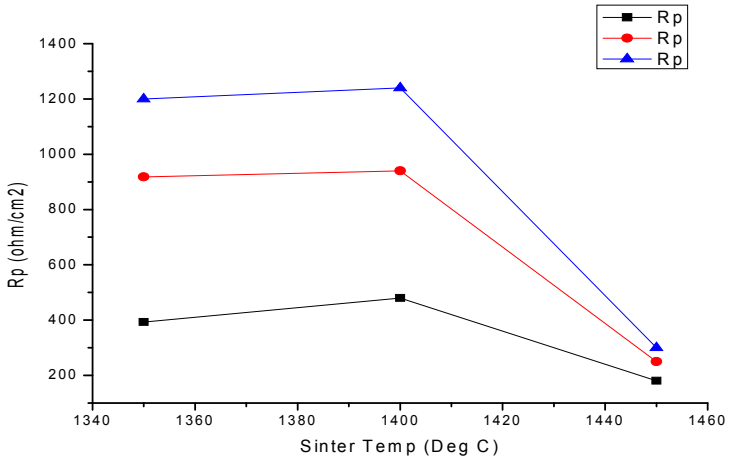

Figure 6.10 Variation of R_p (polarization resistance) for titanium samples sintered at different temperatures

From the potentiodynamic polarization curves and Electrochemical Impedance Spectroscopy (Nyquist Plots in figures 6.7, 6.8 and 6.9), from figure 6.10 and tables 6.4, 6.5 and 6.6, it is clearly evident that, as sintering temperature of the PM titanium is changed from 1350°C to 1400°C, initially there is a small increment in polarization resistance, that means, its corrosion tendency diminished. But, in contrast, when sintering temperature is increased further from 1400°C to 1450°C, its polarization resistance decreased sharply, that means its corrosion tendency will be increased. So, we can conclude that, corrosion tendency increases phenomenally as sintering temperature approaches 1450°C.

6.3.4 Optical Images

After the corrosion tests, the PM titanium samples were examined in an Optical microscope at 500X and 1000X magnifications respectively, as shown in Figure 6.11 to 6.13.

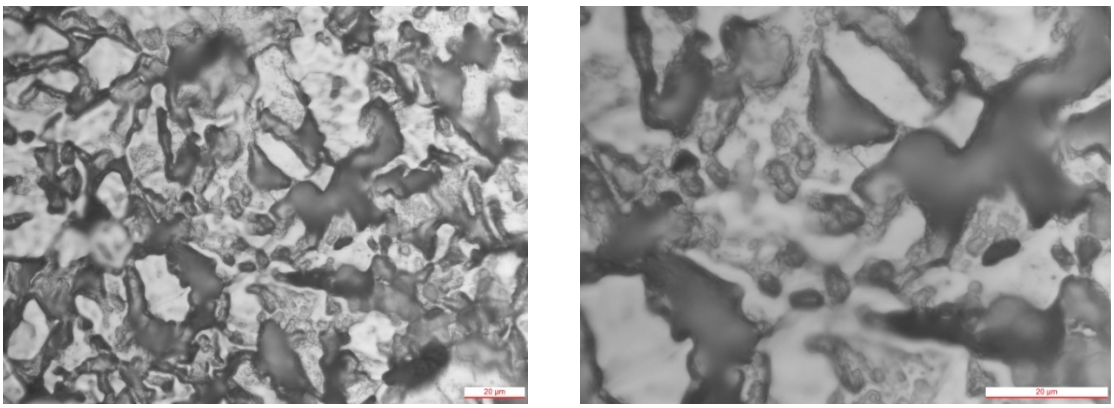

(a) 500X magnification (b) 1000X magnification

Figure 6.11 Optical micrographs of titanium sample sintered at 1350°C

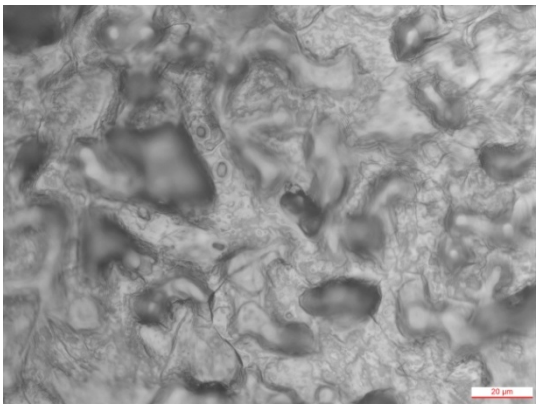

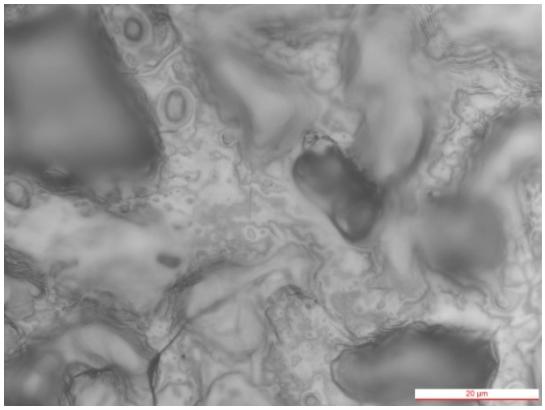

(a) 500X magnification (b) 1000X magnification

Figure 6.12 Optical micrographs of titanium sample sintered at 1400°C

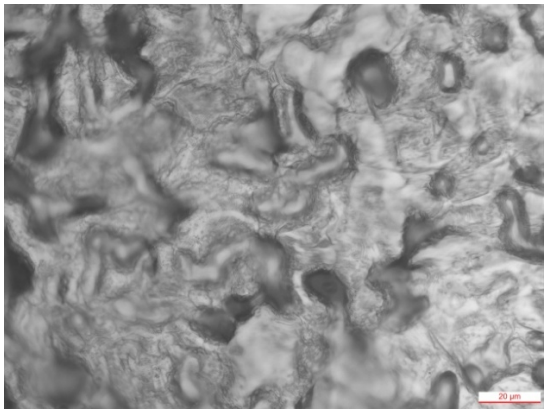

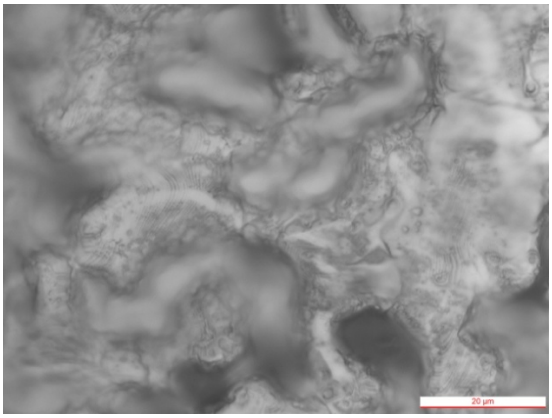

(a) 500X magnification (b) 1000X magnification

Figure 6.13 Optical micrographs of titanium sample sintered at 1450°C

From optical micrograph images (figures 6.11, 6.12 and 6.13) we can see a whitish tone has appeared over the surface of the PM titanium samples. This is due to the formation of passive titanium oxide layer over the outer surface of the samples. This passive oxide layer protects titanium from further corrosion and simultaneous decay.

6.4 Closure

In this work commercially pure titanium powder metallurgy parts have been formed by sintering at three different temperatures, namely, 1350°C, 1400°C and 1450°C. The corrosion behavior of all the samples sintered at different sintering temperatures is investigated in Hank's solution using Tafel's polarization technique. Electro-chemical measurements reveal an increase in corrosion rate for PM titanium samples sintered at higher sinter temperatures. Better corrosion resistance of CP-Ti samples sintered at 1350°C and 1400°C suggests that these samples can be used for bio-medical implants.

CHAPTER 7

CONCLUSIONS AND SCOPE FOR FUTURE WORK

Outline of the Chapter: *7.1 Conclusions, 7.2 scope for future work*

7.1 CONCLUSIONS

The present dissertation focuses on the processing, characterization, cold forging behavior, machining analysis and corrosion behavior of press and sinter formed commercially pure titanium powder metallurgy parts. The following conclusions are being arrived upon from the research works.

- Powder Metallurgy route of manufacturing is found to be successful to fabricate titanium powder metallurgy components. The soundness of the P/M parts is affected by the effective compaction of the metal powder in a Universal Testing Machine and finally sintering them in a high vacuum furnace fitted with a diffusion pump. The magnitude of the vacuum is to the tune of 10^{-4} Torr. Therefore, by controlling the process parameters like compaction load, sintering temperature, powder size, etc. improved mechanical properties of the sintered parts can be achieved.
- The density, micro-hardness and metallurgical study by scanning electron microscope of the sintered titanium samples revealed that as compaction load and sintering temperature has been increased gradually, density, micro-hardness and other related properties were enhanced drastically. It is found that the green density, sintered density and relative density maintain a linear relationship with respect to sintering temperature.
- The deformation pattern during the forging of metal powder preform is quite different from that of cast or wrought metals and is a function of both relative density and hydrostatic stress. The deformation characteristics of metal powder preforms during axisymmetric compression have been considered for this situation. The problem of die-load, during compression test, was researched by applying an appropriate interfacial friction law and plasticity theory for permeable metals. The percentage decrease in height during compression was taken as a criterion for evaluating the formability of metal powder preforms. It was discovered that the relative density of the titanium powder preforms increase with increase in compacting pressure and

sintering temperature. Since, a powder metallurgy part comprises porosity, hence, at the time of forging, initially the pores close-up, later on, as we go on increasing the forging load, deformation sets in. During forging, it was seen that, compaction and compression take place simultaneously. The work is observed to be successful for the evaluation of die-loads during forging of porous metals like PM titanium components by the utilization of 'upper bound theory'.

- The machining analysis focused on the non-conventional machining, i.e., wire-cut electro discharge machining process on sintered titanium parts. Since, titanium is one of the hardest of metals; hence Wire-EDM is an easy and alternative option to machine titanium. Moreover, by alternating the process parameters while machining, we can easily modify the machining characteristics such as metal removal rate, surface roughness and other machining characteristics of the finished products.
- The corrosion study of the sintered titanium samples disclosed that titanium has very good corrosion resistance properties. It is due to the fact that; a very thin but secure layer of titanium oxide is formed on the surface of the bare titanium when it is exposed to air or water. As the sintering temperature increased the corrosion resistance decreased.

From the aforesaid inferences it can be opined that bio-medical implants such as human prosthesis and dental implants can be easily manufactured through press-and-sinter method and thereby minor modification of the implants can be done though cold forging process, and further if at all machining is required, it can be easily accomplished though wire-EDM route.

7.2 SCOPE FOR FUTURE WORK

The present investigation was aimed at studying the cold forging, machining and corrosion behavior of sintered titanium powder metallurgy parts. However, for production of sintered titanium samples with improved properties, it is recommended that further research be directed along the lines mentioned below.

- The present research work focused on commercially pure titanium, but newer research work may target on manufacturing some titanium composites with enhanced mechanical as well as bio-compatible properties.
- Future research may also concentrate on how to make threads on the titanium samples in order to make it suitable for dental implants.
- Some more parameters can be varied in the machining analysis in order to study their effect on the machining characteristics of sintered titanium.
- Last but not the least, if other than conventional powder metallurgy route, hot iso-static pressing or cold iso-static compaction followed by sintering may be used to prepare the titanium parts, then newer type of titanium samples with different microstructural and mechanical properties can be formed.

REFERENCES

[1] "Titanium" (http://www.britannica.com/eb/article-9072643/titanium); Encyclopædia Britannica, Retrieved 7 June 2018.

[2] David R. Lide ed. (2005), CRC Handbook of Chemistry and Physics, Internet Version, <http://www.hbcpnetbase.com>, CRC Press, BocaRaton, FL, ISBN 0-8493-0486-5.

[3] Robert E. Krebs, (2006), *the History and Use of Our Earth's Chemical Elements: A Reference Guide* (2nd Edition); Westport, CT: Greenwood Press; ISBN 0-313-33438-2.

[4] "Titanium" (https://en.wikipedia.org/wiki/Titanium); Retrieved 7 June 2018.

[5] C. N. Elias, J. H. C. Lima, R. Valiev, M. A. Meyers, (2008), *Biomedical applications of titanium and its alloys***,** J. Miner. Met. Mater. Soc. 60; pp. 46-49.

[6] S.E. Mirvis, F. Geisler, J.N. Joslyn, H. Zrebeet, (1988), *Use of titanium wire in cervical spine fixation as a means to reduce MR artifacts*, American Journal of Neuro Radiology; 9, pp. 1229-1231.

[7] R.L. Saha, KT Jacob, (1986), *Casting of Titanium and its alloys*, Def. Sci. J. Vol 36 (6), pp. 121-141.

[8] L.M.R. de Vasconcellos, M.V. de Oliveira, M.L. de A Graca, L.G.O. de Vasconcellos, Y.R. Carvalho, C.A.A. Cairo, (2008), *Porous Titanium Scaffolds Produced by Powder Metallurgy for Biomedical Applications*, Materials Research, Vol. 11, No. 3, pp. 275-280.

[9] C. Leyens, M. Peters, (2003), *Titanium and titanium alloys: Fundamentals and applications*; Wiley-VCH GmbH, ISBN 3-527-30534-3.

[10] R. J. Narayan, (2012), ASM Handbook, Vol. 23, pp. 224-226: *Materials for Medical Devices*, ASM International, ISBN-10: 1-61503-827-2.

[11] W. J. Kroll, (1940), *Method for the Manufacturing of Titanium and Alloys Thereof*, US Patent 2,205,854.

[12] P. C. Angelo, R. Subramanian, (2012), *Powder Metallurgy: Science, Technology and Applications*, PHI, India, ISBN-978-81-203-3281-2.

[13] C. M. Ward-Close, A. B. Godfrey, S. R Thompson, (2005), *Titanium made the EDO way should see prices drop*, Metal Powder Report, 60(7-8), 20-25, https://doi.org/10.1016/S0026-0657(05)70451-3.

[14] G. Lutjering, J. C. Williams, (2003), *Titanium* (second edition), Springer Verlag.

[15] F. H. (Sam) Froes, (2005), *Powder Metallurgy of Titanium Alloys*, DOI:10.1533/9780857098900.2.202.

[16] C. G. McCracken, (2010), "Manufacture of hydride-dehydride low oxygen Ti-6Al-4V (Ti-6-4) powder incorporating a novel powder de-oxidation step "Euro PM Conference and (2010).

[17] S. M. Abkowitz, D. Abkowitz, H. Fisher, D. Main, (2011), *Affordable PM Titanium – Microstructure, Properties and Products*, MPIF Conference.

[18] Di Hu, Aleksei Dolganov, Mingchan Ma, Biyash Bhattacharya, Matthew T. Bishop, George Z. Chen, (2017); Development of the Fray-Farthing-Chen Cambridge Process: Towards the Sustainable Production of Titanium and Its Alloys; JOM, Vol. 70(2), https://doi.org/10.1007/s11837-017-2664-4.

[19] F. H. (Sam) Froes, (2013), *Titanium Powder Metallurgy: Developments and opportunities in a sector poised for growth*, Powder Metallurgy Review, Vol 2 (4), pp. 29-43.

[20] J. Black, M. Dekker, (1983), Book Review: *Biological Performance of Materials: Fundamentals of Biocompatibility* - (Vol. 8, Biomedical engineering and instrumentation series).

[21] P. Parida, A. Behera, S. Mishra, (2012), *Classification of Biomaterials used in Medicine, International*, Journal of Advances in Applied Science, 1 pp. 31-35.

[22] G. Manivasagam, D. Dhinasekaran, A. Rajamanickam, (2010), *Biomedical Implants: Corrosion and* **its** *Prevention - A Review*, Recent Patents on Corrosion Science, 2 pp. 40-54.

[23] M. Long, H.J. Rack, (1998), *Titanium alloys in total joint replacement — a materials science perspective*, Biomaterials, 19(18), pp. 1621-1639.

[24] D.W. Hoeppner, V. Chandrasekaran, (1994), Fretting in orthopaedic implants: A review, Wear, 173(1-2), pp. 189-197.

[25] J. Pan, D. Thierry, C. Leygraf, (1996), *Electrochemical impedance spectroscopy study of the passive oxide film on titanium for implant application*, Electrochimica Acta, 41(7-8), pp.1143-1153.

[26] M. Geetha, A.K. Singh, R. Asokamani, A.K. Gogia, (2009), *Ti based biomaterials, the ultimate choice for orthopaedic implants – A review*, Progress in Materials Science, 54(3), pp. 397-425.

[27] H. Hermawan, D. Ramdan, J.R.P. Djuansjah, (2011), *Metals for Biomedical Applications*, in: R. Fazel-Rezai (Ed.) Biomedical Engineering - From Theory to Applications, InTech.

[28] W.A. Lane, (1895), *Some remarks on the treatment of fractures*, The British Medical Journal, 1 pp.861-863.

[29] T. Ma, P. Wan, Y. Cui, G. Zhang, J. Li, J. Liu, Y. Ren, K. Yang, L. Lu, (2012), *Cytocompatibility of High Nitrogen Nickel-Free Stainless Steel for Orthopedic Implants*, Journal of Materials Science & Technology, 28(7), pp.647-653.

[30] S. Mischler, A.I. Munoz, (2013), *Wear of CoCrMo alloys used in metal-on-metal hip joints: A tribocorrosion appraisal*, Wear, 29, pp.1081-1094.

[31] M.T. Mathew, M.J. Runa, M. Laurent, J.J. Jacobs, L.A. Rocha, M.A. Wimmer, (2011), *Tribocorrosion behavior of CoCrMo alloy for hip prosthesis as a function of loads: A comparison between two testing systems*, Wear, 271, pp.1210-1219.

[32] Y. Yan, A. Neville, D. Dowson, S. Williams, (2006), *Tribocorrosion in implants - assessing high carbon and low carbon Co-Cr-Mo alloys by in situ electrochemical measurements*, Tribol Int, 39, pp.1509-1517.

[33] S. Kalpakjian, S. R. Schmid, (2015), *Manufacturing Process for Engineering Materials*, 5th Edition, Pearson, India.

[34] Y. Torres, J.J. Pavo´ N, I. Nieto, J.A. Rodri´ Guez, (2011), *Conventional Powder Metallurgy Process and Characterization of Porous Titanium for Biomedical Applications,* Metallurgical and Materials Transactions B, 42B, pp. 891-900.

[35] C. N. Elias, J. H. C. Lima, R. Valiev, M. A. Meyers, (2008), *Biomedical applications of titanium and its alloys*,J. Miner. Met.Mater. Soc. 60, pp. 46-49.

[36] M. T. Mohammed, Z. A. Khan, A. N. Siddiquee, (2014), *Beta titanium alloys: the lowest elastic modulus for biomedical applications: a review*, Int. J. Chem. Nucl. Met.Mater. Eng. 8(8), pp. 752 – 757.

[37] M. Niinomi, T. Hattori, K. Morikawa, T. Kasuga, A. Suzuki, H. Fukui, S. Niwa, (2002), *Development of low rigidity β-type titanium alloy for biomedical applications*, Mater. Trans. JIM, 43 (12), pp. 2970 – 2977.

[38] M. Greger, M. Cerny, L. Kander, J. Kliber, (2009), *Structure and properties of titanium implants*, Metall. 48 (4), pp. 249 – 252.

[39] S. Zherebtsov, G. Salishchev, R. Galeyev, K. Maekawa, (2005), *Mechanical Properties of Ti-6Al-4V titanium alloy with submicrocrystalline structure produced by severe plastic deformation*, Mater. Trans. JIM, 49 (9), pp. 2020 – 2025.

[40] T. Threrujirapapong, K. Kondoh, H. Imai, J. Umeda, B. Fugetsu, (2009), *Mechanical Properties of titanium matrix composite reinforced with low cost carbon black via powder metallurgy processing*, Mater. Trans. JIM, 50 (12), pp. 2757 – 2762.

[41] C. Santulli, F. Billi, (2002), *Normal and off-axis compression tests of biocompatible titanium dental implants monitored by acoustic emission*, J. Mater. Sci. Lett. 21, pp. 727–730.

[42] R. O. Ritchie, D. L. Davidson, B. L. Boyce, J. P. Campbell, O. Roder, (1999), *High-cycle fatigue of Ti-6Al-4V*, Fatigue Fract. Eng. Mater.Struct. 22, pp. 621 – 631.

[43] R. K. Nalla, B. L. Boyce, J. P. Campbell, J. O. Peters, R. O. Ritchie, (2002), *Influence of microstructure on high-cycle fatigue of Ti-6Al-4V: Bimodal vs. lamellar structures*, Metall. Mater. Trans. A 33A, pp. 899 – 918.

[44] W. Chen, Y. Yamamoto, W. H. Peter, S. B. Gorti, A. S. Sabau, M. B. Clark, S. D. Nunn, J. O. Kiggans, C. A. Blue, J. C. Williams, B. Fuller, K. Akhtar, (2011), *Cold compaction study of Armstrong process Ti-6Al-4V powder*s, Powder Technol. 214, pp. 94-99.

[45] W. Chen, Y. Yamamoto, W. H. Peter, M. B. Clark, S. D. Nunn, J. O. Kiggans, T. R. Muth, C. A. Blue, J. C. Williams, K. Akhtar, (2012), *The investigation of die-pressing and sintering behavior of ITP CP-Ti and Ti-6Al-4V powders*, J. Alloy. Compd. 541, pp. 440-447.

[46] B. Behrens, E. Gastan, N. Vahed, (2010), *Application of tool vibration in die-pressing of Ti-powder*, Prod. Eng. Res. Devel. 4, pp. 545 – 551.

[47] H. Choe, S. M. Abkowitz, S. Abkowitz, D. C. Dunand, (2005), *Effect of tungsten additions on the mechanical properties of Ti-6Al-4V*, Mater. Sci. Eng., A, 396, pp. 99 – 106.

[48] H. Choe, S. Abkowitz, S. M. Abkowitz, (2008), *Influence of processing on the mechanical properties of Ti-6Al-4V-based composites reinforced with 7.5 mass% TiC and 7.5 mass% W*, Mater. Trans., JIM, 49 (9), pp. 2153 – 2158.

[49] A. Afrin, A. B. Sulong, N. Muhamad, J. Syarif, M. I. Ramli, (2014), *Material processing of hydroxyapatite and titanium alloy (HA/Ti) composite as implant materials using powder metallurgy: a review*, Mater. Des. 55, pp. 165 – 175.

[50] M. Ghorbani, A. Afshar, N. Ehsani, M. R. Saeri, C. C. Sorrell, (2002), *Interface characterization of plasma sprayed hydroxyapatite coat on Ti-6Al-4V*, Int. J. Eng. Trans. B, 15(2), pp.173 – 182.

[51] V. M. Imayev, R. A. Gaisin, R. M. Imayev, (2018), *Microstructure and mechanical properties of near α titanium alloy based composites prepared in situ by casting and subjected to multiple hot forging*, Journal of Alloys and Compounds, 762, pp. 555-564.

[52] R. A. Gaisin, V. M. Imayev, R. M. Imayev, (2017), *Effect of hot forging on microstructure and mechanical properties of near α titanium alloy/TiB composites produced by casting*, Journal of Alloys and Compounds, 723, pp. 385-394.

[53] Matthew S. Dahar, Sesh A. Tamirisakandala, John J. Lewandowski, (2018), *Evolution of fatigue crack growth and fracture behavior in gamma titanium aluminide Ti-43.5Al-4Nb-1Mo-0.1B (TNM) forgings*, International Journal of Fatigue, 111, pp. 54-69.

[54] M. Bambach, A. Emdadi, I. Sizova, U. Hecht, F. Pyczak, (2018), *Isothermal forging of titanium aluminides without beta-phase — Using non-equilibrium phases produced by spark plasma sintering for improved hot working behaviour*, Intermetallics, 101, pp. 44-55.

[55] H. Miura, M. Kobayashi, T. Aoba, H. Aoyama, T. Benjanarasuth, (2018), *An approach for room-temperature multi-directional forging of pure titanium for strengthening*, Materials Science and Engineering: A, 731, pp. 603-608.

[56] Z. Bézi, G. Krállics, M. El-Tahawy, P. Pekker, J. Gubicza, (2018), *Processing of ultrafine-grained titanium with high strength and good ductility by a combination of multiple forging and rolling,* Materials Science and Engineering: A, 688, pp. 210-217.

[57] Xian Zheng Lu, Luen Chow Chan, (2018), *X-ray CT assisted damage identification in warm forging,* Procedia Manufacturing, 15, pp. 535-541.

[58] Irina Sizova, Markus Bambach, (2017), *Hot workability and microstructure evolution of pre-forms for forgings produced by additive manufacturing*, Procedia Engineering, 207, pp. 1170-1175.

[59] Antonino Ducato, Gianluca Buffa, Livan Fratini, Rajiv Shivpuri, (2014), *Influence of geometrical ratios in forgeability of complex shapes during hot forging of Ti-6Al-4V alloy*, Procedia Engineering, 81, pp. 516-521.

[60] Ali Mamedov, Hakan Ozturk, Taner Makas, (2017), *Investigation of mechanical and microstructural properties of Ti-6Al-4V alloy depending on hot forging process parameters,* Procedia Engineering, 207, pp. 2155-2160.

[61] B. Isik, A. Kentli, (2014), *The prediction of surface temperature in drilling Ti6Al4V*, Arch. Met. Mater.59 (2), pp. 467 – 471.

[62] E. A. Rahim, S. Sharif, Z. A. Ahmad, A. S. Mohruni, I. A. Syed, (2005), *Machinability investigation when drilling titanium alloys*, International Conference on Leading Edge Manufacturing in 21st Century, Nagoya, Japan.

[63] P. K. Shetty, R. Shetty, D. Shetty, F. Rehaman, T. K. Jose, (2014), *Machinability study on dry drilling of titanium alloy Ti-6Al-4V using L9 orthogonal array*, International Conference on Advances in Manufacturing and Materials Engineering (AMME2014), Procedia Materials Science 5, pp. 2605 – 2614.

[64] A. Kumar, V. Kumar, J. Kumar, (2013), *Multi-response optimization of process parameters based on response surface methodology for pure titanium using WEDM process*, Int. J. Adv. Manuf. Technol. 68, pp. 2645–2668.

[65] A. Kumar, V. Kumar, J. Kumar, (2012), *Prediction of Surface Roughness in Wire Electric Discharge Machining (WEDM) Process based on Response Surface Methodology*, Int. J. Eng. Technol. 2(4), pp. 708-719.

[66] D. S. Badkar, K. S. Pandey, G. Buvanashekaran, (2013), *Development of RSM- and ANN-based models to predict and analyze the effects of process parameters of laser-hardened commercially pure titanium on heat input and tensile strength*, Int. J. Adv. Manuf. Technol. 65, pp. 1319–1338.

[67] M. Manjaiah, S. Narendranath, S. Basavarajappa, V. N. Gaitonde, (2014), *Wire electric discharge machining characteristics of titanium-nickel shape memory alloy*, Trans. Nonferrous Met. Soc. China, 24, pp. 3201−3209.

[68] M. M. Rahman, Md. A. R. Khan, K. Kadirgama, M.A. Maleque, R. A. Bakar, (2011), *Parametric Optimization in EDM of Ti-6Al-4V using Copper Tungsten Electrode and Positive Polarity: A Statistical Approach*, Mathematical Methods and Techniques in Engineering and Environmental Science, 13th WSEAS Conference Proceedings, pp. 24-29.

[69] Farnaz Nourbakhsh, K. P. Rajurkar, A. P. Malshe, Jian Cao, (2013), *Wire electro-discharge machining of titanium alloy*, Proceedings of the First CIRP Conference on Biomanufacturing, Procedia CIRP 5, pp. 13 – 18.

[70] M.P. Garg, A. Jain, G.Bhushan, (2014), *An Investigation of Wire Electric Discharge Machining of High Temperature Titanium Alloy*, Proceedings of the 5th International & 26th All India Manufacturing Technology, Design and Research Conference (AIMTDR 2014) IIT Guwahati, Assam, India, pp. 862-1 -862-6.

[71] Munmun Bhaumik, Kalipada Maity, (2018), *Effect of different tool materials during EDM performance of titanium grade 6 alloy*, Engineering Science and Technology, an International Journal, 21(3), pp. 507-516.

[72] Binoy Kumar Baroi, Siddhartha Kar, Promod Kumar Patowari, Electric Discharge Machining of Grade 2 Titanium alloy and its parametric study, (2018), Materials Today: Proceedings, 5 (2), Part 1, pp. 5004-5011.

[73] Sonja Kieren-Ehses, Martin Bohley, Peter Arrabiyeh, Benjamin Kirsch, Jan C. Aurich, (2018), *Influence of different metal working fluids when micro-machining CP-Titanium with 50 µm diameter micro end mills*, Procedia CIRP, 71, pp. 198-202.

[74] Hongyan Jing, Ming Zhou, Jianwei Yang, Shengzuo Yao, (2018), *Stable and Fast Electrical Discharge Machining Titanium Alloy with MIMO Adaptive Control System,* Procedia CIRP, 68, pp. 666-671.

[75] Aimin Yang, Yang Han, Yuhang Pan, Hongwei Xing, Jinze Li, *Optimum surface roughness prediction for titanium alloy by adopting response surface methodology*, (2017), Results in Physics, 7, pp. 1046-1050.

[76] Jianfei Sun, Shun Huang, Tianming Wang, Wuyi Chen, (2018), *Research on surface integrity of turning titanium alloy TB6*, Procedia CIRP, 71, pp. 484-489.

[77] S. M. Ravi Kumar, Suneel Kumar Kulkarni, (2017), *Analysis of hard machining of titanium alloy by Taguchi method*, Materials Today: Proceedings, 4 (10), pp. 10729-10738.

[78] Dong Yang, Zhanqiang Liu, Xiao Xiao, Feng Xie, (2018), *The Effects of Machining-induced Surface Topography on Fatigue Performance of Titanium Alloy Ti-6Al-4V,*Procedia CIRP, 71, pp. 27-30.

[79] B. Kasemo, (1983), *Biocompatibility of titanium implants: Surface science aspects*, The Journal of Prosthetic Dentistry, 49, pp. 832-837.

[80] J.W. Schultze, M.M. Lohrengel, (2000), *Stability, reactivity and breakdown of passive films, Problems of recent and future research*, Electrochimica Acta, 45, pp. 2499-2513.

[81] C. Coddet, A.M. Craze, G. Beranger, (1987), *Measurements of the adhesion of thermal oxide films: application to the oxidation of titanium*, J Mater Sci, 22, pp. 2969-2974.

[82] D. Reyes-Coronado, G. Rodríguez-Gattorno, M.E. Espinosa-Pesqueira, C. Cab, R.d. Coss, G. Oskam, (2008), *Phase-pure TiO_2 nanoparticles: anatase, brookite and rutile*, Nanotechnology, 19(14), 145605.

[83] M. Pourbaix, (1984), *Electrochemical corrosion of metallic biomaterials*, Biomaterials, 5(3), pp. 122-134.

[84] E. J. Kelly, (1982), *Electrochemical Behavior of Titanium*, J.O. Bockris, B.E. Conway, R. White (Eds.) Modern Aspects of Electrochemistry, Springer US, pp. 319-424.

[85] J.E. Sundgren, P. Bodö, I. Lundström, (1986), *Auger electron spectroscopic studies of the interface between human tissue and implants of titanium and stainles*s steel, Journal of Colloid and Interface Science, 110(1), pp. 9-20.

[86] J.M. Anderson, (1992), *The bone-biomaterial interface*. J. E. Davies, (ed.), University of Toronto Press, Toronto, Canada, 1991, Journal of Biomedical Materials Research, 26(10), pp. 1395-1396.

[87] A. Dalmau, V. Gui˜nón Pina, F. Devesa, V. Amigó, A. Igual Mu˜noz, (2013), *Influence of fabrication process on electrochemical and surface properties of Ti–6Al–4V alloy for medical applications*, Electrochimica Acta 95, pp. 102 – 111.

[88] M. Long, H.J. Rack, (1998), *Titanium alloys in total joint replacement—a materials science perspective*, Biomaterials, 19(18), pp. 1621–1639.

[89] I. Milosev, M. Metikos-Hukovi´c, H.H. Strehblow, (2000), *Passive film on orthopaedic TiAlV alloy formed in physiological solution investigated by X-ray photoelectron spectroscopy*, Biomaterials 21(20), pp. 2103-2113.

[90] X. Liu, P.K. Chu, C. Ding, (2004), *Surface modification of titanium, titanium alloys, and related materials for biomedical applications*, Materials Science and Engineering R: Reports 47(3-4), pp. 49-121.

[91] G. Adamek, J. Jakubowicz, (2010), *Microstructure of the mechanically alloyed and electrochemically etched Ti–6Al–4V and Ti–15Zr–4Nb nanocrystalline alloys*, Materials Chemistry and Physics 124(2-3), pp. 1198-1204.

[92] Y.L. Jo, C.M. Lee, H.S. Jang, N.S. Lee, J.H. Suk, W.H. Lee, (2007), *Mechanical properties of fully porous and porous-surfaced Ti–6Al–4V implants fabricated by electro-discharge-sintering*, Journal of Materials Processing Technology 194(1-3), pp. 121-125.

[93] Montasser M. Dewidar, J.K. Lim, (2008), *Properties of solid core and porous surface Ti–6Al–4V implants manufactured by powder metallurgy*, Journal of Alloys and Compounds, 454(1-2), pp. 442-446.

[94] V. Barranco, M.L. Escudero, M.C. García-Alonso, (2011), *Influence of the microstructure and topography on the barrier properties of oxide scales generated on blasted Ti6Al4V surfaces*, Acta Biomaterialia, 7(6), pp. 2716-2725.

[95] A. Bandyopadhyay, F. Espana, V.K. Balla, S. Bose, Y. Ohgami, N.M. Davies, (2010), *Influence of porosity on mechanical properties and in vivo response of Ti6Al4V implants*, Acta Biomaterialia 6(4), pp. 1640-1648.

[96] P. F. Thomson, (1986), *Densification of sintered metal compacts by cold deformation*, Journal of Mechanical Working Technology, 13(2), pp. 219-227.

[97] *P. Ramakrishnan, (2013), Automotive applications of powder metallurg*y, Advances in Powder Metallurgy, pp. 493-519.

[98] G. Sutradhar, A.K. Jha, S. Kumar, (1995), *Cold forging of sintered iron-powder preforms*, Journal of Materials Processing Technology, 51, pp. 369-386.

[99] Edmond Ilia, Kevin Tutton, Mike O'Neill, (2005), *Forging a way towards a better mix of PM automotive steels*, Metal Powder Report, 60(3), pp. 38-44.

[100] A. K. Jha and S. Kumar, (1983), *Forging of metal powder performs*, Int. J. Mach. Tool Design Res. 23(4), pp. 201-212.

[101] L. M. M. Alves, P. A. F. Martins, and J. M. C. Rodrigues, (2006), *A new yield function for porous materials*, J. Mater. Process. Tech. 179(1-3), pp. 36-43.

[102] A. K. Jha, S. Kumar, (1978), *Deformation characteristics and fracturing of sintered copper powder strips during cold forging*, J. Mech. Work Technol. 16(145), 1988. Sci. Technol. 22(2), pp. 45.

[103] S. Malayappan and G. Esakkimuthu, (2006), *Barreling of aluminium solid cylinders during cold upsetting with differential frictional conditions at the faces*, Int. J. Adv. Manuf. Tech. 29, pp. 41-48.

[104] P. Kumar, R. K. Ranjan, and R. Kumar, (2011), *Mechanics of deformation during open die forging of sintered preform: comparative study by equilibrium and upper bound methods*, ARPN Journal of Engineering and Applied Sciences, 6(6), pp. 83-93.

[105] B. W. Rooks, (1974), *The effect of die temperature on metal flow and die wear during high speed hot forging*, Proc. 15th Int. MTDR conference held in Birmingham, UK, Macmillan, London, pp. 487.

[106] T. Tabata, S. Masaki, K. Hosokawa, (1980), *Int. J. Powder Metal, Powder Techno,* 16 (149).

[107] H.H. Uhlig, (1948), *The Corrosion Handbook*, John Wiley & Sons, New York.

APPENDIX

Annexure 1

Comparative Survey Table of some important past works on development of titanium

Sl.	Year	Author	Findings
1	1983	Kasemo	Found that titanium is an exceedingly reactive metal and it has strong affinity towards oxygen. An oxide layer of 10 Armstrong can form over it in micro-seconds
2	2002	Santulli et al.	Performed compression tests on cast-Ti dental inserts
3	2002	Ghorbani et al.	Examined the interface behaviour of plasma sprayed hydroxyapatite coating on Ti-6Al-4V bio-implants
4	2008	Elias et al.	Detailed that titanium is the best bio-perfect material
5	2009	Greger et al.	Examined the production of nano-structured Ti through ECAP process
6	2010	Bandyopadhyay et al.	Created penetrable Ti-6Al-4V utilizing Laser Engineered Net Shaping and performed in vivo examination, acquiring higher porosity of the samples
7	2011	Torres et al.	Contemplated the impact of process parameters on micro-structure and mechanical properties on P/M Ti
8	2011	Chen et al.	Studied the cold compaction behavior of Armstrong process CP-Ti and Ti-6Al-4V samples
9	2012	Kumar et al.	Built up a quadratic model for dimensional deviation to connect dominating machining parameters on WEDM of Grade 2 Titanium
10	2013	Nourbakhsh et al.	Studied the impact of Zn-covered metal wire on WEDM of Ti compared to brass wire
11	2013	Dalmau et al.	Researched the electro-chemical conduct of rolled and sintered Ti-6Al-4V by various electro-chemical strategy
12	2014	Mohammed et al.	Checked that titanium is utilized in biomedical applications owing to its high specific strength, great corrosion obstruction and lower elastic modulus
13	2014	Shetty et al.	Performed machinability examination on cast Ti-6Al-4V using L9 orthogonal array
14	2014	Manjaiah et al.	Considered improvement of Surface roughness and MRR through WEDM of Ti-Ni Shape Memory Alloy (SMA)
15	2017	Mamedov et al.	Introduced a numerical modelling of Ti-6Al-4V forging
16	2017	Sizova et al.	Studied the microstructure advancement amid heat-treatment and hot-working of Ti-6Al-4V samples prepared by Selective Laser Melting
17	2017	Kumar et al.	Optimized the surface roughness of Ti-alloy during turning in a CNC machine through L9 orthogonal array
18	2018	Imayev et al.	Examined the forging characteristics of near alpha Ti-alloy (VT18U) cast with TiB and TiC
19	2018	Banbach et al.	Investigated hot forgeability of TNB-V5 created by Spark Plasma Sintering
20	2018	Yang et al.	Characterized surface topography in peripheral milling of Ti-6Al-4V

Annexure 2

Technical Specification of the Universal Testing Machine

- Maximum capacity – 400 kN
- Model – KUT 40
- Sl. No. – 2K7/85
- Make – Ratnakar Enterprises, Maharashtra, India

Technical Specification of the Tubular Furnace (Pre-heater)

- Installed power – 4 kW
- Voltage required – 230 V
- Phase – single
- Maximum temperature in working space – 1000 °C
- Heating tube material – Quartz
- Working space medium – nitrogen gas
- Make – Therelek Furnaces Pvt. Ltd. Thane, India

Technical Specification of the Electric Resistance Batch-type Vacuum Furnace

- Installed power – 31 kW
- Rated capacity of the heating chamber – 28 kW
- Shut-off capacity – $27^{+2.7}$ kW
- Nominal temperature in working space – 2000 °C
- Stability of the rated power maintenance during the control of heating of automatic control system - ± 1 %
- Working space dimensions – width: 100 mm; length: 300 mm; height: 100 mm
- Batch weight – 12 ± 0.5 kg
- Working space medium – vacuum
- Ultimate residual pressure in cold condition of electric furnace – 6.65×10^{-3} Pa or 5×10^{-5} mm of Hg
- Rated supply line voltage – 380/220 V
- Current rated frequency – 50 Hz
- Number of heater phases – 1
- Water flow-rate cooling – $1.6^{+0.2}$ m^3/hour or 27 litres/hour

- Electric furnace dimensions – width: 1800 mm; length: 1450 mm; height: 1510 mm
- Electric furnace weight – 1.1 ton

The Russian make electric furnace (Model No. CHB3-1.3.1/20H2) with tungsten heaters and screen thermal insulation made of tungsten and molybdenum consists of – a heating chamber, a diffusion pump operated vacuum unit, a water cooling system, a furnace transformer, a control desk and a microprocessor based controller – 'POTAP-100'. If this furnace is required to be operated at a gas supply, then maximum gas pressure is not to exceed 0.02 MPa and cooling water temperature gradient is 20 °C between inlet and outlet.

Technical Specification of the Scanning Electron Microscope

- Magnification – 5 to 3,00,000X
- Resolution – 3 nm
- Accelerating voltage – 0 to 30 kV (In 55 steps)
- Maximum working space dimension – 90 mm × 90 mm
- Filament - Tungsten
- Fully computer controlled
- Make / Model – JEOL JSM-6360 (Japan)

Technical Specification of the Microhardness Tester

- Test mode – Automatic focus
- Test Scale – Vickers Hardness (HV), Knoop Hardness (HK), Fracture toughness (KC)
- CCD Camera – Inter-line method 1/3 inch 0.8 Megapixel monochrome
- Reading speed – Shortest 0.5 sec / 1 point
- Reading reproducibility – ±0.5 %
- Unit of minimum measurement – 0.1 μm
- Minimum indentation reading – 20 μm for 50× object length
- Display magnification – 2000×; 800×; 400×; 200×
- Measurement view – 55 μm; 140 μm; 280 μm; 560 μm
- Load – 100 gmf for 15 sec
- Make / Model – AMT-X7 BFS MATSUZAWA (Japan)

Annexure 3

Comparison of theoretical load vs deformation curves with experimental load vs deformation curves

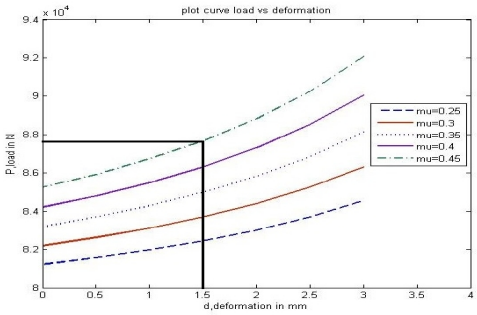

Figure 4.8
(Theoretical)

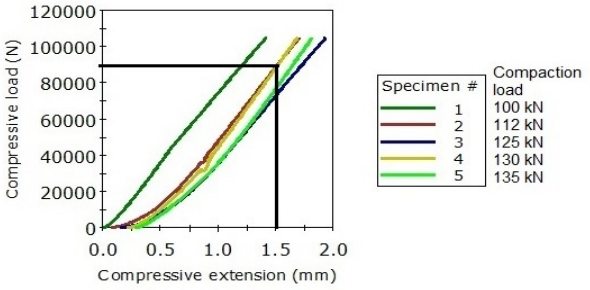

Figure 4.9
(Experimental)

Load vs deformation diagrams

From the comparative evaluation of load vs deformation curves, we can clearly state that the nature of the curves in both cases are identical. In case of theoretical load-deformation curves, up to 81000N, no deformation sets in, however, in case of experimental load-deformation curves, negligible deformation starts initially, because of the closing of pores in the preforms. To create a compression of 0.5 mm, theoretical load required varies from 81000N to 86000N (depending upon the friction coefficient μ; $0.25 < \mu < 0.45$), whereas experimental load required is 20000N, which is much less than the theoretical one. It happens because, the interfacial friction condition actually taken place between the surfaces is quite different than assumed frictional conditions. On the other hand, to generate a deformation of 1.5 mm, theoretical load required is nearly 88000N for μ=0.45, whereas actual load required for specimen 4 (compacted at 130 kN) was 90000N, which is quite similar. From this we can presume that, the friction factor for specimen 4, which was compacted at 130 kN is near about 0.45.

Annexure 4

Corrosion Data

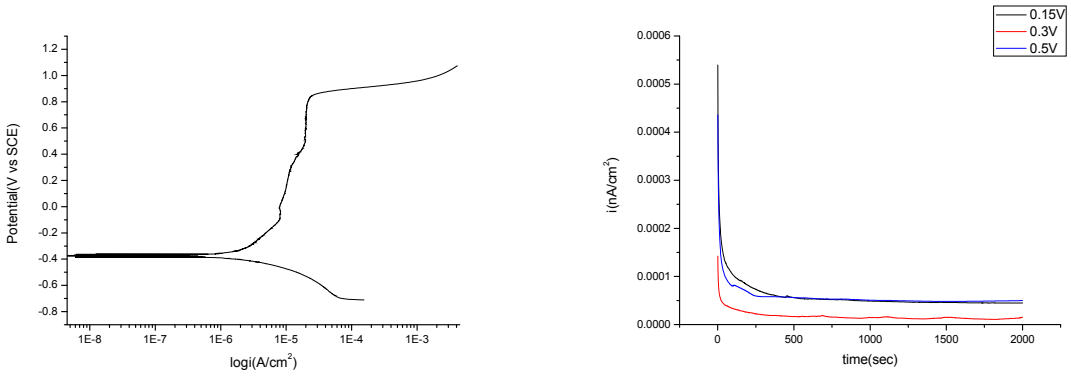

(a) (b)

Potentiodynamic polarization curve (a) and polarization current plots (b) for as-received Ti-samples sintered at 1350 °C [Similar plots also generated for 1400 °C and 1450 °C]

Experimental set-up

- Reference electrode – Saturated Calomel Electrode (SCE)
- Counter electrode – Platinum / Graphite
- Working electrode – Titanium
- Electrolyte solution – Simulated Body Fluid (SBF)

Chemical composition of Simulated Body Fluid

Ion	Concentration/mol m^3	
	SBF	Human Blood Plasma
Na^+	142.0	142.0
K^+	5.0	5.0
Mg^{2+}	1.5	1.5
Ca^{2+}	2.5	2.5
Cl^-	147.8	103.0
HCO_3^-	4.2	27.0
HPO_4^{2-}	1.0	1.0
SO_4^{2-}	0.5	0.5